Using TLS-measured Tree Attributes to Estimate the Above Ground Biomass of Individual Small Black Spruce Trees in Canadian Boreal Forest Peatlands

by

Steven Wagers

A thesis submitted in partial fulfillment of the requirements for the degree of

Master of Science

Earth and Atmospheric Sciences
University of Alberta

Abstract

Earth's changing climate poses a number of potential issues for people around the globe. It has become increasingly important for researchers to have the ability to collect good data and build accurate, robust climate models that can help influence the direction of policy makers to mitigate the effects of climate change on as many people as possible. One important measurement pertaining to climate modelling is above ground biomass (AGB), for its ability to describe the amount of carbon stored within living vegetation, such as trees. Measuring AGB directly requires that trees be destructively sampled and weighed. An alternative to this method is to use allometric equations that are based on other, more easily measurable tree attributes as a way of estimating AGB. Advances in technology and the emergence of laser scanning technology has allowed for fast, highly detailed tree measurements. In the first chapter, this thesis explores the importance of developing accurate AGB models to measure the amount of carbon stored in forest ecosystems, and the ways laser scanning technology has changed the way researchers are able to measure the tree attributes needed for these equations. The research questions and hypotheses of this thesis are then posed based on the emergent uses of these technologies, and the needs for biomass mapping.

In the second chapter, Terrestrial Laser Scanning (TLS) was used to develop point clouds of plots of small black spruce (*Picea mariana* L.) trees in the Taiga plains ecozone of the Northwest Territories. Tree attributes were measured to build allometric models to estimate individual tree AGB. The measurements used as predictor variables in the allometric equations created in this thesis were crown area, crown diameter, height, individual tree volume from a quantitative structure model (QSM), minimum bounding box volume of individual tree point clouds, diameter at breast height (DBH), and the products of crown area and height, crown

diameter and height, and DBH and height. Multiple forms of these equations were created using both ordinary least squares (OLS) and weighted least squares (WLS) regressions, with either tree height or ground-measured biomass determining how much weight each tree received in the models. Model predictions were cross validated and ranked by average tree error, average RMSE and average adjusted R^2. The best model was then tested against other established models to determine its viability. This thesis uses TLS point clouds to explore the applicability of tree attributes that can also be easily measured from airborne platforms such as airborne- and UAV laser scanners (ALS and ULS respectively) and provides the allometric equations that can be used for a common species found in a typical peatland environment in the Taiga Plains ecozone. A preliminary experiment to assess if the models using crown size and height could have the potential to be used with point clouds created by airborne methods was conducted. To simulate the decreasing point densities that are generally seen in ALS and ULS point clouds, rasters of varying cell size looking down on the trees were used to measure crown attributes such as crown area and crown diameter. A sensitivity analysis was then done to show how the AGB estimates given by equations provided by the best models using these tree attributes were affected as the raster cell size increased.

The third chapter of this thesis examines the significance of the models created in Chapter 2, and comments on the implications of the results obtained. Potential future studies, including the possibility of flying scanning missions and using the AGB models from this thesis are also discussed.

Preface

This thesis is an original work by Steven Wagers. The research conducted in this thesis is the culmination of a joint effort between the Remote Sensing group at the Northern Forestry Centre under the direction of Dr. Guillermo Castilla with support from the Government of the Northwest Territories, and the Centre for Earth Observation Sciences led by Dr. G.A. Sanchez-Azofeifa, who also provided the terrestrial laser scanner used in Chapter 2.

Terrestrial Laser Scanning of the trees used in Chapter 2 were collected by Michelle Filiatrault and me. Drying, weighing and lab measurements of trees were done by Tyler Rea, Nicole Wozney and Mihai Voicu. The project was designed by Guillermo Castilla and myself, and I performed the data analysis and curation. I also compiled the information in Chapters 1 and 3.

Acknowledgements

I would like to thank my supervisor, Dr. Arturo Sanchez-Azofeifa for taking a chance on me and giving me the opportunity to join his lab and learn about Terrestrial Laser Scanning and remote sensing. Under his tutelage, I have grown a lot as a scientist, and I have gotten the chance to take part in some exciting projects that I otherwise never would have had the chance to do. I am very grateful to be working at CEOS and look forward to the future work that we will do together in the coming years.

I would also like to thank Dr. Guillermo Castilla for his guidance and for imparting his knowledge to me and helping me to turn this project into a reality. His patience and ability to explain his own thought processes in an easily understandable manner has helped me to improve the way that I approach science and to develop the tools necessary to be successful in this field. Additionally, I would like to recognize Michelle Filiatrault for being a great source of support and helping me to get acclimatized working as a scientist, not to mention the wealth of knowledge that she has imparted to me as well.

Dr. Benoit Rivard, who served on my supervisory committee, also provided very valuable feedback throughout this degree, and I want to thank him for taking an interest in my work and helping me to critically analyze what I am doing in an effort to create the best final product possible.

The entire group at CEOS has been amazing as well, providing feedback and being available to discuss new ideas. In particular, I would like to thank Felipe Alencastro, Jose Antonio Guzman, and Connor Bax for their willingness to share their knowledge of remote sensing science, processing point clouds, and for their valuable feedback that helped me to move forward with my work.

I would be remiss if I did not thank my family for all their support in getting me to where I am today. My father, Eric Wagers, my mother, Brigitta Wagers, and my sister, Annette Wagers have all been instrumental in supporting me and keeping me in the right frame of mind to make this thesis a reality. They have always been there for me when I was struggling through some of the tougher portions of this degree, and I would certainly not have been able to do it without them.

Finally, I would like to acknowledge the financial support I received from the University of Alberta and from Natural Resources Canada to allow me to do this work.

Table of Contents

List of Tables

List of Figures

Chapter 1 -- Introduction

1.1 Carbon, Biomass, and the Climate System

Climate change is one of the biggest global threats to the health and well-being of humanity. Changes in local weather patterns have been observed and linked to the warming climate, with many regions around the world showing increased precipitation (Westra et al., 2013). A 12% increase in record-breaking rainfall events was observed globally from 1980-2010 compared to what would be expected in a situation where the climate remained stable (Lehmann et al., 2015). These increases in precipitation are projected to lead to an increase in the frequency of flood events, affecting millions of people even if the average global temperature increase is held to 2°C (Hirabayashi et al., 2013). Warm summers in the Arctic have been linked to slower-moving weather systems in the Northern Hemisphere, increasing the risk of more persistent extreme weather events such as heatwaves (Kornhuber & Tamarin-Brodsky, 2021), which are also becoming more frequent in recent years (Coumou et al., 2013; Sun et al., 2014). Higher average global temperature affects the oceans as well, through processes of thermal expansion, changes in terrestrial water storage, and melt water from glaciers and the Antarctic and Greenland ice sheets (Frederikse et al., 2020). These processes can cause the average sea level (ASL) to rise, which poses not only a physical threat to coastal cities and countries around the world (Dasgupta et al., 2009), but a financial one as well. A recent study by Abadie (2018) predicted the potential cumulative damages associated with sea level rise due to climate change to be in the trillions of US dollars for many of the world's largest coastal cities by the year 2100. The potential impacts of climate change, both in terms of human lives and financial costs, highlight the importance of having a strong and intimate knowledge of all components of the climate system. Such knowledge would allow for better predictions of future climate scenarios that can be used to create policies to best mitigate these costs and develop adaptive strategies to deal with the climate impacts anticipated in the coming decades.

One such component that plays a critical role in the Earth's climate system is the carbon cycle, which exists as multiple interlinked reservoirs, where carbon is able to flow from one reservoir to the next (Ciais et al., 2013). In the atmosphere, carbon is found in two of the three main drivers of climate change: carbon dioxide (CO_2) and methane (CH_4) (Ciais et al., 2013). These gases are called greenhouse gases, because they absorb outgoing infrared radiation from

the Earth, and then reemit it in a random direction, meaning that some of the radiation is sent back towards the Earth (McFarland et al., 2007). It is this greenhouse effect that makes the Earth capable of supporting liquid water (McFarland et al., 2007), but as atmospheric greenhouse gas concentrations increase, so too does the average global temperature. CO_2 is a particularly prevalent greenhouse gas, accounting for ~76 % of global greenhouse gas emissions (IPCC, 2014) and contributing ~80% of the increase in radiative forcing since 1990 (Butler & Montzka, 2021). Atmospheric greenhouse gas concentrations have been rising for hundreds of years since The Industrial Revolution. In 1750, the atmospheric CO_2 concentration was around 278 ppm (Ciais et al., 2013), but has since increased to nearly 420 ppm in 2021 (NASA Global Climate Change, 2021). The current concentration is higher than at any other point in the last 800,000 years (Ciais et al., 2013). This rapid increase can be primarily attributed to human activity, such as fossil fuel burning and changing land use (Bandh et al., 2021; Ciais et al., 2013), which releases carbon that was previously stored in other reservoirs like the biosphere and lithosphere into the atmosphere.

Fortunately, processes exist within the carbon cycle to remove carbon from the atmosphere. One of the most important processes for doing this comes from the interactions between the atmosphere and the biosphere. Vegetation removes carbon dioxide from the atmosphere through the process of photosynthesis, in which carbon dioxide, water and energy from sunlight is converted into oxygen and glucose, which can be stored in plant tissue as starch (Gibbs & Latzko, 1979). In this way, large vegetated areas, like forests, can act as carbon sinks (Annighöfer et al., 2016; X. Chen et al., 2018; Reichstein & Carvalhais, 2019; Vashum, 2012) storing carbon in vegetative tissue and preventing it from contributing to the greenhouse effect. Globally, it is estimated that forests contain roughly 660 Pg of carbon, of which almost 300 Pg is stored in living biomass (FAO, 2020). Carbon makes up roughly half of the dry biomass (Brown, 1997; X. Chen et al., 2018; Houghton, 2008; Vashum, 2012), making biomass a vital quantity in the monitoring of carbon stocks. This is pertinent to forests which make up between 70 and 90% of the planet's terrestrial biomass (Houghton, 2008; Lucas et al., 2015; Reichstein & Carvalhais, 2019).

1.2 Uncertainties in Climate Modelling and Biomass Modelling

Unfortunately, there are still many uncertainties in the carbon cycle that can propagate through to the climate models. These models depend on inputs from many different components such as the atmosphere, biosphere, and hydrosphere that are also linked to one another (Gettelman & Rood, 2016). Carbon can flow between these components, and small changes in one process can propagate through to other processes where they can become magnified or cause unforeseen feedbacks (Bonan, 2008). This means it is critical to understand the exchange processes between the different components with a high degree of certainty so a complete picture of the carbon cycle and its adaptive capabilities can be built (Gettelman & Rood, 2016). Because of the vast extent of Earth's forests (roughly a third of the land surface (Reichstein & Carvalhais, 2019)) and their role in removing CO_2 from the atmosphere, the carbon exchange between the atmosphere and forests is particularly important (Bonan, 2008).

It is also important to consider that while vegetation plays a major role in storing carbon, it cannot do so indefinitely. When trees die and decompose, or are burned, the carbon that was previously stored within the plant tissue is once again released into the atmosphere, turning them from sinks into sources of CO_2 (Fearnside, 2000; Zhao et al., 2021). What happens to the carbon and the amount of biomass that is subject to burns is another area of uncertainty within climate modelling (Fearnside, 2000), which further indicates the need for accurate, real-time biomass estimation methods so that carbon released in wildfires can be properly accounted for. The vegetation residence time for carbon is still not well understood either, and is a significant contributor to the uncertainty of many climate models (Friend et al., 2014). Developing methods to estimate biomass quickly and accurately over large areas could be a significant step towards understanding these residence times, as it would allow for higher temporal resolution observations to monitor changes in biomass and, by extension, carbon stocks.

It is known that carbon fluxes are tightly linked to vegetation biomass stocks on a decadal scale, as plants will adjust to the amount of CO_2 in the air around them to a certain extent, but depending on the methods used for modelling global vegetation carbon stocks, predictions may vary from observed amounts by up to 27% (Reichstein & Carvalhais, 2019). Accurate biomass measurements are needed to accurately estimate carbon stocks, but it can be difficult and time-consuming to measure biomass directly, because this requires physically weighing the trees, which can only be done by harvesting them first (Brown, 1997; Picard et al., 2012; Sah et al., 2004). Instead, allometric equations are commonly used to quantify the relationship between

biomass and other, more easily measured variables like diameter at breast height (DBH) and height (Annighöfer et al., 2016; Hyyppä et al., 2020; Navar, 2010; Picard et al., 2012). There are two kinds of allometric biomass models: Generic and species-specific. Generic models are used to predict the biomass of multiple different species of trees, such as all coniferous trees or all broadleaf trees in an area, but they have been shown to be less accurate in their estimations than species-specific models (Annighöfer et al., 2016; Buech & Rugg, 1989; Martinez et al., 2020; Sah et al., 2004). Although species-specific models may be preferred in many cases, the ones that exist tend to favour larger, merchantable trees, as opposed to younger, smaller trees which can contribute a notable portion of biomass, particularly when considering regions that are recovering from disturbances (Annighöfer et al., 2016). As such, there is a need for species-specific biomass equations for small trees. While many allometric equations have been shown to predict above ground biomass (AGB) with considerable accuracy, they often require DBH as an input variable (Abich et al., 2019; Puc-Kauil et al., 2020). Recent studies have shown, however, that incorporating crown size into these equations can lead to more accurate estimates of AGB (Forrester et al., 2021; Jucker et al., 2017). This suggests that it is possible to estimate AGB of trees using estimates of height and crown size without the need for measuring DBH at all, which could be particularly useful when using airborne measurement methods.

1.3 The Role of Technology in Forestry and Biomass Estimation

New technologies have had a large impact on the methods used to estimate biomass in forest inventories. One of the most significant technological advances comes in the form of laser scanners. The types of laser scanning most commonly used in forestry studies include airborne- (ALS) (Holopainen et al., 2013; Mielcarek et al., 2020; Vauhkonen et al., 2014), Unmanned Aerial Vehicle- (ULS) (Colomina & Molina, 2014; Hyyppä et al., 2020), terrestrial- (TLS) (Holopainen et al., 2013; Liang et al., 2016, 2018), mobile- (MLS) (Holopainen et al., 2013; Liang, Hyyppä, et al., 2014), and personal- (PLS) (S. Chen, Liu, et al., 2019; Liang, Kukko, et al., 2014; Stal et al., 2021) laser scanning systems. These machines measure the time it takes for a laser pulse emitted by the scanner to travel to a reflective object, and return to a sensor on the device (also known as a time-of-flight measurement) (Beraldin et al., 2010). For ALS, ULS, and MLS, a Global Navigation Satellite System (GNSS) and an inertial measurement unit (IMU) are necessary to properly position obtained data (S. Chen, Liu, et al., 2019; Holopainen et al., 2013;

Hyyppä et al., 2020; Vauhkonen et al., 2014). Using the known speed of light in air, it is then possible to calculate the distance between the scanner and the reflective object. The end result from these scans is a 3D digital representation of the scanned area in the form of a point cloud (Beraldin et al., 2010).

Of the five methods listed, ALS has been used in forestry the longest, with ties to the profiling LiDAR used in the 1980's (Lim et al., 2003). In the 1990's ALS was used to measure plot level attributes before being adapted to measure individual tree attributes in 1999 (Vauhkonen et al., 2014). One of the main strengths of ALS is its ability to scan large areas of land in a relatively short period of time, with minimal ground truth data required (Brede et al., 2017; Vosselman & Maas, 2010). This allows for more potential remote data collection than ground-based methods. Point densities of the resultant point clouds tend to be lower than the other methods (generally between 1 and 10 pts/m^2) (Brede et al., 2017) however, and because scans are conducted from above the trees, dense multistory canopies can prevent the laser pulses from hitting the ground and understory (Vosselman & Maas, 2010). This effect is known as occlusion, and it occurs when the laser pulse is fully reflected by one object preventing anything behind the initial object to be seen. Being unable to visualize the lower portions of the trees makes it difficult to measure DBH directly and in situations where it is possible to measure from above the methods required need higher point densities than those typical of ALS point clouds (Harikumar et al., 2017). This is a significant drawback as DBH has historically been one of the most important tree attributes in forestry (Liang et al., 2016).

ULS is similar to ALS in that it is often used to scan from above the tree canopy, meaning understory and lower portions of trees are often highly occluded, although recent studies have shown that it is possible to scan below the canopy as well (Hyyppä et al., 2020). While these methods show promise, one of the major challenges faced with below canopy flights is that the GNSS signal is inconsistent, making it unreliable for measuring the scanner's position (Hyyppä et al., 2020). To overcome this a simultaneous localization and mapping (SLAM) system that builds a self-contained map to allow for accurate positioning of data points is needed (Hyyppä et al., 2020). ULS often results in higher point densities than ALS, and there has been some success in recent studies evaluating the possibility of using ULS to directly measure DBH (Brede et al., 2017; Jaakkola et al., 2017). These studies required high point density point clouds

and less accuracy was observed in the direct measurements when compared to TLS scans, indicating further study is needed to develop these methods.

TLS technologies were first used for forest inventory studies in the early 2000s and have since become one of the most common methods of laser scanning used in forestry (Liang et al., 2016). This system uses a ground-based scanner mounted on a tripod and usually has a range of 100-300 m (Liang et al., 2016) meaning that the coverage is considerably smaller than ALS. The tradeoff is that TLS provides a higher level of detail than any other laser scanning method available to date (Wang, Pyörälä, et al., 2019), with millimetre-level ranging precision (Liang et al., 2016, 2018). Instead of the time-of-flight ranging method described above that uses a discrete laser pulse, some TLS systems emit a continuous signal and use a phase shift sensor to measure the reflected waves and estimate the range for out-of-phase return signals (Calders et al., 2020). Although the phase shift method is fast and the sensors that employ it are lightweight and provide high resolution data, they also have a lower signal to noise ratio than their time-of-flight counterparts, thus the time-of-flight TLS systems are more commonly used when studying forests and vegetation (Calders et al., 2020). Many studies have shown the ability of TLS to accurately measure specific tree attributes like height and DBH (Cabo et al., 2018; Ghimire et al., 2017; Liang et al., 2018; G. Liu et al., 2018). One method often used with TLS point clouds is to create a quantitative structure model (QSM) that fits cylinders over structural shapes detected in the point cloud. These QSMs can be used to estimate a tree's volume, which can also be a useful predictor of biomass (Calders et al., 2015; S. Chen, Feng, et al., 2019). This has been shown to be effective for large structures on large trees (e.g. stems) but varying results have been reported as the diameter of the structures (e.g. branches) decreases (Hackenberg et al., 2015; Lau et al., 2018; Takoudjou et al., 2018). This indicates that more research is necessary to determine the extent to which QSMs can accurately model small tree structures. Like the other types of laser scanners, one of the biggest challenges facing TLS is occlusion. The accuracy of attribute measurements and tree detection decreases with younger, smaller trees, particularly in dense plots, where physical characteristics like DBH are smaller, and therefore more likely to be missed by the scanner due to occlusion effects (Liang et al., 2018). Furthermore, because the scanner operates near the ground surface, the lower portions of trees are often better measured than the canopy where branches and foliage may prevent the laser pulses from reaching treetops, leading to underestimated heights (Holopainen et al., 2013; Liang et al., 2018). Tree stems and

lower branches can create occlusion in the horizontal plane on trees located farther away from the scanner, so it is often a good practice to scan from multiple locations to mitigate occlusion effects (Liang et al., 2018).

MLS systems consist of a 3D scanner, camera, GNSS receiver, and IMU mounted on a mobile platform (Wang, Chen, et al., 2019), allowing for greater mobility than a TLS system (Liang, Hyyppä, et al., 2014). When GNSS is available, they can produce point clouds with centimetre-level positioning accuracy (W. Liu et al., 2020). As such, they are often used in urban studies where the signal is likely to be strong and where terrain poses few obstacles (Liang et al., 2014). In forests, canopy cover can cause the satellite signal to be intermittent and unreliable, and terrain is often rough (S. Chen, Liu, et al., 2019; Liang, Hyyppä, et al., 2014). In recent years, however, methods have been developed for improving positioning accuracy when GNSS signal is unavailable (Kukko et al., 2017; W. Liu et al., 2019, 2020; Mao et al., 2015; Shao et al., 2020), potentially making MLS a more attractive option for future forestry studies.

PLS is another relatively new technology that has shown potential for use in forestry over the last decade (S. Chen, Liu, et al., 2019; Gollob et al., 2020a, 2020b; Liang, Kukko, et al., 2014). These systems use SLAM technology to accurately position data points and provide higher registration accuracy than MLS, which requires a clear GNSS signal (S. Chen, Liu, et al., 2019). Furthermore, they are lightweight and their mobility makes them an attractive option over the other, bulkier ground-based scanners (TLS and MLS) (S. Chen, Liu, et al., 2019; Liang, Kukko, et al., 2014), but TLS still provides more precise estimates of tree attributes (Gollob et al., 2020b). PLS is still a new technology and there are few studies examining its usability in a forestry context, but the early results suggest that while more study is needed, it has high potential to become an important and accurate ground-based measurement tool in forestry in the future (Gollob et al., 2020b).

1.4 The Canadian Boreal Forest

Having these new technologies available in Canada is valuable because of the country's vast expanse of boreal forest. Boreal forests are known to play a major role in global carbon storage, accounting for roughly a third of terrestrial carbon stocks (Zhao et al., 2021) and they make up the second largest forest biome in the world at 27% of the global forest area (FAO, 2020). They form a band circling the planet across northern latitude countries in Asia, North

America, and Europe and are characterized by their extensive coniferous forests, bogs, fens, lakes, and wetlands (Zhang, 2019). The temperature at these latitudes is highly variable throughout the year, ranging from as low as -50°C in the Winter to ~20°C in the Summer. Canada is home to 24% of the world's boreal forests (Zhang, 2019), stretching across 270 million hectares from the Yukon Territory to Newfoundland (Natural Resources Canada, 2013). Only 54% of this forest is managed, however, and it is estimated that the managed portion stores 28 Pg of carbon, while the amount of carbon stored in unmanaged forest is currently unknown (Kurz et al., 2013). Roughly a quarter of Canada's boreal forest is peatland (Wieder et al., 2006), and there has been significant research done showing that peatlands are important carbon sinks (Alexandrov et al., 2020; Treat et al., 2019). The majority of the carbon stored in peatlands can be found in the soil (Kurz et al., 2013; Magnan et al., 2020; Tarnocai et al., 2009), but the contribution from AGB should not be ignored because it has a high interannual variability due to disturbances like wildfire and insect infestation, and it can provide insight into the sustainability of forestry practices in an area (Kurz et al., 2013). Additionally, it is predicted that as the climate warms and dries out peatland soil, more carbon will be stored in trees (Magnan et al., 2020), once again implying the need for easily obtained biomass estimates for these regions to monitor these changes.

The most common tree species in peatland environments across the Canadian boreal forest is black spruce (*Picea mariana*, L.) particularly in nutrient poor peatlands where they are often the only tree species present (Smith et al., 2007). In these regions, the black spruce's height is often stunted (Smith et al., 2007), making it important to have accurate biomass estimation models for these smaller trees. Current models for estimating the AGB of black spruce require DBH as an input variable (Alemdag, 1983; Bhatti et al., 2006; Ung et al., 2008) or are not recommended for small trees (Singh, 1984). Models that can accurately estimate the AGB of small black spruce trees in peatland environments using tree variables that can be easily measured by the airborne scanners mentioned above (e.g. ALS, ULS) can help to provide better and more up-to-date biomass inventories for these regions.

1.5 Hypotheses and Objectives

With the background information laid out, it is clear that forest biomass modelling (and by extension, carbon storage) will play an important role in future climate studies as humanity

attempts to understand and mitigate the effects of climate change over the next century. Advances in technology will surely be instrumental for expanding this knowledge, and in particular, the rise of laser scanners has opened many doors for new methods to study forests. As these technologies improve and become cheaper, faster, more accurate and more mobile, the results obtained from them will improve as well.

TLS currently provides the highest quality laser scanning data (Wang, Pyörälä, et al., 2019) and it can be used to develop high quality point cloud estimates than can be used as the foundation for models to predict AGB for individual trees. Based on the importance of biomass estimates for carbon stock calculations and climate studies, as well as the fact that black spruce is a dominant tree species found in peatlands across the Canadian boreal forest, it is necessary to focus on building robust biomass estimation models that can predict AGB of this tree species accurately and quickly while taking advantage of advances in technology. Therefore, this thesis examines the following hypotheses:

1. TLS scans produce highly detailed point clouds that can be used to measure tree attributes with a high level of accuracy. These measurements can then be used to develop allometric equations to accurately estimate the AGB of black spruce between 1.3 and 5 metres tall in boreal peatland environments.
2. Allometric models that use crown size and height as predictors will provide comparable performance for trees between 1.3 and 5 metres tall to the model currently used by Canada's National Forestry Inventory that relies on DBH and height.

Based on these hypotheses, the following objectives were established:

1. Evaluate the ability of TLS to measure multiple tree attributes of small black spruce in peatland environments.
2. Develop allometric models to estimate AGB using the TLS-derived measurements obtained in the first objective, and determine which predictors lead to the best performing models.
3. Assess the ability of the developed equations to estimate AGB by comparing their estimations to those of other established models.

This research will provide significant insight into the predictors used in allometric equations and the role that new technology has in obtaining measurements of those predictors by fitting

and testing models using multiple variables measured using TLS point clouds. Specifically, the models in Chapter 2 that are fitted using predictors that can also potentially be measured by ALS and ULS could have important implications on methods used to estimate AGB in the future without ever having to set foot on the ground. This study also provides a significant case study of the use of TLS to measure small trees, because while TLS has been used to accurately measure many tree attributes on larger, merchantable trees (Cabo et al., 2018; Ghimire et al., 2017; Liang et al., 2018; G. Liu et al., 2018), the accuracy of these measurements decreases as the trees get smaller (Liang et al., 2018). In situations where it is no longer possible to measure these attributes accurately, this thesis provides the framework for developing alternative methods to overcome this obstacle. Finally, by focusing on black spruce trees in peatland environments, this study provides valuable insight on the most prominent tree species found in a common ecosystem across Canada. The equations presented in this thesis could be a valuable tool for forest biomass inventory, while also laying the foundation for further studies to fully utilize technology that has rapidly become an intrinsic part of forestry research.

1.6 References

Abadie, L. M. (2018). Sea level damage risk with probabilistic weighting of IPCC scenarios: An application to major coastal cities. *Journal of Cleaner Production*, *175*, 582–598. https://doi.org/10.1016/j.jclepro.2017.11.069

Abich, A., Mucheye, T., Tebikew, M., Gebremariam, Y., & Alemu, A. (2019). Species-specific allometric equations for improving aboveground biomass estimates of dry deciduous woodland ecosystems. *Journal of Forestry Research*, *30*(5), 1619–1632. https://doi.org/10.1007/s11676-018-0707-5

Alemdag, I. S. (1983). Mass Equations and Merchantability Factors for Ontario Softwoods. *Canadian Forestry Service*, *Information Report*, 1–24.

Alexandrov, G. A., Brovkin, V. A., Kleinen, T., & Yu, Z. (2020). The capacity of northern peatlands for long-term carbon sequestration. *Biogeosciences*, *17*(1), 47–54. https://doi.org/10.5194/bg-17-47-2020

Annighöfer, P., Ameztegui, A., Ammer, C., Balandier, P., Bartsch, N., Bolte, A., Coll, L., Collet, C., Ewald, J., Frischbier, N., Gebereyesus, T., Haase, J., Hamm, T., Hirschfelder, B., Huth, F., Kändler, G., Kahl, A., Kawaletz, H., Kuehne, C., … Mund, M. (2016). Species-specific and generic biomass equations for seedlings and saplings of European tree species. *European Journal of Forest Research*, *135*(2), 313–329. https://doi.org/10.1007/s10342-016-0937-z

Bandh, S. A., Shafi, S., Peerzada, M., Rehman, T., Bashir, S., Wani, S. A., & Dar, R. (2021). Multidimensional analysis of global climate change: A review. *Environmental Science and Pollution Research*, *28*(20), 24872–24888. https://doi.org/10.1007/s11356-021-13139-7

Beraldin, J.-A., Blais, F., & Lohr, U. (2010). Laser Scanning Technology. In *Airborne and Terrestrial Laser Scanning*. Whittles Publishing. http://ebookcentral.proquest.com/lib/ualberta/detail.action?docID=3417283

Bhatti, J. S., Errington, R. C., Bauer, I. E., & Hurdle, P. A. (2006). Carbon stock trends along forested peatland margins in central Saskatchewan. *Canadian Journal of Soil Science*, *86*(Special Issue), 321–333. https://doi.org/10.4141/S05-085

Bonan, G. B. (2008). Forests and Climate Change: Forcings, Feedbacks, and the Climate Benefits of Forests. *Science*, *320*(5882), 1444–1449. https://doi.org/10.1126/science.1155121

Brede, B., Lau, A., Bartholomeus, H. M., & Kooistra, L. (2017). Comparing RIEGL RiCOPTER UAV LiDAR Derived Canopy Height and DBH with Terrestrial LiDAR. *Sensors*, *17*(10), 2371. https://doi.org/10.3390/s17102371

Brown, S. (1997). *Estimating Biomass and Biomass Change of Tropical Forests: A Primer*. Food & Agriculture Org.

Buech, R. R., & Rugg, D. J. (1989). Biomass relations of shrub components and their generality. *Forest Ecology and Management*, *26*(4), 257–264. https://doi.org/10.1016/0378-1127(89)90086-8

Butler, J. H., & Montzka, S. A. (2021). *The NOAA Annual Greenhouse Gas Index (AGGI)*. https://gml.noaa.gov/aggi/aggi.html

Cabo, C., Ordóñez, C., López-Sánchez, C. A., & Armesto, J. (2018). Automatic dendrometry: Tree detection, tree height and diameter estimation using terrestrial laser scanning. *International Journal of Applied Earth Observation and Geoinformation*, *69*, 164–174. https://doi.org/10.1016/j.jag.2018.01.011

Calders, K., Adams, J., Armston, J., Bartholomeus, H., Bauwens, S., Bentley, L. P., Chave, J., Danson, F. M., Demol, M., Disney, M., Gaulton, R., Krishna Moorthy, S. M., Levick, S. R., Saarinen, N., Schaaf, C., Stovall, A., Terryn, L., Wilkes, P., & Verbeeck, H. (2020). Terrestrial laser scanning in forest ecology: Expanding the horizon. *Remote Sensing of Environment*, *251*, 112102. https://doi.org/10.1016/j.rse.2020.112102

Calders, K., Newnham, G., Burt, A., Murphy, S., Raumonen, P., Herold, M., Culvenor, D., Avitabile, V., Disney, M., Armston, J., & Kaasalainen, M. (2015). Nondestructive estimates of above-ground biomass using terrestrial laser scanning. *Methods in Ecology and Evolution*, *6*(2), 198–208. https://doi.org/10.1111/2041-210X.12301

Chen, S., Feng, Z., Chen, P., Khan, T. U., & Lian, Y. (2019). Nondestructive Estimation of the Above-Ground Biomass of Multiple Tree Species in Boreal Forests of China Using Terrestrial Laser Scanning. *Forests*, *10*(11), 936–936. https://doi.org/10.3390/f10110936

Chen, S., Liu, H., Feng, Z., Shen, C., & Chen, P. (2019). Applicability of personal laser scanning in forestry inventory. *PLOS ONE*, *14*(2), e0211392. https://doi.org/10.1371/journal.pone.0211392

Chen, X., YE, C., Li, J., & Chapman, M. A. (2018). Quantifying the Carbon Storage in Urban Trees Using Multispectral ALS Data. *IEEE Journal of Selected Topics in Applied Earth Observations and Remote Sensing*, *11*(9), 3358–3365. https://doi.org/10.1109/JSTARS.2018.2859957

Ciais, P., Sabine, C., Bala, G., Bopp, L., Brovkin, V., Canadell, J., Chhabra, A., DeFries, R., Galloway, J., Heimann, M., Jones, C., Le Quere, C., Myneni, R. B., Piao, S., & Thornton, P. (2013). Carbon and Other Biogeochemical Cycles. In T. F. Stocker, D. Qin, G.-K. Plattner, M. Tignor, S. K. Allen, J. Boschung, A. Nauels, Y. Xia, V. Bex, & P. M.

Midgley (Eds.), *Carbon and Other Biogeochemical Cycles. In: Climate Change 2013: The Physical Science Basis. Contribution of Working Group I to the Fifth Assessment Report of the Intergovernmental Panel on Climate Change*. Cambridge University Press.

Colomina, I., & Molina, P. (2014). Unmanned aerial systems for photogrammetry and remote sensing: A review. *ISPRS Journal of Photogrammetry and Remote Sensing*, *92*, 79–97. https://doi.org/10.1016/j.isprsjprs.2014.02.013

Coumou, D., Robinson, A., & Rahmstorf, S. (2013). Global increase in record-breaking monthly-mean temperatures. *Climatic Change*, *118*(3), 771–782. https://doi.org/10.1007/s10584-012-0668-1

Dasgupta, S., Laplante, B., Meisner, C., Wheeler, D., & Yan, J. (2009). The impact of sea level rise on developing countries: A comparative analysis. *Climatic Change*, *93*(3), 379–388. https://doi.org/10.1007/s10584-008-9499-5

FAO. (2020). *Global Forest Resources Assessment 2020: Main report*. FAO. https://doi.org/10.4060/ca9825en

Fearnside, P. M. (2000). Global Warming and Tropical Land-Use Change: Greenhouse Gas Emissions from Biomass Burning, Decomposition and Soils in Forest Conversion, Shifting Cultivation and Secondary Vegetation. *Climatic Change*, *46*(1), 115–158. https://doi.org/10.1023/A:1005569915357

Forrester, D. I., Dumbrell, I. C., Elms, S. R., Paul, K. I., Pinkard, E. A., Roxburgh, S. H., & Baker, T. G. (2021). Can crown variables increase the generality of individual tree biomass equations? *Trees*, *35*(1), 15–26. https://doi.org/10.1007/s00468-020-02006-6

Frederikse, T., Landerer, F., Caron, L., Adhikari, S., Parkes, D., Humphrey, V. W., Dangendorf, S., Hogarth, P., Zanna, L., Cheng, L., & Wu, Y.-H. (2020). The causes of sea-level rise since 1900. *Nature*, *584*(7821), 393–397. https://doi.org/10.1038/s41586-020-2591-3

Friend, A. D., Lucht, W., Rademacher, T. T., Keribin, R., Betts, R., Cadule, P., Ciais, P., Clark, D. B., Dankers, R., Falloon, P. D., Ito, A., Kahana, R., Kleidon, A., Lomas, M. R., Nishina, K., Ostberg, S., Pavlick, R., Peylin, P., Schaphoff, S., … Woodward, F. I. (2014). Carbon residence time dominates uncertainty in terrestrial vegetation responses to future climate and atmospheric CO2. *Proceedings of the National Academy of Sciences*, *111*(9), 3280–3285.

Gettelman, A., & Rood, R. B. (2016). Essence of a Climate Model. In A. Gettelman & R. B. Rood (Eds.), *Demystifying Climate Models: A Users Guide to Earth System Models* (pp. 37–58). Springer. https://doi.org/10.1007/978-3-662-48959-8_4

Ghimire, S., Xystrakis, F., & Koutsias, N. (2017). Using Terrestrial Laser Scanning to Measure Forest Inventory Parameters in a Mediterranean Coniferous Stand of Western Greece. *PFG – Journal of Photogrammetry, Remote Sensing and Geoinformation Science*, *85*(4), 213–225. https://doi.org/10.1007/s41064-017-0024-1

Gibbs, M., & Latzko, E. (Eds.). (1979). *Photosynthesis II*. Springer Berlin Heidelberg. https://doi.org/10.1007/978-3-642-67242-2

Gollob, C., Ritter, T., & Nothdurft, A. (2020a). Forest inventory with long range and high-speed Personal Laser Scanning (PLS) and Simultaneous Localization and Mapping (SLAM) technology. *Remote Sensing*, *12*(9). https://doi.org/10.3390/RS12091509

Gollob, C., Ritter, T., & Nothdurft, A. (2020b). Comparison of 3D Point Clouds Obtained by Terrestrial Laser Scanning and Personal Laser Scanning on Forest Inventory Sample Plots. *Data*, *5*(4), 103. https://doi.org/10.3390/data5040103

Hackenberg, J., Wassenberg, M., Spiecker, H., & Sun, D. (2015). Non Destructive Method for Biomass Prediction Combining TLS Derived Tree Volume and Wood Density. *Forests*, *6*(4), 1274–1300. https://doi.org/10.3390/f6041274

Harikumar, A., Bovolo, F., & Bruzzone, L. (2017). An approach to conifer stem localization and modeling in high density airborne LiDAR data. *Image and Signal Processing for Remote Sensing XXIII*, *10427*, 104270Q. https://doi.org/10.1117/12.2279526

Hirabayashi, Y., Mahendran, R., Koirala, S., Konoshima, L., Yamazaki, D., Watanabe, S., Kim, H., & Kanae, S. (2013). Global flood risk under climate change. *Nature Climate Change*, *3*(9), 816–821. https://doi.org/10.1038/nclimate1911

Holopainen, M., Kankare, V., Vastaranta, M., Liang, X., Lin, Y., Vaaja, M., Yu, X., Hyyppä, J., Hyyppä, H., Kaartinen, H., Kukko, A., Tanhuanpää, T., & Alho, P. (2013). Tree mapping using airborne, terrestrial and mobile laser scanning – A case study in a heterogeneous urban forest. *Urban Forestry & Urban Greening*, *12*(4), 546–553. https://doi.org/10.1016/j.ufug.2013.06.002

Houghton, R. A. (2008). Biomass. In S. E. Jørgensen & B. D. Fath (Eds.), *Encyclopedia of Ecology* (pp. 448–453). Academic Press. https://doi.org/10.1016/B978-008045405-4.00462-6

Hyyppä, E., Hyyppä, J., Hakala, T., Kukko, A., Wulder, M. A., White, J. C., Pyörälä, J., Yu, X., Wang, Y., Virtanen, J.-P., Pohjavirta, O., Liang, X., Holopainen, M., & Kaartinen, H. (2020). Under-canopy UAV laser scanning for accurate forest field measurements. *ISPRS*

Journal of Photogrammetry and Remote Sensing, *164*, 41–60. https://doi.org/10.1016/j.isprsjprs.2020.03.021

IPCC. (2014). *Climate Change 2014: Mitigation of Climate Change. Contribution of Working Group III to the Fifth Assessment Report of the Intergovernmental Panel on Climate Change* (O. Edenhofer, R. Pichs-Madruga, Y. Sokona, E. Farahani, S. Kadner, K. Seyboth, A. Adler, I. Baum, S. Brunner, P. Eickemeier, B. Kriemann, J. Savolainen, S. Schlömer, C. von Stechow, T. Zwickel, & J. C. Minx, Eds.). Cambridge University Press. https://www.ipcc.ch/report/ar5/wg3/

Jaakkola, A., Hyyppä, J., Yu, X., Kukko, A., Kaartinen, H., Liang, X., Hyyppä, H., & Wang, Y. (2017). Autonomous Collection of Forest Field Reference—The Outlook and a First Step with UAV Laser Scanning. *Remote Sensing*, *9*(8), 785. https://doi.org/10.3390/rs9080785

Jucker, T., Caspersen, J., Chave, J., Antin, C., Barbier, N., Bongers, F., Dalponte, M., Ewijk, K. Y. van, Forrester, D. I., Haeni, M., Higgins, S. I., Holdaway, R. J., Iida, Y., Lorimer, C., Marshall, P. L., Momo, S., Moncrieff, G. R., Ploton, P., Poorter, L., … Coomes, D. A. (2017). Allometric equations for integrating remote sensing imagery into forest monitoring programmes. *Global Change Biology*, *23*(1), 177–190. https://doi.org/10.1111/gcb.13388

Kornhuber, K., & Tamarin-Brodsky, T. (2021). Future Changes in Northern Hemisphere Summer Weather Persistence Linked to Projected Arctic Warming. *Geophysical Research Letters*, *48*(4), e2020GL091603. https://doi.org/10.1029/2020GL091603

Kukko, A., Kaijaluoto, R., Kaartinen, H., Lehtola, V. V., Jaakkola, A., & Hyyppä, J. (2017). Graph SLAM correction for single scanner MLS forest data under boreal forest canopy.

ISPRS Journal of Photogrammetry and Remote Sensing, *132*, 199–209. https://doi.org/10.1016/j.isprsjprs.2017.09.006

Kurz, W. A., Shaw, C. H., Boisvenue, C., Stinson, G., Metsaranta, J., Leckie, D., Dyk, A., Smyth, C., & Neilson, E. T. (2013). Carbon in Canada's boreal forest—A synthesis. *Environmental Reviews*, *21*(4), 260–292. https://doi.org/10.1139/er-2013-0041

Lau, A., Bentley, L. P., Martius, C., Shenkin, A., Bartholomeus, H., Raumonen, P., Malhi, Y., Jackson, T., & Herold, M. (2018). Quantifying branch architecture of tropical trees using terrestrial LiDAR and 3D modelling. *Trees*, *32*(5), 1219–1231. https://doi.org/10.1007/s00468-018-1704-1

Lehmann, J., Coumou, D., & Frieler, K. (2015). Increased record-breaking precipitation events under global warming. *Climatic Change: An Interdisciplinary, International Journal Devoted to the Description, Causes and Implications of Climatic Change*, *132*(4), 501. https://doi.org/10.1007/s10584-015-1434-y

Liang, X., Hyyppä, J., Kaartinen, H., Lehtomäki, M., Pyörälä, J., Pfeifer, N., Holopainen, M., Brolly, G., Francesco, P., Hackenberg, J., Huang, H., Jo, H.-W., Katoh, M., Liu, L., Mokroš, M., Morel, J., Olofsson, K., Poveda-Lopez, J., Trochta, J., … Wang, Y. (2018). International benchmarking of terrestrial laser scanning approaches for forest inventories. *ISPRS Journal of Photogrammetry and Remote Sensing*, *144*, 137–179. https://doi.org/10.1016/j.isprsjprs.2018.06.021

Liang, X., Hyyppä, J., Kukko, A., Kaartinen, H., Jaakkola, A., & Yu, X. (2014). The Use of a Mobile Laser Scanning System for Mapping Large Forest Plots. *IEEE Geoscience and Remote Sensing Letters*, *11*(9), 1504–1508. https://doi.org/10.1109/LGRS.2013.2297418

Liang, X., Kankare, V., Hyyppä, J., Wang, Y., Kukko, A., Haggrén, H., Yu, X., Kaartinen, H., Jaakkola, A., Guan, F., Holopainen, M., & Vastaranta, M. (2016). Terrestrial laser scanning in forest inventories. *ISPRS Journal of Photogrammetry and Remote Sensing*, *115*, 63–77. https://doi.org/10.1016/j.isprsjprs.2016.01.006

Liang, X., Kukko, A., Kaartinen, H., Hyyppä, J., Yu, X., Jaakkola, A., & Wang, Y. (2014). Possibilities of a Personal Laser Scanning System for Forest Mapping and Ecosystem Services. *Sensors*, *14*(1), 1228–1248. https://doi.org/10.3390/s140101228

Lim, K., Treitz, P., Wulder, M., St-Onge, B., & Flood, M. (2003). LiDAR remote sensing of forest structure. *Progress in Physical Geography: Earth and Environment*, *27*(1), 88–106. https://doi.org/10.1191/0309133303pp360ra

Liu, G., Wang, J., Chen, Y., Liu, Z., & Dong, P. (2018). Estimating individual tree height and diameter at breast height (DBH) from terrestrial laser scanning (TLS) data at plot level. *Forests*, *8*(2). https://doi.org/10.3390/f9070398

Liu, W., Li, Z., Li, Y., Sun, S., & Sotelo, M. A. (2020). Using Weighted Total Least Squares and 3-D Conformal Coordinate Transformation to Improve the Accuracy of Mobile Laser Scanning. *IEEE Transactions on Geoscience and Remote Sensing*, *58*(1), 203–217. https://doi.org/10.1109/TGRS.2019.2935744

Liu, W., Li, Z., Sun, S., Malekian, R., Ma, Z., & Li, W. (2019). Improving Positioning Accuracy of the Mobile Laser Scanning in GPS-Denied Environments: An Experimental Case Study. *IEEE Sensors Journal*, *19*(22), 10753–10763. https://doi.org/10.1109/JSEN.2019.2929142

Lucas, R. M., Mitchell, A. L., & Armston, J. (2015). Measurement of Forest Above-Ground Biomass Using Active and Passive Remote Sensing at Large (Subnational to Global)

Scales. *Current Forestry Reports*, *1*(3), 162–177. https://doi.org/10.1007/s40725-015-0021-9

Magnan, G., Garneau, M., Le Stum-Boivin, É., Grondin, P., & Bergeron, Y. (2020). Long-Term Carbon Sequestration in Boreal Forested Peatlands in Eastern Canada. *Ecosystems*, *23*(7), 1481–1493. https://doi.org/10.1007/s10021-020-00483-x

Mao, Q., Zhang, L., Li, Q., Hu, Q., Yu, J., Shaojun Feng, Washington Ochieng, & Hanlu Gong. (2015). A Least Squares Collocation Method for Accuracy Improvement of Mobile LiDAR Systems. *Remote Sensing*, *7*(6), 7402–7424. https://doi.org/10.3390/rs70607402

Martinez, J., Martínez-Garza, C., & Cámara, L. (2020). Species-specific or generic allometric equations: Which option is better when estimating the biomass of Mexican tropical humid forests? *Carbon Management*, *11*, 1–9. https://doi.org/10.1080/17583004.2020.1738823

McFarland, E. L., Hunt, J. L., & Campbell, J. L. (2007). *Energy, physics and the environment*. Cengage Learning.

Mielcarek, M., Kaminska, A., & Sterenczak, K. (2020). Digital Aerial Photogrammetry (DAP) and Airborne Laser Scanning (ALS) as Sources of Information about Tree Height: Comparisons of the Accuracy of Remote Sensing Methods for Tree Height Estimation. *REMOTE SENSING*, *12*(11). https://doi.org/10.3390/rs12111808

NASA Global Climate Change. (2021, June 21). *Carbon Dioxide Concentration | NASA Global Climate Change* [Government]. Climate Change: Vital Signs of the Planet. https://climate.nasa.gov/vital-signs/carbon-dioxide

Natural Resources Canada. (2013, July 11). *Boreal forest*. Natural Resources Canada. https://www.nrcan.gc.ca/our-natural-resources/forests/sustainable-forest-management/boreal-forest/13071

Navar, J. (2010). Methods od Assessment of Aboveground Tree Biomass. In *Biomass*. IntechOpen. https://doi.org/10.5772/9768

Picard, N., Saint-André, L., & Henry, M. (2012). *Manual for building tree volume and biomass allometric equations from filed measurement to prediction*. Food and Agriculture Organization of the United Nations (FA0). http://www.fao.org/docrep/018/i3058e/i3058e.pdf

Puc-Kauil, R. (1), Ángeles-Pérez, G. (1), Valdéz-Lazalde, J. r. (1), Reyes-Hernández, V. j. (1), Pérez-Rodríguez, P. (1), Dupuy-Rada, J. m. (2), Schneider, L. (3), & García-Cuevas, X. (4). (2020). Allometric equations to estimate above-ground biomass of small-diameter mixed tree species in secondary tropical forests. *IForest*, *13*(3), 165–174. https://doi.org/10.3832/ifor3167-013

Reichstein, M., & Carvalhais, N. (2019). Aspects of Forest Biomass in the Earth System: Its Role and Major Unknowns. *Surveys in Geophysics*, *40*(4), 693–707. https://doi.org/10.1007/s10712-019-09551-x

Sah, J. P., Ross, M. S., Koptur, S., & Snyder, J. R. (2004). Estimating aboveground biomass of broadleaved woody plants in the understory of Florida Keys pine forests. *Forest Ecology and Management*, *203*(1), 319–329. https://doi.org/10.1016/j.foreco.2004.07.059

Shao, J., Zhang, W., Mellado, N., Wang, N., Jin, S., Cai, S., Luo, L., Lejemble, T., & Yan, G. (2020). SLAM-aided forest plot mapping combining terrestrial and mobile laser

scanning. *ISPRS Journal of Photogrammetry and Remote Sensing*, *163*, 214–230. https://doi.org/10.1016/j.isprsjprs.2020.03.008

Singh, T. (1984). *Biomass Equations for Six Major Tree Species of the Northwest Territories* (pp. 1–30). Environment Canada, Canadian Forestry Service.

Smith, K. B., Smith, C. E. S., Forest, S. F., & Richard, A. J. (2007). *A Field Guide to the Wetlands of the Boreal Plains Ecozone of Canada*. Ducks Unlimited Canada.

Stal, C., Verbeurgt, J., De Sloover, L., & De Wulf, A. (2021). Assessment of handheld mobile terrestrial laser scanning for estimating tree parameters. *Journal of Forestry Research*, *32*(4), 1503–1513. https://doi.org/10.1007/s11676-020-01214-7

Sun, Y., Zhang, X., Zwiers, F. W., Song, L., Wan, H., Hu, T., Yin, H., & Ren, G. (2014). Rapid increase in the risk of extreme summer heat in Eastern China. *Nature Climate Change*, *4*(12), 1082–1085. https://doi.org/10.1038/nclimate2410

Takoudjou, S. M., Ploton, P., Sonké, B., Hackenberg, J., Griffon, S., Coligny, F. de, Kamdem, N. G., Libalah, M., Mofack, G. I., Moguédec, G. L., Pélissier, R., & Barbier, N. (2018). Using terrestrial laser scanning data to estimate large tropical trees biomass and calibrate allometric models: A comparison with traditional destructive approach. *Methods in Ecology and Evolution*, *9*(4), 905–916. https://doi.org/10.1111/2041-210X.12933

Tarnocai, C., Canadell, J. G., Schuur, E. a. G., Kuhry, P., Mazhitova, G., & Zimov, S. (2009). Soil organic carbon pools in the northern circumpolar permafrost region. *Global Biogeochemical Cycles*, *23*(2). https://doi.org/10.1029/2008GB003327

Treat, C. C., Kleinen, T., Broothaerts, N., Dalton, A. S., Dommain, R., Douglas, T. A., Drexler, J. Z., Finkelstein, S. A., Grosse, G., Hope, G., Hutchings, J., Jones, M. C., Kuhry, P., Lacourse, T., Lähteenoja, O., Loisel, J., Notebaert, B., Payne, R. J., Peteet, D. M., …

Brovkin, V. (2019). Widespread global peatland establishment and persistence over the last 130,000 y. *Proceedings of the National Academy of Sciences*, *116*(11), 4822–4827.

Ung, C.-H., Bernier, P., & Guo, X.-J. (2008). Canadian national biomass equations: New parameter estimates that include British Columbia data. *Canadian Journal of Forest Research*, *38*(5), 1123–1132. https://doi.org/10.1139/X07-224

Vashum, K. (2012). Methods to Estimate Above-Ground Biomass and Carbon Stock in Natural Forests—A Review. *Journal of Ecosystem & Ecography*, *02*. https://doi.org/10.4172/2157-7625.1000116

Vauhkonen, J., Maltamo, M., McRoberts, R. E., & Næsset, E. (2014). Introduction to Forestry Applications of Airborne Laser Scanning. In M. Maltamo, E. Næsset, & J. Vauhkonen (Eds.), *Forestry Applications of Airborne Laser Scanning: Concepts and Case Studies* (pp. 1–16). Springer Netherlands. https://doi.org/10.1007/978-94-017-8663-8_1

Vosselman, G., & Maas, H.-G. (2010). *Airborne and Terrestrial Laser Scanning*. Whittles Publishing. http://ebookcentral.proquest.com/lib/ualberta/detail.action?docID=3417283

Wang, Y., Chen, Q., Zhu, Q., Liu, L., Li, C., & Zheng, D. (2019). A Survey of Mobile Laser Scanning Applications and Key Techniques over Urban Areas. *REMOTE SENSING*, *11*(13). https://doi.org/10.3390/rs11131540

Wang, Y., Pyörälä, J., Liang, X., Lehtomäki, M., Kukko, A., Yu, X., Kaartinen, H., & Hyyppä, J. (2019). In situ biomass estimation at tree and plot levels: What did data record and what did algorithms derive from terrestrial and aerial point clouds in boreal forest. *Remote Sensing of Environment*, *232*, 111309. https://doi.org/10.1016/j.rse.2019.111309

Westra, S., Alexander, L. V., & Zwiers, F. W. (2013). Global Increasing Trends in Annual Maximum Daily Precipitation. *Journal of Climate*, *26*(11), 3904–3918. https://doi.org/10.1175/JCLI-D-12-00502.1

Wieder, R., Vitt, D., & Benscoter, B. (2006). Peatlands and the Boreal Forest. In *Ecol. Stud.* (Vol. 188, pp. 1–8). https://doi.org/10.1007/978-3-540-31913-9_1

Zhang, J. (2019). Boreal forests and taiga. In *Salem Press Encyclopedia of Science*. Salem Press. https://login.ezproxy.library.ualberta.ca/login?url=https://search.ebscohost.com/login.aspx?direct=true&db=ers&AN=94981257&site=eds-live&scope=site

Zhao, B., Zhuang, Q., Shurpali, N., Köster, K., Berninger, F., & Pumpanen, J. (2021). North American boreal forests are a large carbon source due to wildfires from 1986 to 2016. *Scientific Reports*, *11*(1). https://doi.org/10.1038/s41598-021-87343-3

Chapter 2 -- Using TLS-measured Tree Attributes to Estimate Above Ground Biomass in Small Black Spruce Trees

Abstract: Terrestrial laser scanning (TLS) has become a useful tool for modelling forest structure and estimating tree parameters such as above ground biomass (AGB). Allometric equations are often used to estimate individual tree AGB as a function of height and diameter at breast height (DBH), but these variables can often be laborious to measure using traditional methods. The main objective of this study was to develop allometric equations using a variety of TLS-measured variables and compare their estimation accuracy to other established equations that rely on DBH and height. The study focusses on small black spruce trees (1.3 – 7 m) located in peatland ecosystems of the Taiga Plains Ecozone in the Northwest Territories, Canada, where the dry weight of nearly 100 small trees sampled in 10 plots were destructively sampled. We fitted power-, quadratic-, and multiple regression power models to estimate AGB using tree attributes derived from TLS including DBH, crown diameter, crown area, height, tree volume and bounding box volume. The equations given by our best models outperformed those obtained from established AGB equations that rely on DBH, even though ours do not require DBH. Our equations lay the groundwork for rapid ground estimation of AGB density (t/ha) for a prominent tree species in the most common ecosystem (treed peatlands) of North America's boreal forest, as well as providing a potential framework for using airborne LiDAR to obtain extensive and accurate AGB reference data in the future.

Keywords: Terrestrial laser scanning; biomass; black spruce; allometric equations.

2.1 Introduction

As Earth's climate changes and governments around the world look for the best ways to meet these changes, the importance of a thorough understanding of the climate system becomes apparent. Greenhouse gases, like carbon dioxide, absorb outgoing infrared radiation from the Earth and reemit it in a random direction, effectively trapping some of this radiation within the atmosphere and warming the surface of the planet (McFarland et al., 2007). The atmospheric content of greenhouse gases has been increasing since 1750, leading to increased average global

temperatures (Ciais et al., 2013). As regional weather patterns change, new socioeconomic challenges pertaining to disaster prevention and mitigation, water availability and population migration will likely become more prevalent for policy makers (Ferguson et al., 2018; Thomas, 2017; Zanhouo & Nana, 2019). The climate models that policy makers rely on to make informed decision rely on known physical laws and processes (like the carbon cycle) to predict future climates based on different scenarios (Gettelman & Rood, 2016). Thus, understanding the interactions between different components of the climate system is necessary to reduce uncertainty in the models (Gettelman & Rood, 2016). Because carbon has such a major influence on the climate system (Ciais et al., 2013), intimate knowledge of the carbon cycle is needed for these climate models. Forests play a major role in the interactions between the atmosphere and biosphere and are some of the most important carbon sinks on Earth because trees absorb carbon dioxide through the process of photosynthesis (Gibbs & Latzko, 1979). This removes carbon from the atmosphere and it stored as biomass (Lorenz & Lal, 2010), which prevents it from contributing to the greenhouse effect.

Roughly half of a tree's above ground biomass (AGB, the dry weight of trees excluding their roots) is made of carbon (Chen et al., 2018; Houghton, 2008; Vashum, 2012), making forests an important component of the climate system because they act as significant sinks of atmospheric carbon (Novotný et al., 2020; Rencz & Auclair, 1978). Canada's boreal forest is one such important region. It covers 270 million hectares (Natural Resources Canada, 2013) and is estimated to contain a third of the world's terrestrial carbon stocks (Zhao et al., 2021) and more than 208 billion tonnes of carbon (Carlson et al., 2009; Wells et al., 2020). Monitoring changes in carbon stocks within forest vegetation means that AGB needs to be monitored accurately. Calculating AGB often involves the use of allometric equations that rely on other tree attributes as predictors (Alemdag, 1983; Chen et al., 2018; M. Disney et al., 2019; Lau et al., 2019; Vashum, 2012). Calibration of these equations is often expensive as they require dozens if not hundreds of harvested trees that need to be processed and weighed, but once calibrated, one can use those tree attributes in the equations to obtain AGB estimates. In Canada, large country-wide efforts have taken place to develop allometric AGB models, such as those put forth by Lambert et al. (Lambert et al., 2005) which were later updated by Ung et al. (Ung et al., 2008). These are the equations currently used by the Canadian National Forest Inventory for individual tree AGB estimation and they rely on height and diameter at breast height (DBH) (Ung et al., 2008). These

are the most commonly used attributes for similar AGB equations in other areas of the world (Calders et al., 2018; Chen et al., 2018; M. Disney et al., 2019).

In recent years, new technologies like Terrestrial Laser Scanners (TLS) have been incorporated into forestry studies and have proven to be effective at measuring tree parameters in forest inventory plots (Kalwar et al., 2021). Scanning with TLS produces highly-detailed, 3D point clouds (Chen et al., 2018) that can be used to locate trees within the plot and measure a number of their attributes with high accuracy (Liang et al., 2016, 2018; Shruthi Srinivasan et al., 2015; Tansey et al., 2009; Y. Wang et al., 2019; Watt & Donoghue, 2005). The resultant point clouds consist of a myriad of points that correspond to a recorded return from a laser pulse emanating from the scanner that reflects off the surface of an object. These point clouds also enable researchers to virtually return to the plot at any point to better interpret field data or check for errors and outliers. Despite the many benefits of TLS, there are some drawbacks as well. Scanning equipment can be expensive and heavy, and the scans themselves can be time consuming (White et al., 2016). Point clouds can sometimes contain data gaps, particularly in dense forests where branches and stems block the laser beam emitted by the scanner from reaching anything behind it (Watt & Donoghue, 2005). This occlusion is one of the biggest concerns when using TLS, often compromising the data's usefulness (Watt & Donoghue, 2005). It can, however, be partially remedied with properly planned scan stations at multiple positions in and around the plot (Abegg et al., 2017; Watt & Donoghue, 2005) or, when considering occlusion effects on leaf area density, by using a multistep process called kriging that creates estimators based on spatial information for regions of the point clouds where data does not exist (Soma et al., 2020). An example of how occlusion can affect data can be seen when measuring DBH. While the DBH of large trees has been accurately measured using TLS in many cases (Ghimire et al., 2017; Heinzel & Huber, 2017; Liu et al., 2018), when parts of the tree stems are occluded, TLS-based DBH measurements become less accurate (Moskal & Zheng, 2011).

One alternative is to use allometric models that do not rely on DBH, and recent studies have shown the potential of crown parameters, such as crown diameter, to accurately estimate AGB (Jucker et al., 2017; Lau et al., 2019). Crown parameters also have the important advantage of being measurable using airborne laser scanning (ALS) assuming high enough point density, whereas measuring DBH in this manner is difficult and requires higher point densities than are normally seen in ALS point clouds (Harikumar et al., 2017). ALS can cover large areas of land

quickly (Malek S et al., 2019), making models that use ALS-obtainable parameters as predictors very attractive for obtaining extensive AGB reference datasets without setting foot on the ground. As such, these models could be particularly useful in ecosystems that are widespread and common across the Canadian boreal forest, like peatlands.

Peatland ecosystems make up around 24% of boreal forests worldwide (R. Wieder et al., 2006) and are prominent in Canada where they cover 13% of the country's land surface (Tarnocai et al., 2011; Warner & Asada, 2006). Black spruce (*Picea mariana* L.) is a dominant species in boreal peatlands (Lieffers, 1986; Rencz & Auclair, 1978), and roughly 70% of black spruce biomass is above ground (Rencz & Auclair, 1978). While AGB makes up only a small portion of the total carbon stored in black spruce peatlands (~3% of the total soil carbon according data from Bona et al. (Bona et al., 2018) and using the mean estimates from the model given in Bona et al. (Bona et al., 2020), the large extent of these ecosystems (over 100 million hectares of Canada's boreal forest) (Thompson et al., 2016) and the fact that black spruce is a dominant species in boreal forest peatlands (Lieffers, 1986; R. K. Wieder et al., 2006), makes their AGB an important carbon sink. Furthermore, of all the carbon pools in Canada's boreal forest, AGB is the most spatially variable, and the one that fluctuates the most due to its vulnerability to wildfires and other disturbances (Kurz et al., 2013). For example, an experimental fire in an Albertan black spruce peatland resulted in 100% tree mortality with around 25% of biomass being combusted and the remainder being added to dead wood carbon pool, compared with the loss of only ~1% of the peat (Thompson et al., 2020). This variability highlights the need for methods that can provide accurate AGB estimates for black spruce in peatlands.

In this study, we develop allometric equations specific to individual black spruce trees shorter than 5 m tall in peatlands of the Taiga Plains ecozone using various model forms and TLS-measured tree attributes, and assess which combinations of predictor variable and model form led to the best estimates of AGB. Of particular interest to us were the models that rely on predictors that can also be measured by ALS (assuming high enough point density). We also assess the use of quantitative structure models (QSMs) for measuring tree attributes like DBH, height, and volume of small black spruce trees as this has been successfully done for mature deciduous trees (Brede et al., 2019; Calders et al., 2015; Lau et al., 2018). Finally, we compare the AGB estimates made by our best models to those made using the equations given by Ung et

al. (Ung et al., 2008) and to those given in Bhatti et al. (another set of equations based on unpublished data specifically for black spruce less than 3 m tall) (Bhatti et al., 2006) to see if ours represent a suitable alternative for accurate AGB estimation.

2.2 Materials and Methods

2.2.1 Study Area

This study was conducted in boreal forest peatlands located in the Northwest Territories in between Hay River, NWT and Fort Simpson, NWT (Figure 1). The study area lies within the mid-boreal Taiga plains ecoregion (Environment and Natural Resources, n.d.), which has average annual temperatures between 1°C and 4.5°C, and mean annual precipitation between 400-460 mm (mostly summer precipitation) (Ecosystem Classification Group et al., 2009). Peatlands in this ecoregion are in the form of flat-topped, peat-rich areas elevated from the surroundings by underlying ice-rich permafrost (peat plateaus), smaller mounds of peat with permafrost and minerals in their cores (palsas), wetlands with parallel rows of peat material (northern ribbed fens), and wetlands with uniformly spread peat material (horizontal fens) (Ecosystem Classification Group et al., 2009).

We selected 10 circular plots that represented a variety of tree heights and densities typical of black spruce peatlands in the study area (Figure 1). Plots were 7.98 m in diameter (50 m^2) and contained anywhere from 23 to 115 trees per plot, most of which were black spruce, but with several (20 out of 606) tamarack (*Larix laricina* (Du Roi) K. Koch) as well.

2.2.2 Plot Characteristics

All trees within the plot were flagged with orange flagging tape and trees on the edge were flagged with pink. Their heights and DBHs were measured using a Haglof Vertex IV and Transponder T3, and a diameter tape, respectively. Ten black spruce trees representing the range of heights found in the plot were then selected for destructive sampling. To identify sample trees, reflective tape was wrapped around the trunk near 1.3 m, blue flagging tape was added to the branches, and a reflective pole with a number from 0-9 was placed next to the trunk. The trees selected for destructive sampling were also measured for their distance and bearing from the centre of the plot to help us locate them in the resultant point clouds later.

2.2.3 Scanning the Plots

All plots were scanned using a Leica C10 Terrestrial Laser Scanner from five different stations: One at the centre of the plot and four at points corresponding to the corners of a square that encompassed the plot. This follows the findings of Abegg et al. (2017) that the plot centre provides the best visibility in a plot, and additional scan locations placed evenly around the plot will reduce occlusion. The C10 can produce colourized point clouds, for which the C10 camera was set to medium image resolution (960 x 960 px). The scan rate for the C10 laser instrument is 50,000 pts/sec, and it has a footprint diameter of 4.5 mm at 50 m range. Scan angles were set to 360° horizontally, and from -45° to 90° vertically. Five TLS targets were placed around the plot so they could be seen from each scan station. These targets were used to align the five scans during the process of registration, where all the scans are combined into a single point cloud of the entire plot. Finally, the plots were photographed by the C10 and by a 360° GoPro from each scan location, as well as from above using a drone to provide extra assistance in locating the destructively sampled trees in the point clouds later.

2.2.4 Destructive Sampling and Biomass Measurements

After each plot was scanned and photographed, the 10 trees selected for destructive sampling were cut down as close to the ground as possible. The trees were then cut into smaller pieces and put in bags marked with the tree's information (plot and tree number) for transportation. Some of the bags were brought to Edmonton, Alberta and were left to dry in a storage area at 60°C until there were no significant differences in weight measurements from day to day, with a minimum sitting time of at least one week. The remainder of the bags were measured in Hay River, NWT and were dried at 65°C for at least 1 week. The trees were then separated into main stem, branches, needles, lichens, and cones and weighed to the closest 100^{th} of a gram. These components will be used in a future study. The total weights of these components were added up to produce the reference values of AGB for each tree.

2.2.5 Point Cloud Processing, Tree Extraction, and Height Measurements

Registration of the point clouds was performed in Leica's Cyclone software (*Leica Cyclone 3D Point Cloud Processing Software*, n.d.). Each scan was imported into the software and the targets were used as anchor points for combining the individual scans. We required the

difference in target location to be less than 6mm when combining two scans, otherwise the constraint for those two targets was disabled for the purposes of registration. Once the scans were registered, the resulting point cloud was imported into CloudCompare (*CloudCompare (v2.11.1)*, n.d.) (an open-source point cloud editing software) for further analysis.

In CloudCompare, each plot point cloud was thinned using the cloud subsampling tool (*CloudCompare (v2.11.1)*, n.d.), with the minimum distance between points set to 1 cm to reduce file size and increase computing speed. The point cloud was then cropped at the plot's circumference. To eliminate any points created by atmospheric debris or false returns, a statistical outlier filter (*CloudCompare (v2.11.1)*, n.d.) was applied, computed as:

$$T = \mu_d + nsigma \cdot \sigma_d \quad (1)$$

where T is the threshold for removal, μ_d is the mean average distance from each point to its 10 nearest neighbours, *nsigma* is the standard deviation multiplier (we used *nsigma* = 1.00), and σ_d is the standard deviation of the average distances of all points in the plot point cloud. Points with an average distance to their 10 nearest neighbours exceeding the threshold (T) were removed.

The trees that were selected for destructive sampling were then identified in the point cloud using the numbered reflective marker sticks and the distance and bearing measurements taken in the field as guides. When these clues were not sufficient to identify the tree, the GoPro images were also consulted to search for the blue flagging tape on selected trees. These trees were manually clipped from the plot point cloud, cleaned so that only points from the selected tree remained, and saved as individual tree point clouds for further analysis. The tree point clouds were manually straightened (i.e., the stem was aligned to the z axis when the tree was leaning) and, following Calders et al. (2015), the tree height was measured as the distance between the maximum and minimum z-coordinates of all the points in each individual point cloud.

2.2.6 Crown Diameter and Crown Area Measurements

Initially, we estimated crown diameter as the mean of two orthogonal pseudo-diameters, but because the crowns of these small trees are irregular, we decided to use a method that relied on 2D rasters to measure crown area and from that, derive crown diameter. We chose 1 cm as the size for the raster cells because it is the minimum distance between points after the point cloud thinning outlined in section 2.2.5. We then created a count raster where the digital number (DN) in each cell was the number of points inside the square vertical prism represented by the cell. An

initial estimate of the crown area was then obtained as the sum of the areas of non-empty cells in that raster. To reduce crown area overestimation caused by cells along the crown perimeter with very few points, non-empty cells were then sorted in ascending order by DN, and the first 1% of cells in the ordered list were set to DN=0 in the count raster. While this had little to no effect at the 1 cm cell level, it became more important when we analyzed the effect of raster cell size in the experiment outlined in section 2.2.10. For the purposes of precisely calculating crown area and the uncertainty of this measurement, we determined which cells were on the perimeter and which were inside the crown by looking at each cell's 4-neighbours (neighbouring cells above, below, and on either side of the cell, but not diagonally adjacent). If the DN ≠ 0 in all four neighbouring cells, the cell was classified as an inner cell, otherwise it was classified as a perimeter cell. Then crown area was estimated as follows:

$$CA = (p \cdot 0.5a) + (i \cdot a), \tag{2}$$

where p is the number of perimeter cells, i is the number of inner cells, and a is the area of a single cell.

The uncertainty of this measurement comes from not knowing whether the points in a perimeter cell are evenly distributed horizontally or if they are situated only on the side of the cell closest to the rest of the crown. Assuming the points were located at the centre of the cell, we can account for this uncertainty as follows:

$$\delta CA = \pm (p \cdot 0.5a). \tag{3}$$

Finally, we calculated crown diameter as the diameter of a circle of area equal to CA:

$$CD = 2\sqrt{CA/\pi}, \tag{4}$$

and deriving the uncertainty of this measurement as:

$$\delta CD = (\delta CA \cdot CD)/(2 \cdot CA \cdot \pi). \tag{5}$$

(N.B. Uncertainty propagation for all predictor measurement uncertainties and model parameters is explained in the Appendix.)

2.2.7 TreeQSM Estimates of Height, DBH and Volume

To evaluate the ability of QSMs to derive estimates of allometric variables, we used TreeQSM (Raumonen et al., 2013), an open source Matlab package that can be used to build

QSMs from point cloud data. TreeQSM provides measurements for height, DBH (as the diameter of the cylinder fitted to the point cloud from 1.1 to 1.5 m) and volume in its output. Each tree point cloud was run through the script five times to mitigate the random nature of the resulting QSMs created by the program, following the practices of other studies that generated multiple QSMs of individual trees to obtain more accurate measurements of tree attributes (M. Disney et al., 2018; Gonzalez de Tanago et al., 2017). The attributes were averaged from the five QSMs and their uncertainty measurements were calculated to give a final measured value for each of these attributes. These estimates were then used as predictors in some of the AGB models we tested. Information on the input parameters used for this step can be found in Table 1.

2.2.8 Bounding Box Volume

Bounding box volume was measured as the volume of the smallest box that encompasses the entire tree point cloud. This was done to expand on the work done by Flade et al. who developed methods to use bounding box volume as a predictor for peatland shrub AGB (Flade et al., 2020). The dimensions of the bounding box can be found by calculating the difference between the maximum and minimum coordinates on each axis. This is done automatically in Cloud Compare (*CloudCompare (v2.11.1)*, n.d.), so we used the box dimensions given within the program.

2.2.9 Fitting and Testing the Models

Our measurements gave us values for several different variables that could be used as predictors for our AGB models. The 9 variables (or products of variables) used in our models were:

1. Crown area;
2. Crown diameter;
3. Height (measured by TLS)
4. The product of crown area and height;
5. The product of crown diameter and height;
6. DBH from QSM;
7. The product of DBH and height;
8. Volume from QSM;

9. Volume of the bounding box of the tree point cloud.

Measurement uncertainties were recorded for each of these variables and combined with model uncertainties using the linear approximation and error propagation formulas outlined in the Appendix. Confidence intervals for the models were measured at the 95% confidence level. Correlation coefficients were also calculated between all individual predictors and lab-measured AGB.

All models were fitted using R's lm() function (R Core Team, 2020) and equations representing three different types of model for each of the predictors (Table 2). The input formula for power models was $log(y) \sim log(x)$ and the resulting coefficients were algebraically converted to fit the power function seen in Table 2. Similarly, multiple regression power models used the input formula $log(y) \sim log(x_1) + log(x_2)$. Quadratic models also required a log transformation of both x and y values before being fit into the lm() function using the formula $y \sim x + x^2$. Estimates were made using the resulting coefficients and then back-transformed to give an estimate of AGB. To account for bias in the back-transformed models, the estimates were multiplied by a correction factor of $\varepsilon = e^{MSE/2}$ where MSE is the mean squared error of the fitted models with log-transformed variables (Baskerville, 1972; Flade et al., 2020; Mascaro et al., 2014).

Models were fitted using both ordinary (OLS) and weighted (WLS) least squares methods and OLS models were tested for heteroskedasticity using the Breusch-Pagan test (Breusch & Pagan, 1979; Zeileis & Hothorn, 2002). For the weighted methods, the weight of each tree i was inversely proportional to the number of trees n_i with dry biomass within 1 kg of that tree:

$$W_i = (N - n_i) / \sum(N\text{-}ni), \tag{6}$$

where N is the total number of trees in the sample. Doing this allowed us to give more weight to bigger trees in the sample, which are less represented than smaller trees. Weights were also used to reduce heteroskedasticity in the residuals of some of our OLS models.

We assessed which of these fitted models performed the best using a 10-fold cross validation (Nwanganga & Chapple, 2020) with each plot acting as a fold to create a scenario analogous to using the model in a non-sampled location (Wenger & Olden, 2012). This method used the trees from 9 out of 10 plots to fit the model, and then tested it on the trees of the left-out plot. We then fit the model again using a different combination of 9 fitting plots and tested on a

different plot than the previous iteration(s). The process was repeated until each plot was used for testing once. During each iteration, we recorded the following model performance metrics,

- Mean average error (MAE);
- Adjusted R^2;
- Root mean squared error (RMSE).

We then used the average of each of these metrics from the completed cross validation to rank the models from 1-42. We also noted the coefficient of variation in RMSE to provide insight on the robustness of the model when it is exposed to new data from different areas of peatland. We then selected the top model for each of the nine predictors above for further analysis.

To assess how our top model fares compared to the published equations of Ung et al. (Ung et al., 2008) and Bhatti et al. (Bhatti et al., 2006) for commercial and small black spruce, respectively, the individual AGB of each tree harvested in this study between 1.3 and 3 m tall (as the Bhatti equations are only applicable to trees shorter than 3 m) was estimated using lab measurements of height and DBH and those equations. These estimates were compared with lab-measured AGB and the resulting RMSE and coefficient of determination were calculated and compared to those from the leave-one-plot-out cross validation of our top model. That is, to allow for a fair comparison, our predicted value for each of the trees ≤ 3 m tall came from the version of our top model that was fitted using all plots except the one where the tree was harvested from. There are also AGB equations specific to black spruce in the Northwest Territories, but they are only suited to trees with DBH > 6 cm (Singh, 1984), and therefore were not used in this study.

2.2.10 Surrogate Point Density Sensitivity Analysis

To assess how decreasing point density would reduce the accuracy of the AGB estimates in a scenario where the point clouds used for tree measurements come from ALS instead of TLS, an exploratory sensitivity analysis was performed using the cell size of the rasters as a proxy for point density of first returns. In addition to the 1 cm cell rasters, we created rasters with cells of increasing size at 5 cm steps up to 50 cm, which assuming 1 point per cell, would act as a surrogate for point densities ranging from 10000 pt/m^2 to 4 pt/m^2. Crown area and crown diameter were determined for each raster using the methods outlined in section 2.6 for the 1 cm

cell rasters. Recomputing tree height for decreasing point densities is not as straightforward and would require real ALS or UAV data (Peng et al., 2021), so we decided to forego the assessment of the impact on tree height.

We then calculated the crown area of each tree for each raster cell size, and used the equations provided by the best model for the product of crown area and height to estimate AGB and compared the results to the lab-measured AGB. We recorded the RMSE and the coefficient of determination to see how these metrics would behave with decreasing point density.

2.3 Results

In total we fitted 42 models to our data using different combinations of TLS-measured predictor variables, model forms, and model fitting methods to estimate AGB. Of the 100 trees harvested in this study (10 in each of the 10 plots), 89 were used in the fitting and final analysis of our models (Table 3) and resulted in an average AGB of 1.63 kg with a range of 0.11 kg to 9.31 kg (full details on all variables collected using TLS can be found in Table 4). Details of the trees that were excluded from modelling and the reasons for their removal can be found in Table 5. Occlusion was the most common issue that led to trees being removed from the analysis. Figure 2 shows examples of occluded and unoccluded point clouds.

2.3.1 Effect of Weights on Final Models

In our sample, 73 trees had a lab-measured AGB of less than 2.50 kg (Figure 3), meaning larger trees were underrepresented when fitting the models. Giving more weight to larger trees in the WLS estimation of model parameters saw our model fits either improve or remain constant (adjusted R^2 and RMSE) across the board (see Figure 4 for one example). In this model (the bounding box volume power model), the p-value of the Breusch-Pagan test for the residuals in the OLS method was 0.14, indicating that the residuals are homoscedastic. However, adding weights to give each interval of the AGB range equal influence on the model resulted in an improved adjusted R^2 (0.89 for WLS, 0.86 for OLS), and a constant RMSE (0.66 kg for both).

2.3.2 QSM Effectiveness

Each of the 89 trees in our study was also run through the TreeQSM script (Raumonen et al., 2013) as outlined in section 2.6. Our average measurement uncertainty for total tree volume

was 1.27 L, roughly 9% of the average total volume. Similar relative uncertainties were observed for DBH (8%) and stem volume (10%). DBH estimation proved unreliable when compared to lab-measured results. The coefficient of determination for observed (lab-measured) vs predicted (QSM) DBH was 0.58, with an RMSE of 2.7 cm, and the bias was +2.0 cm (relative to the mean observed DBH, this is 115% and 86% respectively). Height estimation from the QSMs was more reliable than for DBH, but still not as good as the simple max(z) – min(z) calculation. QSM-obtained heights returned a coefficient of determination of 0.97 and an RMSE of 0.20 m, while the max-min method returned a coefficient of determination of 0.97 and an RMSE of 0.18 m. In terms of AGB, estimates given by our best model (crown area and height multiple regression power model, outlined in section 3.3) gave an average adjusted R^2 value of 0.94 and an average RMSE of 0.34 kg (21.0% of the average AGB of the sample), whereas the same model using QSM-measured height instead of TLS-measured height gave an average adjusted R^2 of 0.94 and an average RMSE of 0.35 kg (21.4% of the average AGB of the sample).

2.3.3 Model Rankings

The multiple regression power models that used the product of crown size (either crown area or crown diameter) and height yielded the best results (Table 6). A graphical representation of the fitted model using the product of crown area and height can be seen in Figure 5. Because crown diameter was a parameter derived from crown area, these two power models returned the same results. The same is true for the two multiple regression models that use the products of crown area and height and crown diameter and height. The fact that they use a separate exponent for each factor makes for a closer fit than in the normal power models where a single exponent applies to the completed product of the factors.

Model parameters and standard errors are reported for the best combination of model type and variable in Tables 7 (multiple regression power models), 8 (power models), and 9 (quadratic models). The standard errors were combined with the recorded measurement uncertainties and plotted as error bars in predicted vs observed AGB scatterplots which can be found in the Figures 6-14). Full rankings for each model type can be seen in Tables 10 (multiple regression power models), 11 (power models), and 12 (quadratic models). Methods and equations for estimating the uncertainty of estimates appear in the Appendix.

2.3.4 Comparisons with Other AGB Estimation Methods

We used a subset of 64 trees to compare our top model's estimates to those made using equations from Ung et al. (Ung et al., 2008) and Bhatti et al. (Bhatti et al., 2006). We could not use the whole sample for this comparison because the equations in Bhatti et al. are only recommended for trees less than 3 m in height (Bhatti et al., 2006), and because four trees from our sample had no lab-measured DBH due to their reconstructed lab-measured heights being less than 1.3 m. Our best model (crown area and height WLS multiple regression power model) outperformed both the other models, even though it does not use DBH. Our estimates had the lowest RMSE of the tested methods at 0.21 kg or 24% of the average biomass of this subset of trees, compared to 0.31 kg (36%) for the Ung estimates, and 0.35 kg (40%) for the Bhatti estimates (Figure 15). The crown area and height model also performed better than another multiple regression WLS model fitted using lab-measured DBH and height as well (not shown).

We also compared the results from the cross validation of the crown area and height multiple regression power model with the estimates given by the equations of Ung et al. (Ung et al., 2008) for the subset of all trees with lab-measured height and DBH (85 of the 89 in the sample). The average RMSE of the crown area and height model in this test was 0.39 kg (23% of the average AGB of this subset) compared to 0.51 kg (30%) in the estimates made using Ung et al.'s equations (Ung et al., 2008). The R^2 also favoured the crown area and height model for this subset, with an R^2 of 0.96 compared to 0.93 for Ung estimates.

Of the predictors used in this study, bounding box volume (r = 0.93), lab-measured DBH (r = 0.90) and TLS-derived height (r = 0.90) were most strongly correlated with AGB, while crown area (r = 0.81) and QSM-measured DBH (r = 0.67) showed the weakest correlation with AGB (Figure 16).

2.3.5 Crown Area Sensitivity Analysis

The simulation of decreasing point density revealed that the AGB estimation errors in the crown area and height multiple regression power model remain low at nominal densities above 16 pts/m^2 (Figures 17 and 18). While both RMSE and R^2 show some worsening over the full range of nominal point densities tested, most of this occurs for lower point densities. The RMSE of the AGB estimates increases from 0.36 kg when using 10000 pts/m^2 to 1.26 kg when using 4 pts/m^2, but only 17% of this increase is seen between 10000 and 16 pts/m^2. A similar pattern is

also observed for R^2. As explained in section 2.10, the impact of decreasing point density on height estimation was not considered in this simulation. Notwithstanding, the threshold we found is consistent with the one suggested in a recent study focused on height estimation of coniferous trees using drone-based lidar point clouds of different point densities, which found that height accuracy worsens at around 17 pts/m^2 (Peng et al., 2021).

2.4 Discussion

2.4.1 Effect of Weights on Final Models

The residuals of most OLS models did not show heteroskedasticity in a Breusch-Pagan test (Breusch & Pagan, 1979; Zeileis & Hothorn, 2002) (the only exception being the power model of the product of crown area and height), but we did notice slightly larger residuals for trees in the higher end of our lab-measured AGB range. A possible reason for this is that there are more trees with low AGB (< 2.5 kg) than there were trees with high AGB (> 2.5 kg). While more smaller trees than larger trees is to be expected in any treed peatland (Lieffers, 1986), it does not translate well to model fitting, because if each point is given the same weight and more points are at the lower end of the range, then the model will tend to fit those points more, leading to larger residuals for the taller trees.

2.4.2 QSM Effectiveness

At the outset of the study, we expected that the QSMs could be used to reliably estimate AGB. Because the trees were small and frequently clustered together, there was often occlusion which caused anomalies in the final QSMs. Stem reconstruction was partial and noisy for most of the trees, making DBH estimates unreliable with a relative RMSE of more than 100% of the average field-measured DBH, which propagated through to the QSM volume estimates. The latter was still used as a single predictor in one of the models, but it was outperformed by other TLS models that also used only single predictors, namely bounding box volume and height.

The QSMs did not provide the kind of consistent results other authors obtained for mature deciduous trees (Calders et al., 2015; Gonzalez de Tanago et al., 2017). This can be seen in the uncertainties resulting from averaging the five iterations of the QSM for each tree, particularly in total tree volume and DBH (see section 3.2). Occlusion played a large role in this as well, as the QSMs rely on the ability to fit cylinders to structural segments of the point cloud (Raumonen et

al., 2013), and when the stems of trees were occluded it made it difficult for TreeQSM to accurately fit cylinders to the stem and get DBH measurements. It should be noted that QSMs produce best results in leaf off conditions (Burt et al., 2013; Zhouxin Xi et al., 2018). We were unable to remove points corresponding to needles effectively, as they are often easily confused with woody structure (D. Wang et al., 2020; Wu et al., 2020). Therefore, we had to run our QSMs with the needles still on in the point cloud, which likely also contributed to the poor results. The AGB estimation error for models that relied on QSM-measured predictors may not be directly related to needles, but the thick branching and foliage created significant occlusion of the stem. Hence, we do not recommend the use of QSMs for AGB estimation of small black spruce trees.

2.4.3 Model Rankings

The best TLS models were the multiple regression power models of crown area (or alternatively, crown diameter) and height, where the two predictors are multiplied, and each has a different exponent. The power models that assigned a single exponent to the product of multiple variables still performed well, but not as well as these models (Table 13). The strength of the multiple regression models comes from their ability to be more flexible when fitting the curve to the data, leading to smaller residuals than the models using only a single exponent. We found that within the multiple regression power models, the crown area and height model performed better than lab-measured DBH and height model, which was unexpected because DBH correlates more strongly with AGB than crown area. A possible explanation for this is in the correlation between predictors. In our sample, crown area and height are less correlated than DBH and height (Figure 16) ($r = 0.65$ to $r = 0.96$ respectively), which is the likely reason why a model using those two variables would be better able to explain the variance in AGB. These findings are consistent with other studies showing that crown size can improve the predictive capabilities of AGB allometric equations in other ecosystems (Forrester et al., 2021; Goodman et al., 2014; Jucker et al., 2017; Lau et al., 2019).

Quadratic models performed slightly worse than power models in most situations except for the QSM-derived DBH. This was, however, the worst performing of all our top models (Table 6), which likely stems from the issues we had getting accurate DBH measurements from the QSMs. When the same model was fitted using lab-measured DBH it had an RMSE of 0.43 kg,

68% lower than the QSM-derived DBH model (this comparison was done using the subset of the 85 trees that had lab-measured DBHs). An important consideration for quadratic models is that, unlike power models, the regression line does not intercept the y axis at y = 0. This means that it is entirely possible to predict negative AGB for small trees. It is possible to force the regression to have an intercept at y = 0, but because our intercepts were generally quite small, we found that doing this caused the model to predict worse for the trees that fell in the range of our sample, so we used the unconstrained models instead.

Although our study included trees between 1.3 and 7 m tall, in practice there were fewer tall trees than short trees in these plots, and the tallest trees that were used in our dataset where slightly over 5 m tall. As such, we recommend that our equations only be used for black spruce trees that are 1.3 to 5 m in height.

The cross-validation methods we used helped prevent the models from being overfitted to the sample data. They were fitted using trees from nine plots and then tested on the final plot, meaning that the performance metrics used to rank the models were obtained based on AGB estimates for trees that had no impact on the fitting of the models. The low coefficients of variation for RMSE in the cross validation (Table 13) provide evidence that the models presented here performed consistently for all the plots between Hay River and Fort Simpson, NWT. As such, we believe that they should work equally well in other boreal peatlands (Wenger & Olden, 2012), however further work is needed to support this assumption.

The model based on bounding box volume ranked third in the final rankings of TLS models (Table 6). Unlike in QSMs, where volume is calculated using an array of cylinders to represent the stem and branches of a tree, bounding box volume is easily computed from the maximum and minimum point coordinates in each axis. We selected this predictor following Flade et al. (Flade et al., 2020) who found that bounding box volume can predict the AGB of boreal shrubs with relative RMSE of 76% when compared to the average AGB of shrubs in their sample. We expand on this idea by applying it to small black spruce trees and show that bounding box volume can be a useful predictor for estimating tree biomass as well, with a relative avg RMSE of 40% and an R^2 of 0.87. Bounding box volume could be useful in situations where the point cloud is not dense enough to reliably estimate crown area, but where there is ancillary high-resolution imagery that can identify the individual small black spruce within the bounding box.

The model based on TLS-measured height was fourth in the ranking, outperforming the models that used QSM-derived attributes, as well as the models that used only crown size as a predictor. The fact that they perform better than the single predictor models based on crown size indicates that height is the more important factor in the top two models, with crown size being a secondary piece of information that can improve on the models built using height alone.

2.4.4 Comparisons with Other AGB Estimation Methods

We found that our best models (using crown size and height as predictors) outperform the other existing model for small black spruce (Bhatti et al., 2006). The mean RMSE from the leave-one-plot-out cross validation of our crown area and height model for the subset of trees shorter than 3m tall was 0.21, compared to 0.35 for the Bhatti equations, even with the latter using lab-measured DBH and height. Furthermore, our best models also outperform the DBH and height model from Ung et al. (Ung et al., 2008) for our sample and therefore could be a preferred alternative when DBH is not available or is hard to measure from TLS, such as where there are many small trees close together. When the AGB is estimated using Ung et al.'s (2008) equations with lab-measured height and DBH, the RMSE is 0.51 kg, 30% of the average AGB. In comparison, the average RMSE of our best model is 0.39 kg, 23% of the average AGB. Our best model requires that the point clouds can be correctly segmented and classified; something that has been shown for tall trees (Budei et al., 2018; Harikumar et al., 2021; Modzelewska et al., 2020), and with some success for small trees and shrubs when they are not part of an understory (Prošek & Šímová, 2019; Reese et al., 2014). The accuracy of our models combined with their potential to estimate AGB without setting foot on the ground (when using high density ALS instead of TLS) makes them an excellent tool to estimate the AGB of individual small black spruce in boreal forest peatlands.

2.4.5 Crown Area Sensitivity Analysis

The sensitivity analysis with increasing raster cell sizes as a proxy for decreasing point density suggests that our best models could perform similarly using ALS data instead of TLS, provided that point density is greater than 16 pts/m^2 in the ALS point cloud. The threshold we found is consistent with the one suggested in a recent study for height estimation of coniferous trees using drone-based lidar point clouds of different point densities, which found that height

accuracy worsens at around 17 pts/m^2 (Peng et al., 2021). However, the observed accuracy loss could start at higher point densities in a real scenario because we assumed no effect on tree height and uniform horizontal distribution of laser pulses. We also used only tree points for the analysis, but true ALS data has both ground and tree points. As such, the point density of the tree point clouds obtained from ALS would likely be considerably lower than the overall point density. While this analysis provides some preliminary insight as to how the crown area component of our best model is affected by decreasing point densities, it is by no means extensive and further analysis using actual airborne data is needed.

2.5 Conclusion

Our best models produced estimates of AGB for black spruce that are comparable in accuracy to estimates derived from widely-used allometric equations first published in Lambert et al. (Lambert et al., 2005) and then updated in Ung et al. (Ung et al., 2008), which require time-consuming field measurements of DBH and height. They have the advantage of not being reliant on DBH, which cannot be reliably measured from the air (Chen et al., 2018; Jucker et al., 2017; Malek S et al., 2019). It can also be difficult to measure from the ground using TLS when the trees are compact and close to each other. Instead, our models use predictors that have the potential to be measured from the air using high-density point clouds, from UAV or airplane, photogrammetry or LiDAR. Our best model uses predictors of tree height and crown size (expressed as either crown area or crown diameter). As such, the model equations presented here could provide a valuable tool for estimating the individual tree AGB of a common species of tree in a prominent ecosystem of the boreal forest. They set the stage for further study on the effect of point density from ALS and UAV scanning on these estimates and in future studies, it could be possible to scale the models up from individual trees to plot level estimates and assess the use of our models to estimate AGB density (t/ha) in blacks spruce peatlands using an area-based approach.

2.6 Tables

Table 1.

Input	Value
inputs.PatchDiam1	1
inputs.PatchDiam2Min	0.001
inputs.PatchDIam2Max	0.008
inputs.lcyl	1
inputs.FilRad	4
inputs.BallRad1	inputs.PatchDiam1 + 0.075
inputs.BallRad2	inputs.PatchDiam2Max + 0.02
inputs.nmin1	3
inputs.nmin2	1
inputs.OnlyTree	1
inputs.Tria	1
inputs.Dist	1
inputs.MinCylRad	0.001
inputs.ParentCor	1
inputs.TaperCor	1
inputs.GrowthVolCor	0
inputs.GrowthVolFac	2.5

Table 2.

Model Type	Equation
Quadratic	$y = exp(\alpha x^2 + \omega x + \beta) \cdot \varepsilon$
Power	$y = \beta \cdot x^{\alpha} \cdot \varepsilon$
Multiple Regression Power	$y = \beta \cdot x_1^{\alpha} \cdot x_2^{\omega} \cdot \varepsilon$

Table 3.

Plot name	# of Black Spruce in Plot	Height for all trees (m)	DBH for all trees (cm)	# of Black Spruce used in Study	Height for sample trees (m)	DBH for sample trees (cm)	Avg AGB for sample trees (kg)
V2B006	52	2.6 ± 1.0 (1.3; 5.7)	2.9 ± 1.5 (0.5; 7.1)	10	2.6 ± 1.0 (1.6; 5.0)	2.8 ± 1.3 (1.5; 6.0)	1.55 ± 1.50 (0.41; 5.42)
V2B009	47	2.4 ± 1.0 (1.3; 5.4)	2.4 ± 1.4 (0.3; 6.2)	10	2.7 ± 1.1 (1.4; 5.1)	2.9 ± 1.5 (1.1; 6.2)	1.93 ± 1.95 (0.37; 6.78)
V2B011	31	2.7 ± 1.3 (1.3; 6.2)	2.9 ± 1.8 (0.3; 6.5)	10	2.7 ± 1.2 (1.3; 4.7)	2.9 ± 1.6 (0.3; 5.1)	1.85 ± 1.19 (0.46; 4.14)
V2B012	23	3.4 ± 1.7 (1.4; 7.7)	3.7 ± 2.4 (0.6; 9.7)	8	3.4 ± 1.5 (1.5; 5.6)	3.7 ± 2.1 (0.9; 6.7)	3.80 ± 3.40 (0.60; 9.31)
V2B015	44	2.0 ± 0.7 (1.4; 4.6)	2.0 ± 1.0 (0.3; 5.9)	8	2.2 ± 0.9 (1.6; 4.4)	2.3 ± 1.2 (0.3; 4.7)	1.02 ± 1.06 (0.11; 3.68)
V2B016	32	3.0 ± 1.2 (1.3; 5.8)	3.1 ± 1.7 (0.4; 6.6)	7	2.9 ± 1.4 (1.3; 5.5)	2.8 ± 1.6 (0.5; 5.4)	1.72 ± 1.52 (0.28; 5.07)
V2B019	92	2.3 ± 0.7 (1.3; 5.0)	1.9 ± 1.1 (0.3; 5.7)	9	2.4 ± 0.8 (1.4; 3.8)	2.1 ± 1.0 (0.7; 4.1)	0.93 ± 0.69 (0.24; 2.48)

V2B022	25	2.3 ± 0.7 (1.5; 4.7)	2.3 ± 1.3 (0.6; 6.3)	10	2.4 ± 0.9 (1.5; 4.7)	2.4 ± 1.5 (1.0; 6.3)	1.50 ± 1.73 (0.51; 6.58)
V2B023	112	2.2 ± 0.8 (1.3; 7.1)	2.1 ± 1.2 (0.3; 6.9)	9	2.5 ± 1.1 (1.5; 4.8)	2.3 ± 1.4 (0.7; 4.8)	1.10 ± 1.24 (0.15; 4.28)
V2B026	115	2.0 ± 0.6 (1.3; 4.6)	1.8 ± 1.1 (0.3; 5.2)	8	2.2 ± 0.6 (1.6; 3.7)	2.3 ± 1.2 (1.2; 5.2)	0.95 ± 0.81 (0.34; 2.95)
Total	573	2.3 ± 1.0 (1.3; 7.7)	2.3 ± 1.4 (0.3; 9.7)	89	2.6 ± 1.1 (1.3; 5.6)	2.6 ± 1.5 (0.3; 6.7)	1.63 ± 1.83 (0.11; 9.31)

Table 4.

Plot name	# of Black Spruce used in Study	TLS Height (m)	QSM DBH (cm)	Crown Area (m^2)	Crown Diameter (m)	Bounding Box Volume (m^3)	QSM Volume (L)	Avg AGB (kg)
V2B006	10	2.50 ± 0.97 (1.54; 4.86)	2.83 ± 2.48 (0.27; 6.91)	0.16 ± 0.11 (0.05; 0.43)	0.42 ± 0.15 (0.26; 0.74)	1.14 ± 1.19 (0.19; 3.65)	10.08 ± 13.24 (0.89; 36.36)	1.55 ± 1.50 (0.41; 5.42)
V2B009	10	2.67 ± 1.06 (1.41; 5.01)	4.85 ± 3.16 (0.39; 11.66)	0.18 ± 0.09 (0.06; 0.35)	0.46 ± 0.12 (0.29; 0.66)	1.20 ± 0.98 (0.18; 3.34)	22.11 ± 29.20 (2.52; 102.71)	1.93 ± 1.95 (0.37; 6.78)
V2B011	10	2.66 ± 1.12 (1.40; 4.59)	5.92 ± 2.99 (0.64; 10.19)	0.23 ± 0.10 (0.08; 0.41)	0.53 ± 0.12 (0.32; 0.72)	1.54 ± 0.88 (0.49; 3.45)	20.42 ± 11.28 (3.14; 37.45)	1.85 ± 1.19 (0.46; 4.14)
V2B012	8	3.19 ± 1.33 (1.42; 5.38)	4.33 ± 2.77 (1.37; 9.98)	0.32 ± 0.21 (0.11; 0.66)	0.61 ± 0.21 (0.37; 0.92)	3.02 ± 2.64 (0.34; 8.14)	27.80 ± 31.73 (4.86; 102.63)	3.80 ± 3.40 (0.60; 9.31)
V2B015	8	2.16 ± 0.88 (1.46; 4.37)	3.43 ± 1.93 (0.92; 7.13)	0.15 ± 0.10 (0.04; 0.35)	0.41 ± 0.15 (0.23; 0.67)	0.94 ± 1.11 (0.14; 3.71)	9.63 ± 13.78 (1.67; 45.38)	1.02 ± 1.06 (0.11; 3.68)
V2B016	7	2.69 ± 1.28 (1.29; 5.12)	4.83 ± 2.49 (0.87; 8.03)	0.17 ± 0.05 (0.08; 0.23)	0.47 ± 0.08 (0.31; 0.54)	1.21 ± 0.67 (0.23; 2.31)	15.95 ± 12.97 (2.23; 39.58)	1.72 ± 1.52 (0.28; 5.07)

V2B019	9	2.24 ± 0.74 (1.36; 3.75)	2.75 ± 1.51 (0.38; 4.54)	0.11 ± 0.05 (0.06; 0.22)	0.37 ± 0.09 (0.27; 0.53)	0.72 ± 0.52 (0.31; 1.69)	5.39 ± 6.11 (0.54; 19.97)	0.93 ± 0.69 (0.24; 2.48)
V2B022	10	2.30 ± 0.87 (1.41; 4.58)	4.48 ± 2.15 (0.66; 8.62)	0.18 ± 0.11 (0.08; 0.49)	0.46 ± 0.13 (0.31; 0.79)	1.10 ± 1.30 (0.30; 4.91)	16.77 ± 23.55 (2.94; 85.96)	1.50 ± 1.73 (0.51; 6.58)
V2B023	9	2.40 ± 1.06 (1.26; 4.73)	3.77 ± 2.63 (0.54; 8.05)	0.10 ± 0.07 (0.04; 0.27)	0.34 ± 0.11 (0.22; 0.59)	0.78 ± 0.86 (0.12; 3.04)	9.94 ± 12.08 (1.87; 39.20)	1.10 ± 1.24 (0.15; 4.28)
V2B026	8	2.04 ± 0.63 (1.43; 3.56)	4.54 ± 2.46 (0.54; 8.91)	0.12 ± 0.05 (0.06; 0.20)	0.38 ± 0.08 (0.28; 0.50)	0.59 ± 0.41 (0.25; 1.44)	9.96 ± 8.94 (1.13; 28.35)	0.95 ± 0.81 (0.34; 2.95)
Total	89	2.48 ± 1.06 (1.26; 5.38)	4.18 ± 2.69 (0.27; 11.66)	0.17 ± 0.12 (0.04; 0.66)	0.44 ± 0.15 (0.22; 0.92)	1.21 ± 1.35 (0.12; 8.14)	14.86 ± 19.55 (0.54; 102.71)	1.63 ± 1.83 (0.11; 9.31)

Table 5.

Tree Reflector Number	Plot	Height (m)	DBH (cm)	Reason for Removal
1	V2B012	1.6	0.6	Missing bags for ground truth measurements.
7	V2B012	2.3	2.0	Overly occluded point cloud of tree.
7	V2B015	1.6	2.8	Missing bags for ground truth measurements.
8	V2B015	1.4	0.6	Overly occluded point cloud of tree.
3	V2B016	4.8	3.9	Tree in tight clump, could not accurately segment.
6	V2B016	1.8	1.6	Tree in tight clump, could not accurately segment.
7	V2B016	3.5	4.5	Overly occluded point cloud of tree.
5	V2B019	2.2	1.6	Could not find tree in plot-level point cloud.
7	V2B023	2.6	2.4	Could not find tree in plot-level point cloud.
5	V2B026	1.7	1.0	Could not find tree in plot-level point cloud.
7	V2B026	1.8	1.1	Overly occluded point cloud of tree.

Table 6.

Model Type	Model Predictors*	Avg MAE	Avg RMSE (kg)	Avg Adj R^2	Final Ranking
Multi Pwr	CAxH and CDxH	0.22	0.34	0.94	1
Pwr	V (Bounding Box)	0.40	0.59	0.89	2
Pwr	H	0.45	0.63	0.88	3
Multi Pwr	DBHxH	0.46	0.64	0.88	4
Pwr	V (QSM)	0.50	0.70	0.82	5
Pwr	CA and CD	0.67	0.95	0.71	6
Quad	DBH	0.84	1.19	0.62	7

*All models in this table were weighted least squares.

Table 7.

x_1	x_2	β	β std err	α	α std err	ω	ω std err	ε
CA	H	0.73	0.13	0.54	0.06	1.68	0.09	1.00
CD	H	0.64	0.10	1.07	0.11	1.68	0.09	1.00
DBH	H	0.16	0.02	0.06	0.07	2.19	0.14	1.00

Table 8.

X	β	β std err	α	α std err	ε
V (Bounding Box)	1.35	0.05	0.97	0.04	1.00
H	0.16	0.02	2.29	0.09	1.00
V (QSM)	0.23	0.03	0.76	0.04	1.00
CA	14.64	2.40	1.29	0.09	1.00
CD	10.73	1.55	2.57	0.18	1.00

Table 9.

X	β	β std err	α	α std err	ω	ω std err	ε
DBH (QSM)	-0.97	0.13	0.40	0.08	0.25	0.15	1.00

Table 10.

	β				α				ω				
Model	**Val**	**CL95-**	**CL95+**	**SE**	**Val**	**CL95-**	**CL95+**	**SE**	**Val**	**CL95-**	**CL95+**	**SE**	**ε**
CAxH OLS	0.75	0.53	1.08	0.14	0.53	0.41	0.64	0.06	1.63	1.44	1.82	0.10	1.04
CAxH WLS	0.73	0.52	1.03	0.13	0.54	0.43	0.65	0.06	1.68	1.50	1.85	0.09	1.00
CDxH OLS	0.66	0.48	0.92	0.11	1.06	0.82	1.29	0.12	1.63	1.44	1.82	0.10	1.04
CDxH WLS	0.64	0.47	0.88	0.10	1.07	0.86	1.29	0.11	1.68	1.50	1.85	0.09	1.00
DBH(QSM)xH OLS	0.17	0.14	0.21	0.02	0.07	-0.06	0.19	0.06	2.08	1.79	2.37	0.15	1.07
DBH(QSM)xH WLS	0.16	0.13	0.19	0.02	0.06	-0.07	0.20	0.07	2.19	1.91	2.46	0.14	1.00

Table 11.

	β				α				
Model	**Val**	**CL95-**	**CL95+**	**SE**	**Val**	**CL95-**	**CL95+**	**SE**	**ε**
CA OLS	10.34	7.09	15.09	1.97	1.17	0.99	1.36	0.09	1.16
CA WLS	14.64	10.56	20.28	2.40	1.29	1.11	1.46	0.09	1.00
CAxH OLS	2.92	2.60	3.28	0.17	0.92	0.84	1.00	0.04	1.06
CAxH WLS	3.14	2.87	3.42	0.14	0.96	0.89	1.02	0.03	1.00
CD OLS	7.79	5.57	10.90	1.32	2.35	1.98	2.71	0.18	1.16
CD WLS	10.73	8.05	14.30	1.55	2.57	2.22	2.92	0.18	1.00
CDxH OLS	1.08	1.02	1.14	0.03	1.38	1.29	1.47	0.05	1.04
CDxH WLS	1.08	1.02	1.15	0.03	1.42	1.34	1.49	0.04	1.00
DBH (QSM) OLS	0.47	0.37	0.59	0.05	0.70	0.54	0.86	0.08	1.25
DBH (QSM) WLS	0.45	0.34	0.60	0.06	0.90	0.73	1.08	0.09	1.00
DBH (QSM)xH OLS	5.31	4.01	7.03	0.75	0.614	0.518	0.710	0.048	1.16
DBH (QSM)xH WLS	7.97	6.27	10.12	0.96	0.729	0.635	0.822	0.047	1.00
H OLS	0.17	0.14	0.20	0.02	2.193	1.992	2.394	0.101	1.07
H WLS	0.16	0.13	0.19	0.02	2.287	2.111	2.463	0.089	1.00
V (Bounding Box) OLS	1.31	1.21	1.41	0.05	0.932	0.852	1.011	0.040	1.06
V (Bounding Box) WLS	1.35	1.26	1.46	0.50	0.969	0.899	1.040	0.036	1.00

V (QSM) OLS	0.25	0.21	0.31	0.03	0.689	0.607	0.772	0.042	1.11
V (QSM) WLS	0.23	0.19	0.28	0.03	0.761	0.685	0.837	0.038	1.00

Table 12.

	β				α				ω				
Model	**Val**	**CL95-**	**CL95+**	**SE**	**Val**	**CL95-**	**CL95+**	**SE**	**Val**	**CL95-**	**CL95+**	**SE**	**ε**
CA OLS	2.94	2.10	3.78	0.42	0.19	-0.05	0.42	0.12	1.88	-0.98	2.79	0.46	1.16
CA WLS	2.72	2.02	3.42	0.35	0.01	-0.21	0.24	0.11	1.33	-0.50	2.16	0.42	1.00
CAxH OLS	1.07	0.96	1.19	0.06	0.06	-0.02	0.13	0.04	1.02	-0.87	1.18	0.08	1.06
CAxH WLS	1.14	1.05	1.23	0.05	0.01	-0.06	0.07	0.03	0.97	-0.84	1.09	0.06	1.00
CD OLS	2.49	1.85	3.14	0.32	0.74	-0.19	1.67	0.47	3.59	-2.00	5.18	0.80	1.16
CD WLS	2.40	1.88	2.92	0.26	0.05	-0.86	0.96	0.46	2.65	-1.21	4.10	0.73	1.00
CDxH OLS	0.05	-0.04	0.13	0.04	0.07	-0.06	0.20	0.07	1.36	-1.27	1.46	0.05	1.04
CDxH WLS	0.07	-0.01	0.15	0.04	0.02	-0.10	0.13	0.06	1.41	-1.32	1.50	0.05	1.00
DBH (QSM) OLS	-0.98	-1.19	-0.78	0.10	0.41	0.28	0.54	0.07	0.14	0.08	0.37	0.11	1.17
DBH (QSM) WLS	-0.97	-1.22	-0.71	0.13	0.40	0.25	0.56	0.08	0.25	0.04	0.54	0.15	1.00
DBH(QSM)xH OLS	3.15	2.68	3.63	0.24	0.21	0.15	0.26	0.03	1.83	-1.48	2.18	0.18	1.10
DBH(QSM)xH WLS	3.14	2.73	3.56	0.21	0.18	0.12	0.24	0.03	1.74	-1.39	2.09	0.18	1.00
H OLS	-1.59	-2.01	-1.18	0.21	0.28	-0.24	0.81	0.27	1.67	-0.66	2.67	0.50	1.07
H WLS	-1.79	-2.22	-1.36	0.22	0.10	-0.40	0.59	0.25	2.09	-1.11	3.08	0.50	1.00

V (Bounding Box) OLS	0.23	0.13	0.33	0.05	0.05	-0.03	0.12	0.04	0.94	-0.86	1.02	0.04	1.06
V (Bounding Box) WLS	0.30	0.20	0.41	0.05	0.00	-0.07	0.07	0.04	0.97	-0.90	1.04	0.04	1.00
V (QSM) OLS	-1.06	-1.32	-0.80	0.13	0.10	0.04	0.16	0.03	0.27	0.00	0.53	0.13	1.10
V (QSM) WLS	-1.25	-1.55	-0.96	0.15	0.06	0.00	0.12	0.03	0.49	-0.22	0.76	0.14	1.00

Table 13.

Model Type	Model	Avg MAE	Ranking 1	Avg RMSE	Ranking 2	Avg Adj R^2	Ranking 3	CV RMSE	Total Sum of Rankings
Multi Pwr	CAxH WLS	0.22	1	0.34	1	0.94	1	0.60	3
Multi Pwr	CDxH WLS	0.22	1	0.34	1	0.94	1	0.60	3
Multi Pwr	CAxH OLS	0.22	1	0.34	1	0.91	5	0.60	7
Multi Pwr	CDxH OLS	0.22	1	0.34	1	0.91	5	0.60	7
Pwr	CDxH WLS	0.25	5	0.37	5	0.93	3	0.52	13
Pwr	CDxH OLS	0.25	5	0.37	5	0.91	5	0.52	15
Quad	CDxH WLS	0.25	5	0.38	7	0.93	3	0.53	15
Quad	CDxH OLS	0.27	8	0.42	8	0.91	5	0.71	21
Pwr	CAxH WLS	0.37	10	0.53	10	0.89	9	0.55	29
Quad	CAxH WLS	0.38	11	0.55	11	0.89	9	0.60	31
Pwr	CAxH OLS	0.36	9	0.52	9	0.86	16	0.53	34
Pwr	V (Bounding Box) WLS	0.40	13	0.58	12	0.89	9	0.60	34
Quad	V (Bounding Box) WLS	0.40	13	0.59	14	0.89	9	0.60	36
Pwr	V (Bounding Box) OLS	0.39	12	0.58	12	0.85	19	0.58	43

Pwr	H WLS	0.45	17	0.63	16	0.88	13	0.74	46
Multi Pwr	DBHxH WLS	0.45	17	0.63	16	0.88	13	0.80	46
Quad	CAxH OLS	0.43	15	0.69	21	0.86	16	0.96	52
Pwr	H OLS	0.45	17	0.62	15	0.84	20	0.73	52
Multi Pwr	DBHxH OLS	0.45	17	0.63	16	0.84	20	0.80	53
Quad	H WLS	0.46	21	0.64	19	0.88	13	0.75	53
Quad	V (Bounding Box) OLS	0.44	16	0.69	21	0.86	16	0.78	53
Quad	H OLS	0.46	21	0.68	20	0.84	20	0.64	61
Pwr	V (QSM) WLS	0.50	24	0.69	21	0.82	23	0.94	68
Quad	V (QSM)WLS	0.49	23	0.77	25	0.82	23	0.83	71
Pwr	V (QSM) OLS	0.52	25	0.71	24	0.75	28	1.00	77
Quad	DBHxH WLS	0.55	26	0.78	26	0.80	25	0.86	77
Quad	DBHxH OLS	0.57	27	0.86	27	0.77	27	0.87	81
Pwr	DBHxH WLS	0.66	29	0.89	28	0.73	29	0.87	86
Quad	V (QSM) OLS	0.57	27	0.96	33	0.78	26	0.89	86
Pwr	CA WLS	0.67	30	0.94	29	0.70	30	0.55	89
Pwr	CD WLS	0.67	30	0.94	29	0.70	30	0.55	89
Quad	CA WLS	0.67	30	0.95	31	0.70	30	0.55	91

Quad	CD WLS	0.67	30	0.95	31	0.70	30	0.55	91
Pwr	CA OLS	0.69	34	0.98	34	0.64	37	0.54	105
Pwr	CD OLS	0.69	34	0.98	34	0.64	37	0.54	105
Quad	CA OLS	0.69	34	1.03	37	0.65	34	0.62	105
Quad	CD OLS	0.69	34	1.03	37	0.65	34	0.62	105
Pwr	DBHxH OLS	0.71	38	0.98	34	0.64	37	0.87	109
Quad	DBH WLS	0.83	40	1.18	39	0.65	34	0.69	113
Quad	DBH OLS	0.81	39	1.21	40	0.62	40	0.72	119
Pwr	DBH WLS	0.91	41	1.23	41	0.55	41	0.69	123
Pwr	DBH OLS	0.92	42	1.28	42	0.47	42	0.71	126

2.7 Figures

Figure 1.

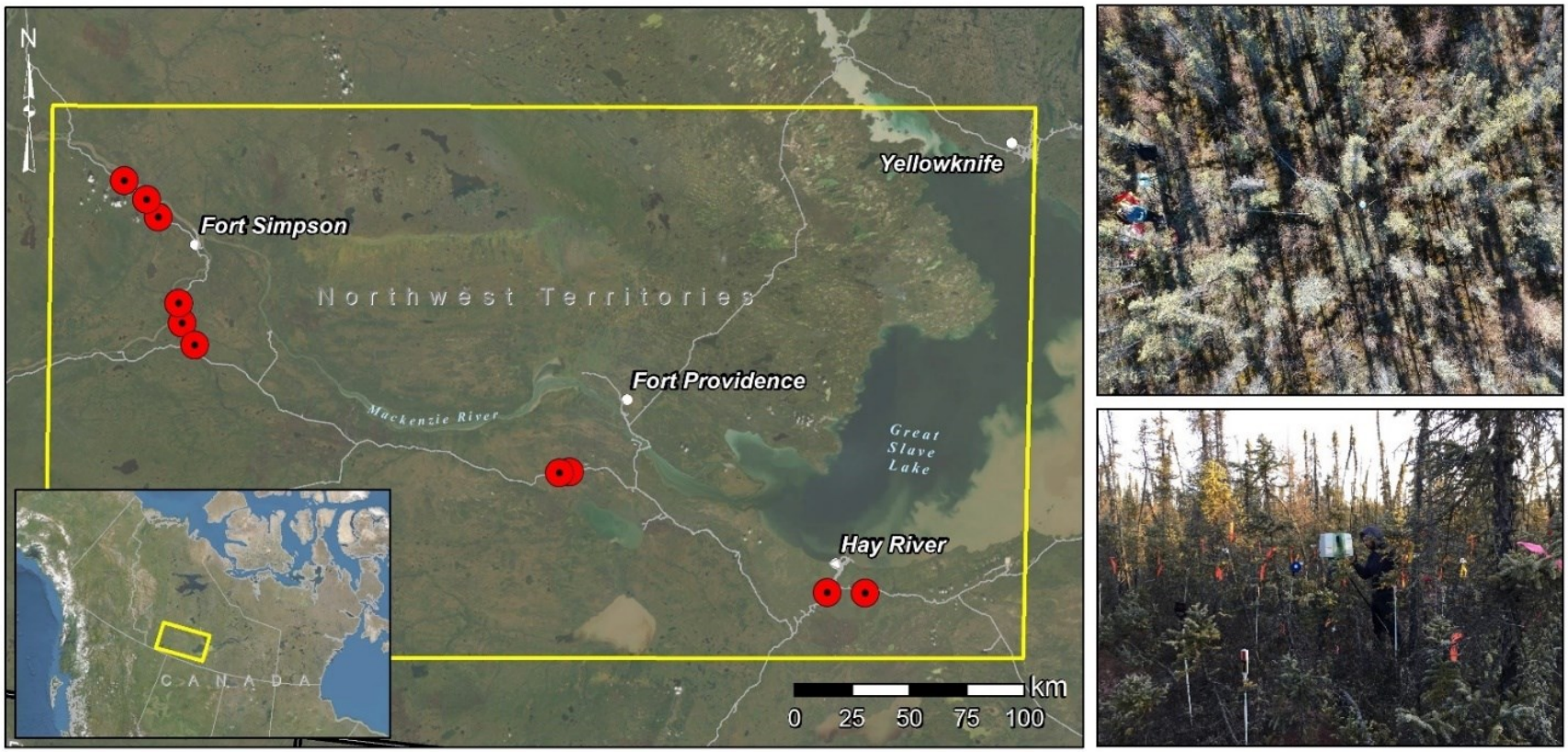

Figure 2.

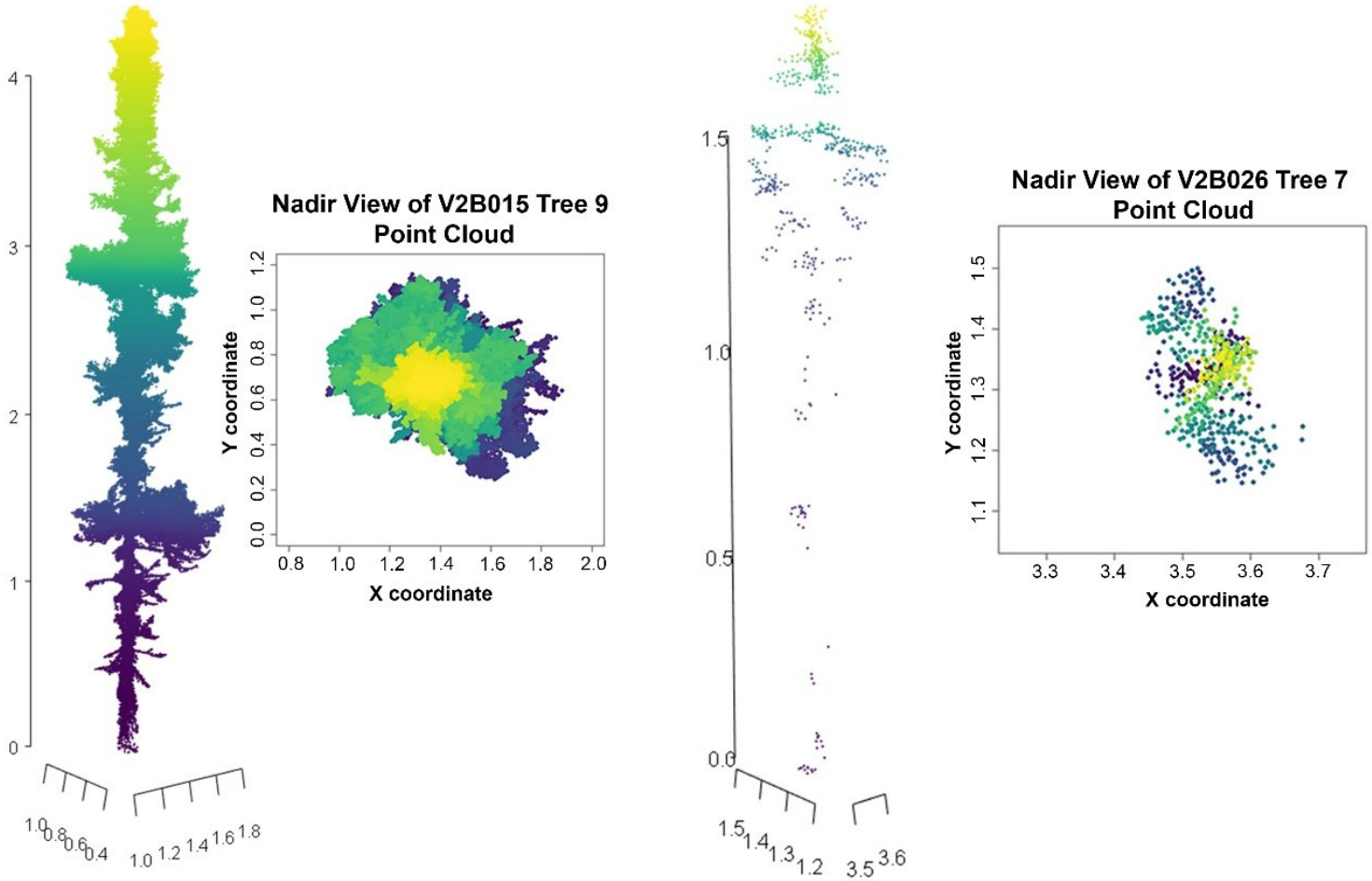
Nadir View of V2B015 Tree 9
Point Cloud
Y coordinate
X coordinate
Nadir View of V2B026 Tree 7
Point Cloud
Y coordinate
X coordinate

A) B)

Figure 3.

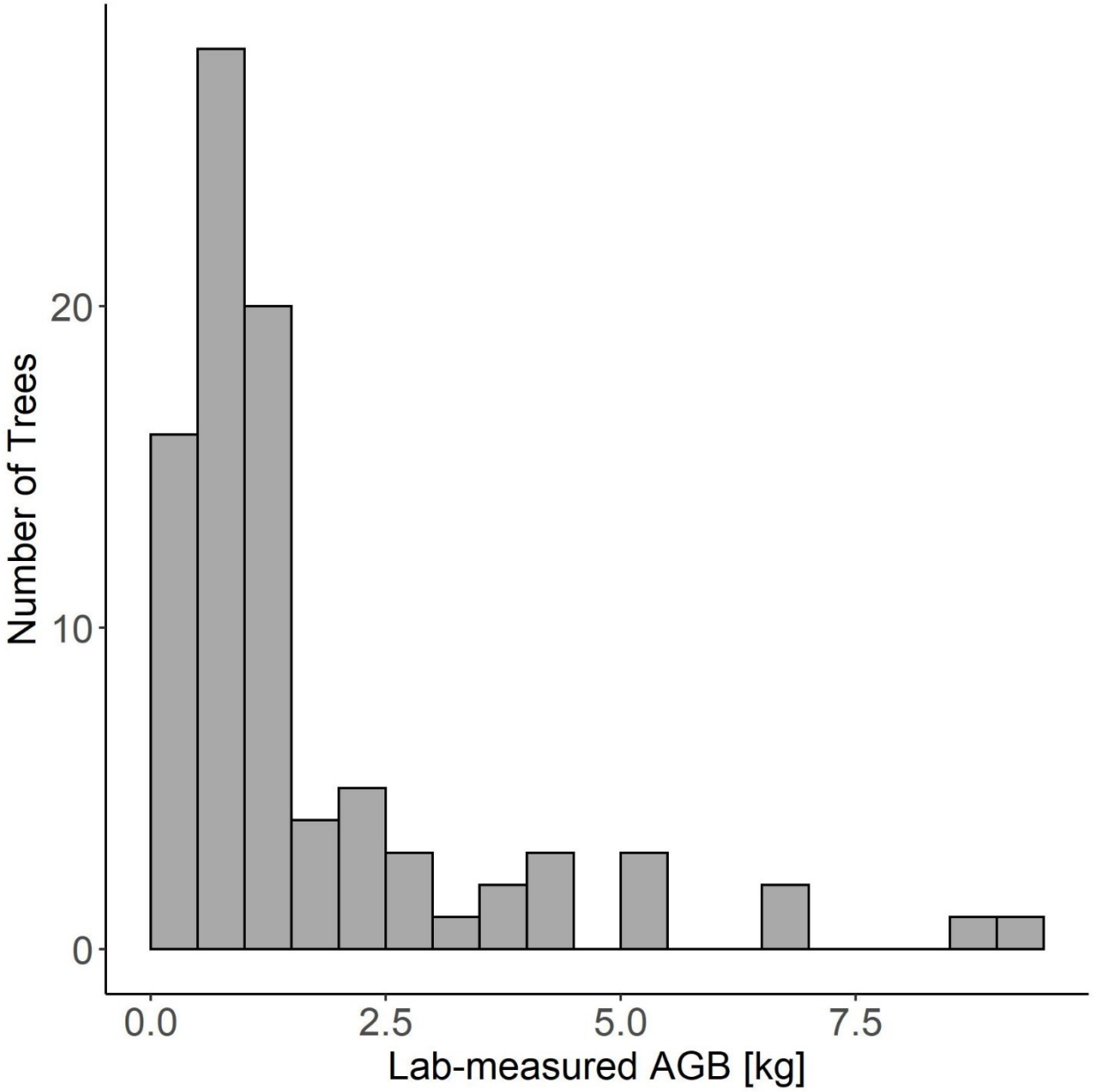

Figure 4.

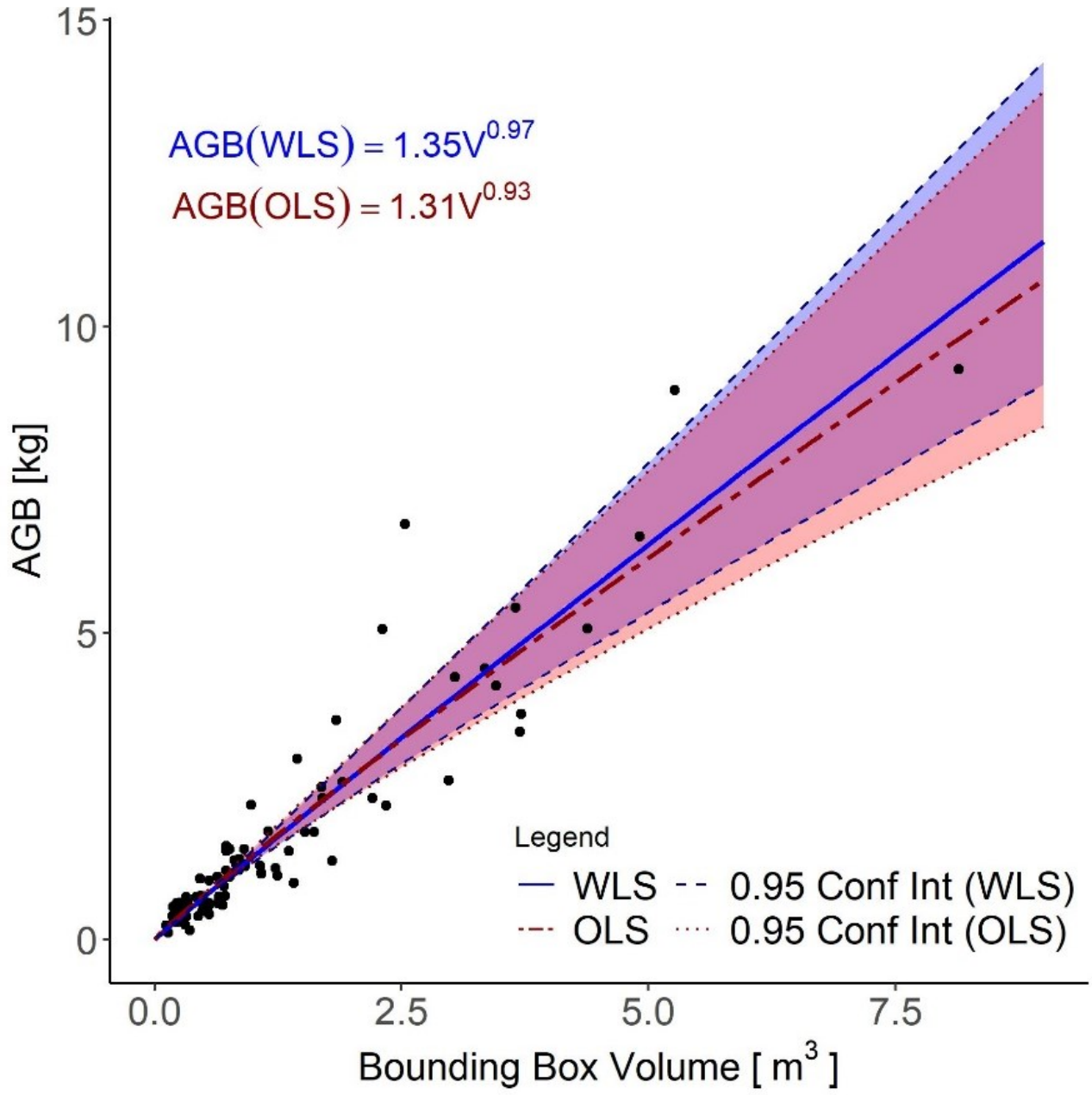
AGB(WLS) = 1.35V^0.97
AGB(OLS) = 1.31V^0.93
AGB [kg]
15
10
5
0
0.0
2.5
5.0
7.5
Bounding Box Volume [m^3]
Legend
WLS
0.95 Conf Int (WLS)
OLS
0.95 Conf Int (OLS)

Figure 5.

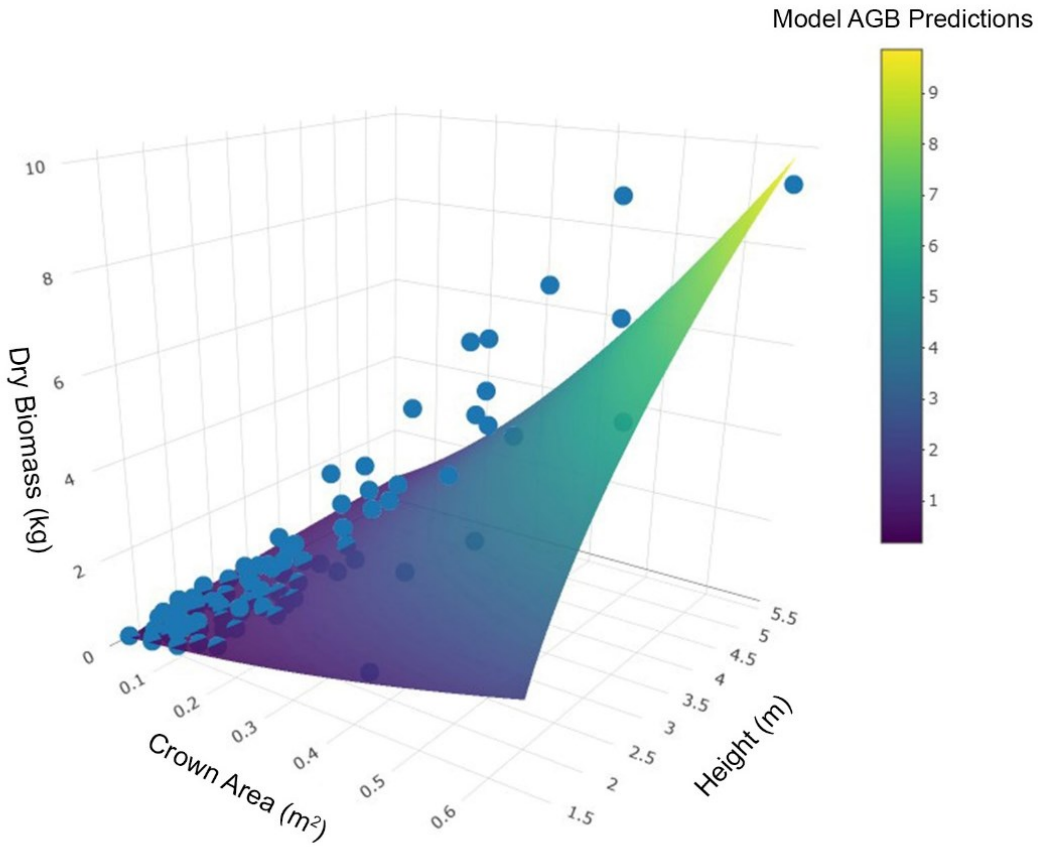

Figure 6.

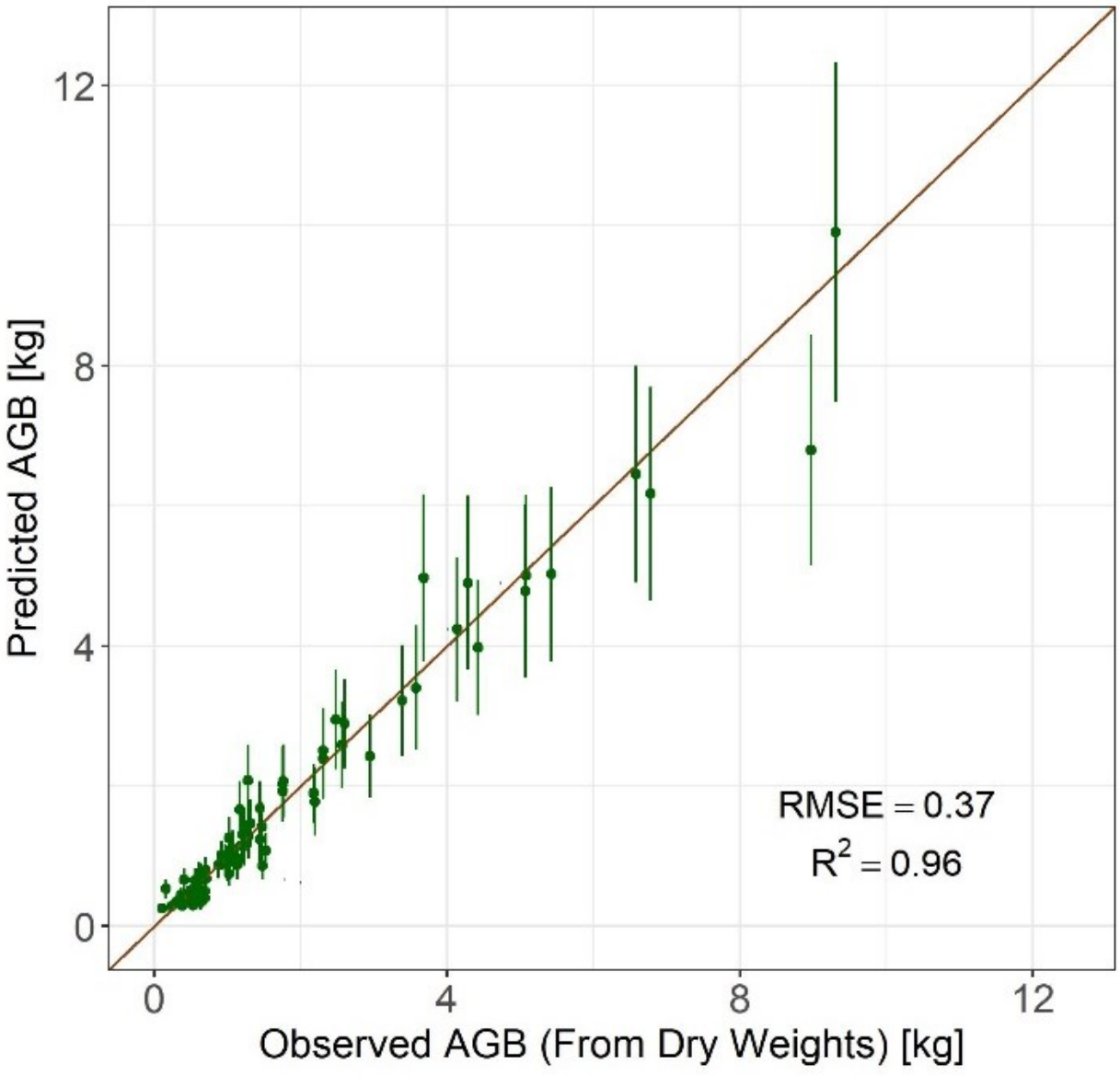
Predicted AGB [kg]
Observed AGB (From Dry Weights) [kg]
0
4
8
12
RMSE = 0.37
R2 = 0.96

Figure 7.

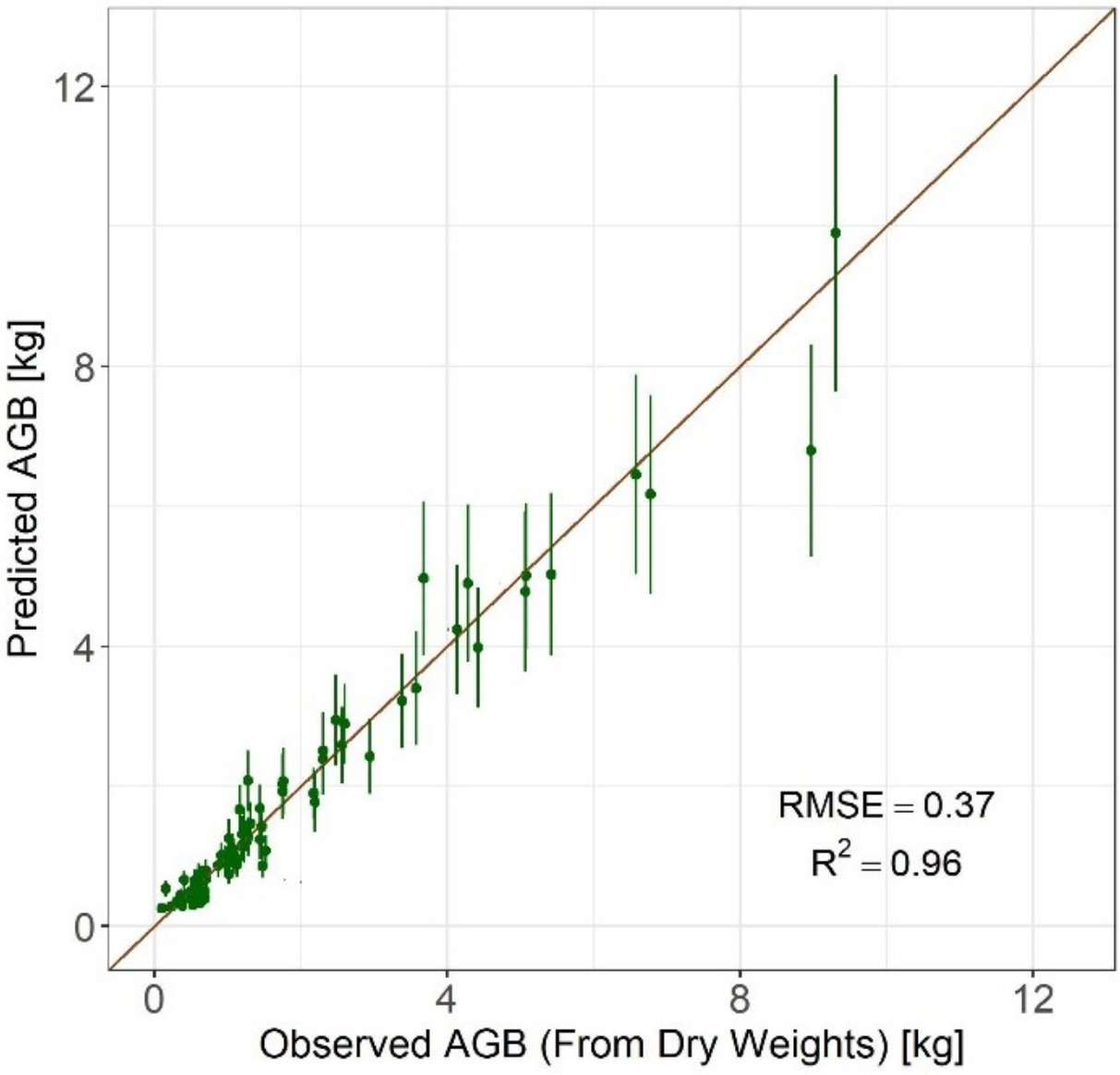
Predicted AGB [kg]
Observed AGB (From Dry Weights) [kg]
0
4
8
12
RMSE = 0.37
R2 = 0.96

Figure 8.

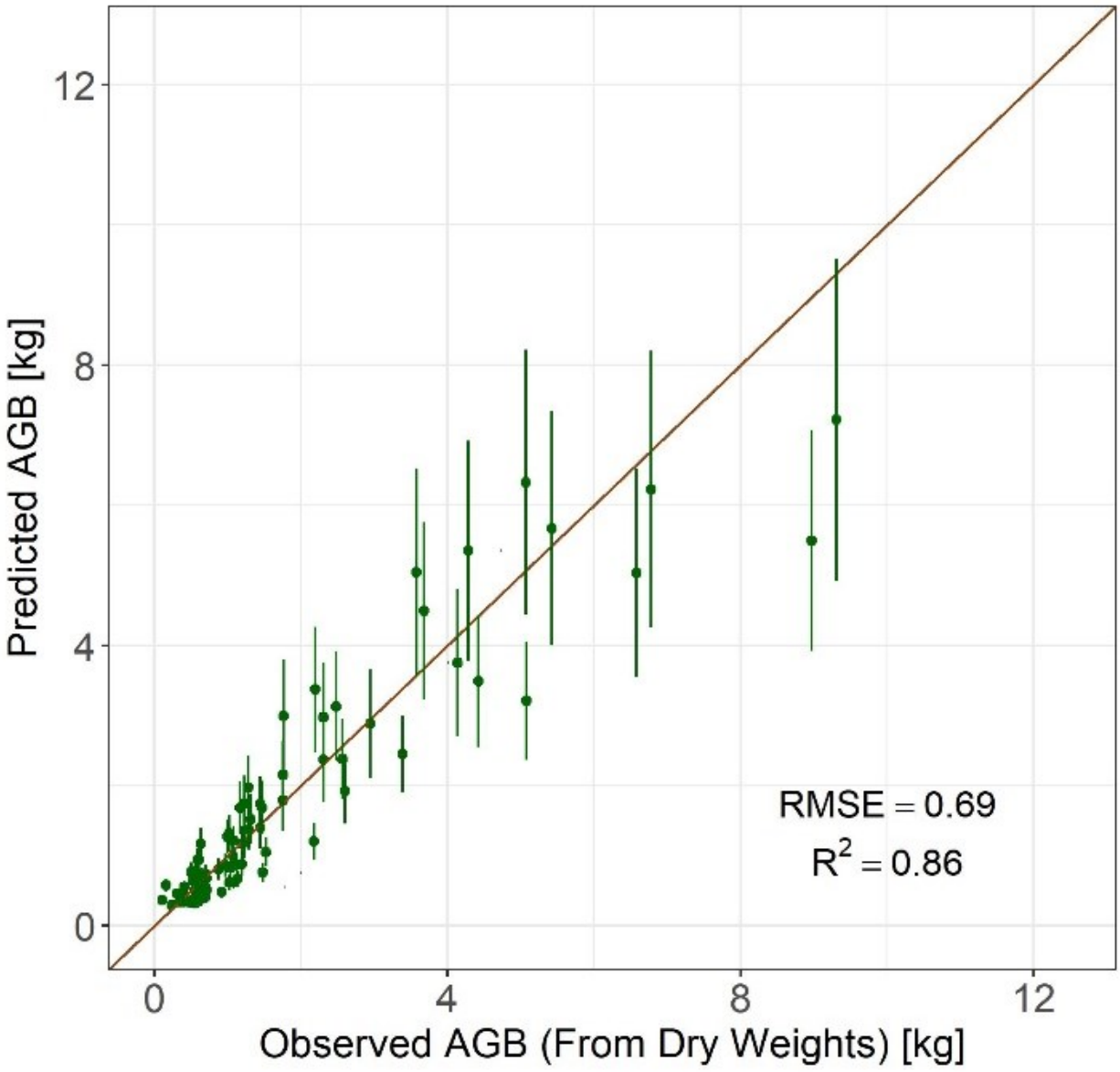
Predicted AGB [kg]
Observed AGB (From Dry Weights) [kg]
0
4
8
12
RMSE = 0.69
R2 = 0.86

Figure 9.

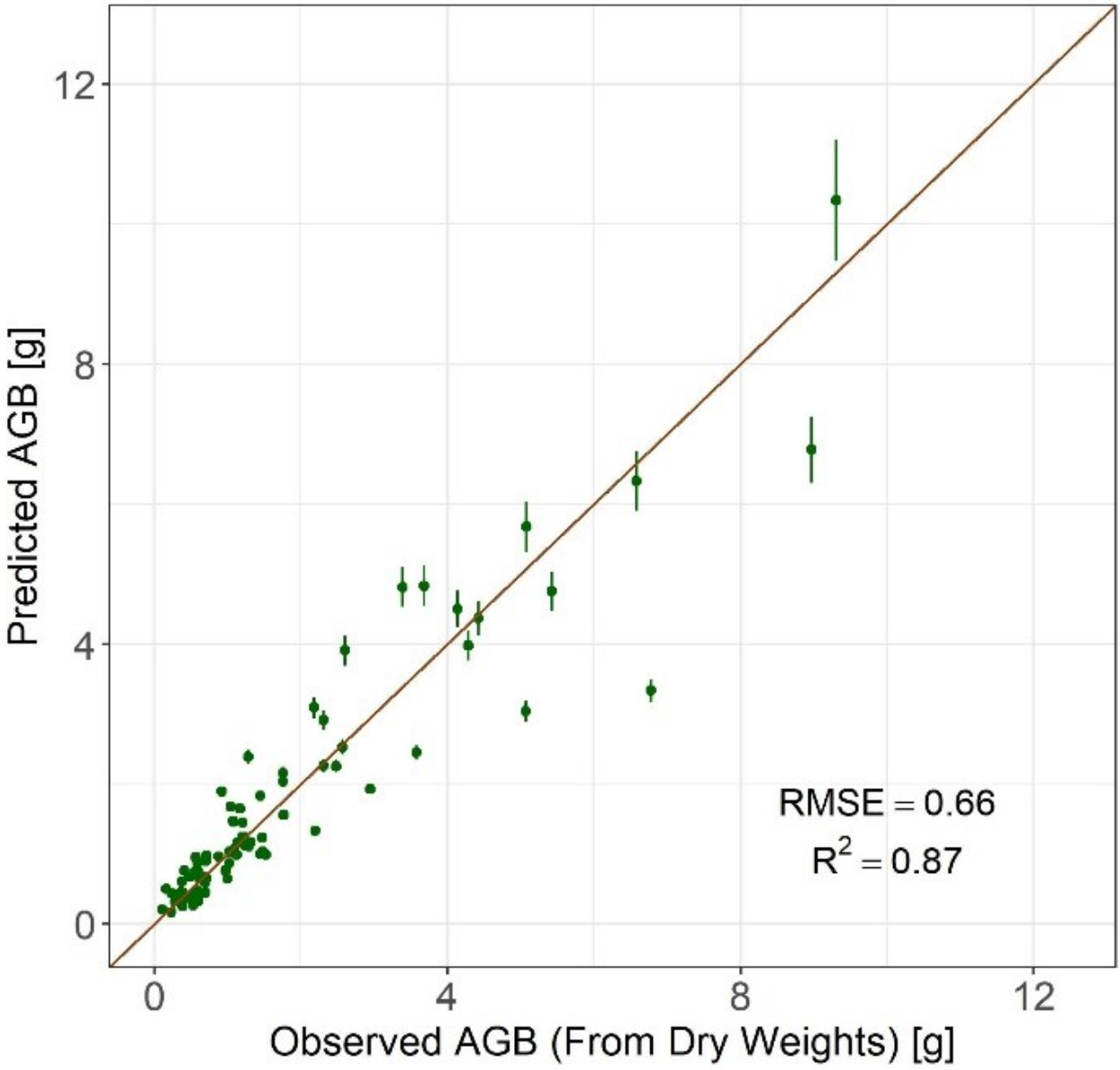
Predicted AGB [g]
Observed AGB (From Dry Weights) [g]
0
4
8
12
RMSE = 0.66
R2 = 0.87

Figure 10.

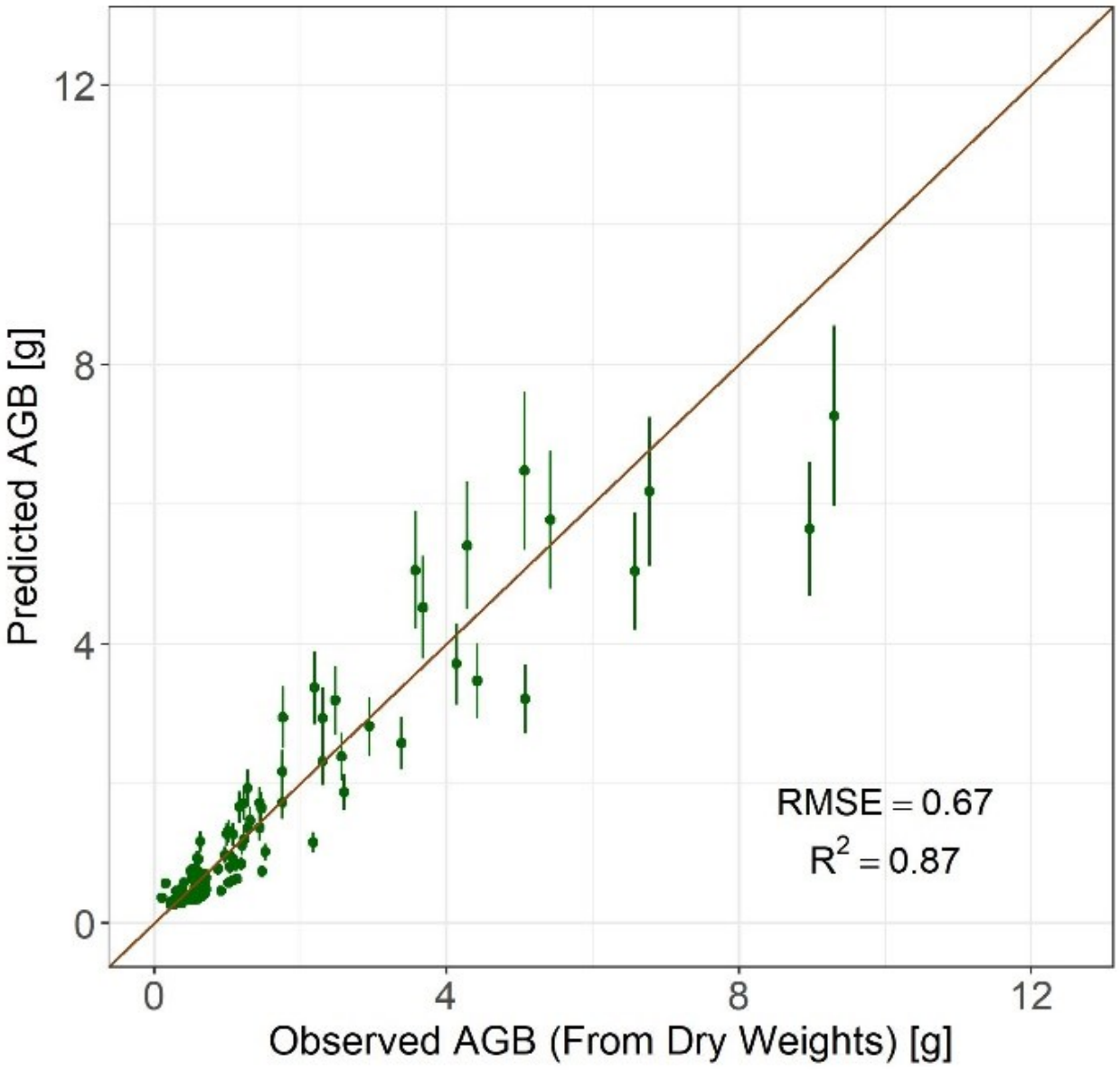
Predicted AGB [g]
Observed AGB (From Dry Weights) [g]
0
4
8
12
RMSE = 0.67
R2 = 0.87

Figure 11.

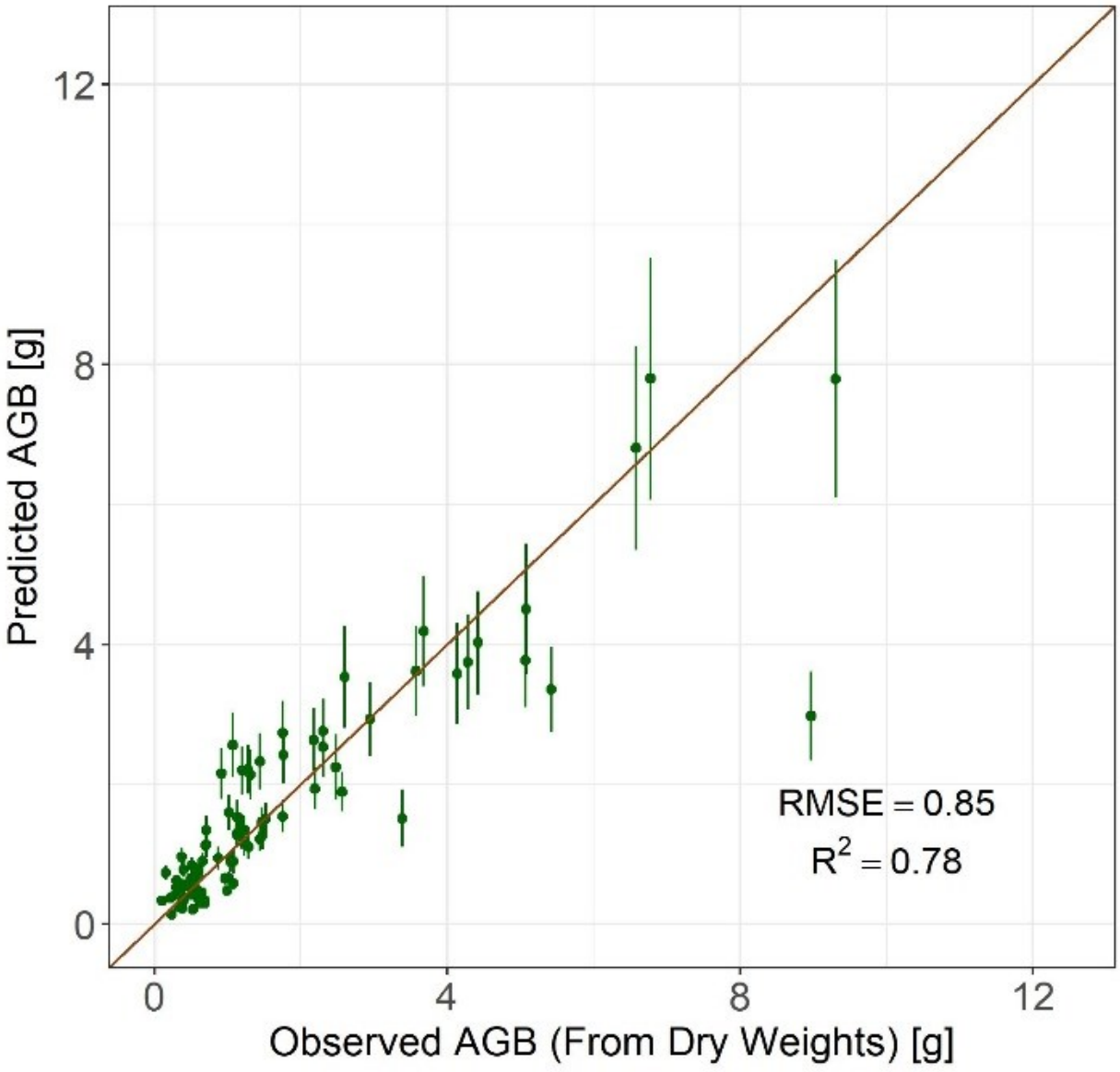
Predicted AGB [g]
Observed AGB (From Dry Weights) [g]
0
4
8
12
RMSE = 0.85
R2 = 0.78

Figure 12.

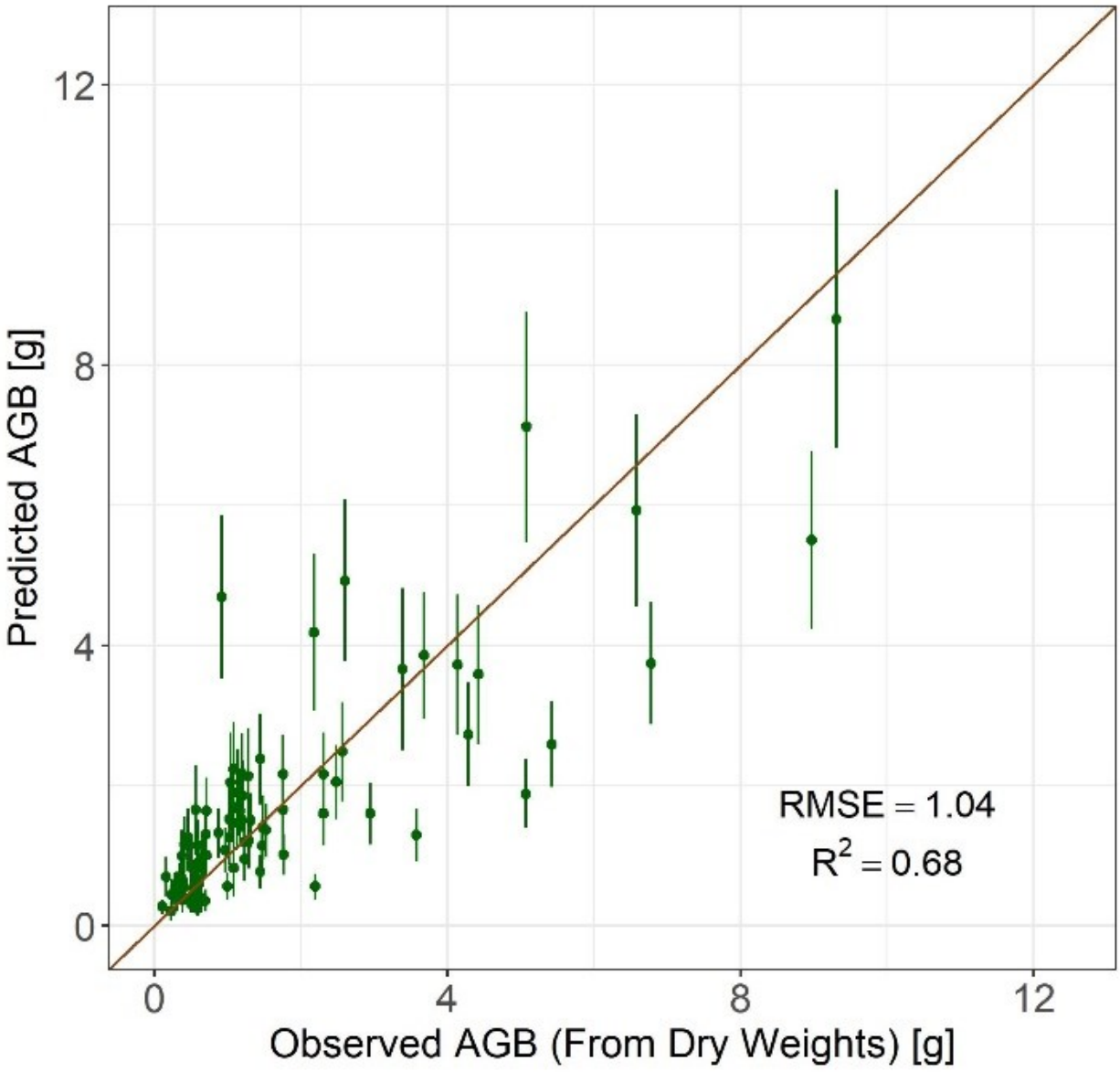
Predicted AGB [g]
Observed AGB (From Dry Weights) [g]
0
4
8
12
RMSE = 1.04
R^2 = 0.68

Figure 13.

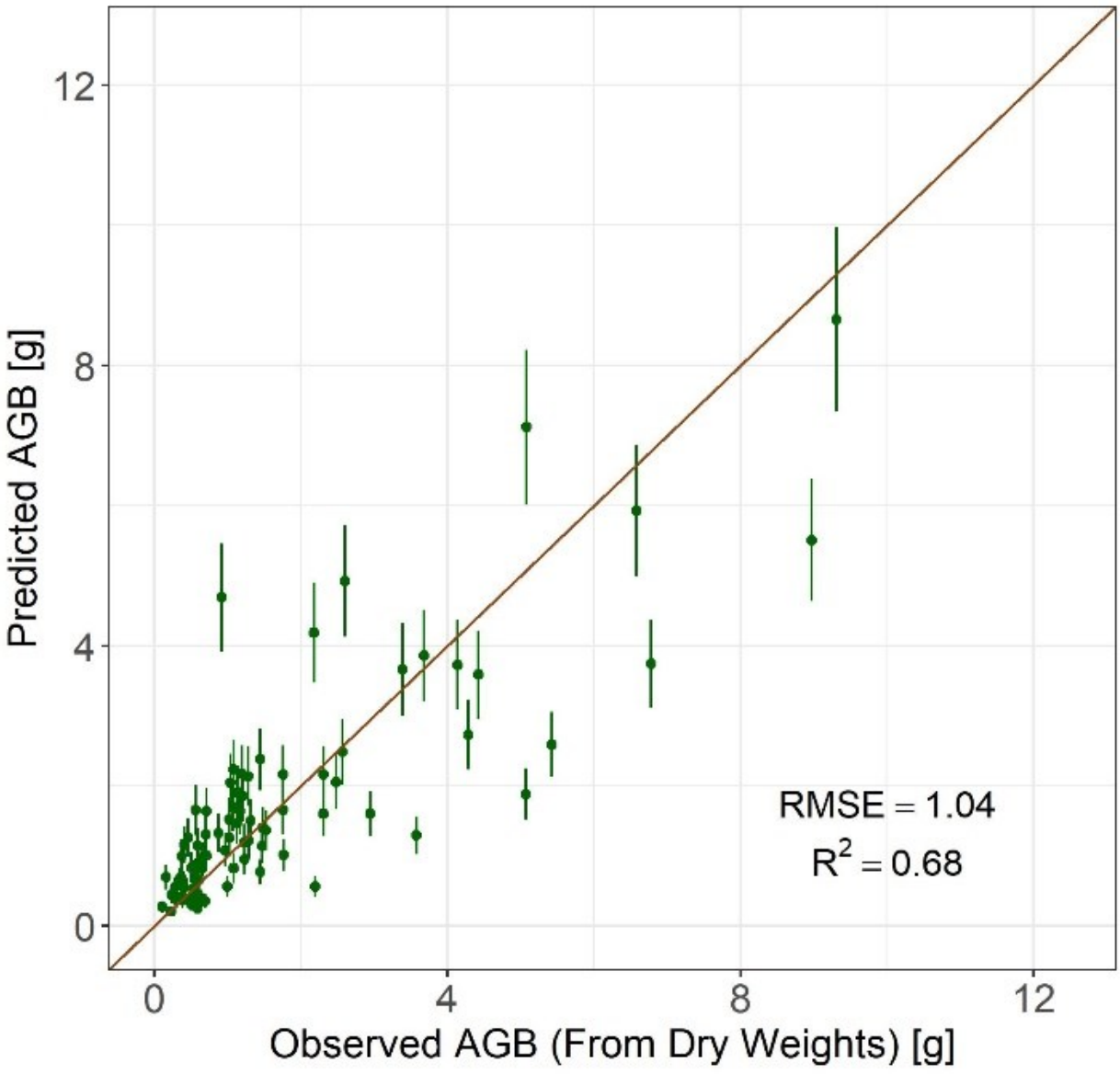
Predicted AGB [g]
Observed AGB (From Dry Weights) [g]
0
4
8
12
RMSE = 1.04
R^2 = 0.68

Figure 14.

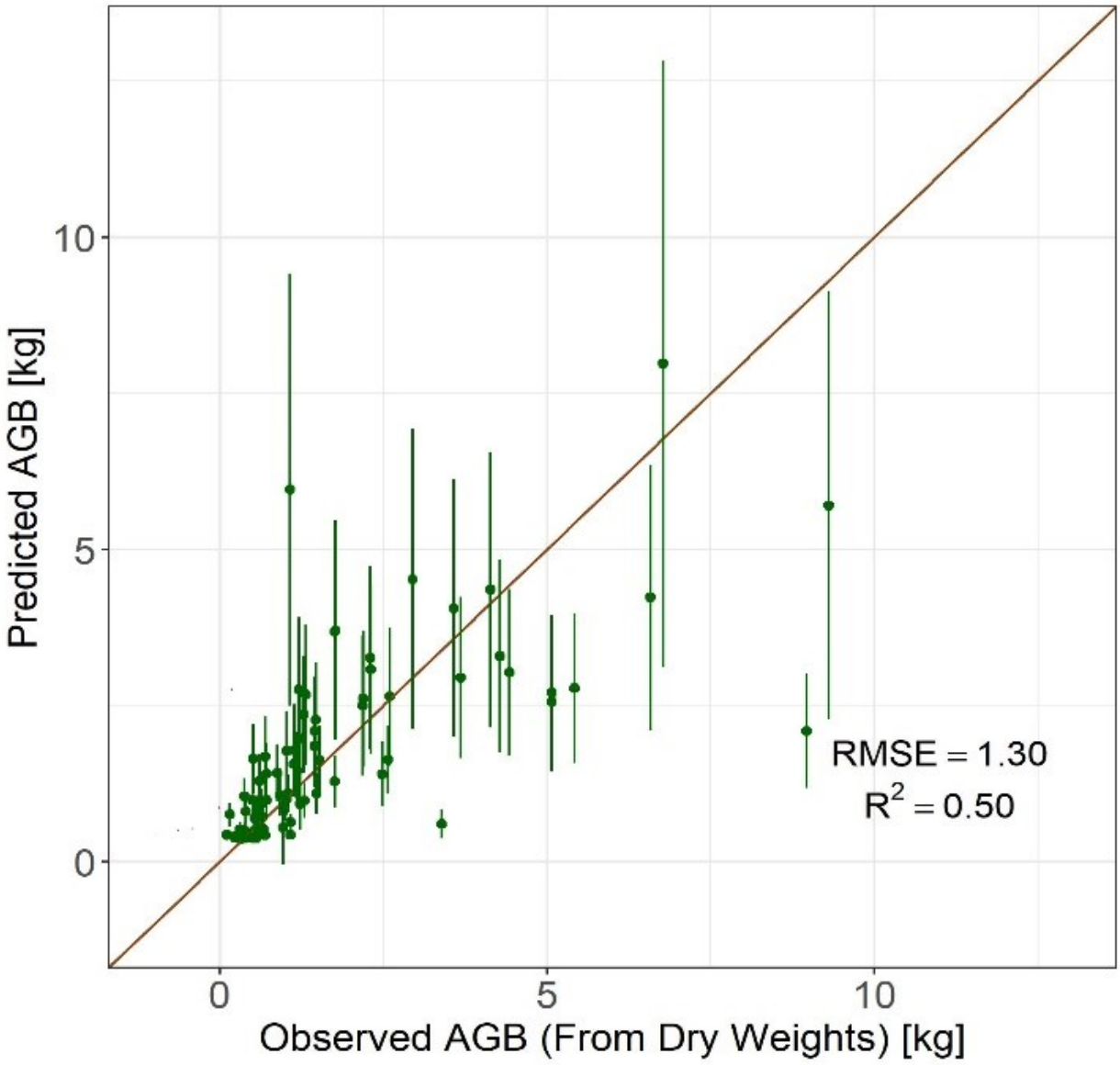
Predicted AGB [kg]
10
5
0
0
5
10
Observed AGB (From Dry Weights) [kg]
RMSE = 1.30
R^2 = 0.50

Figure 15.

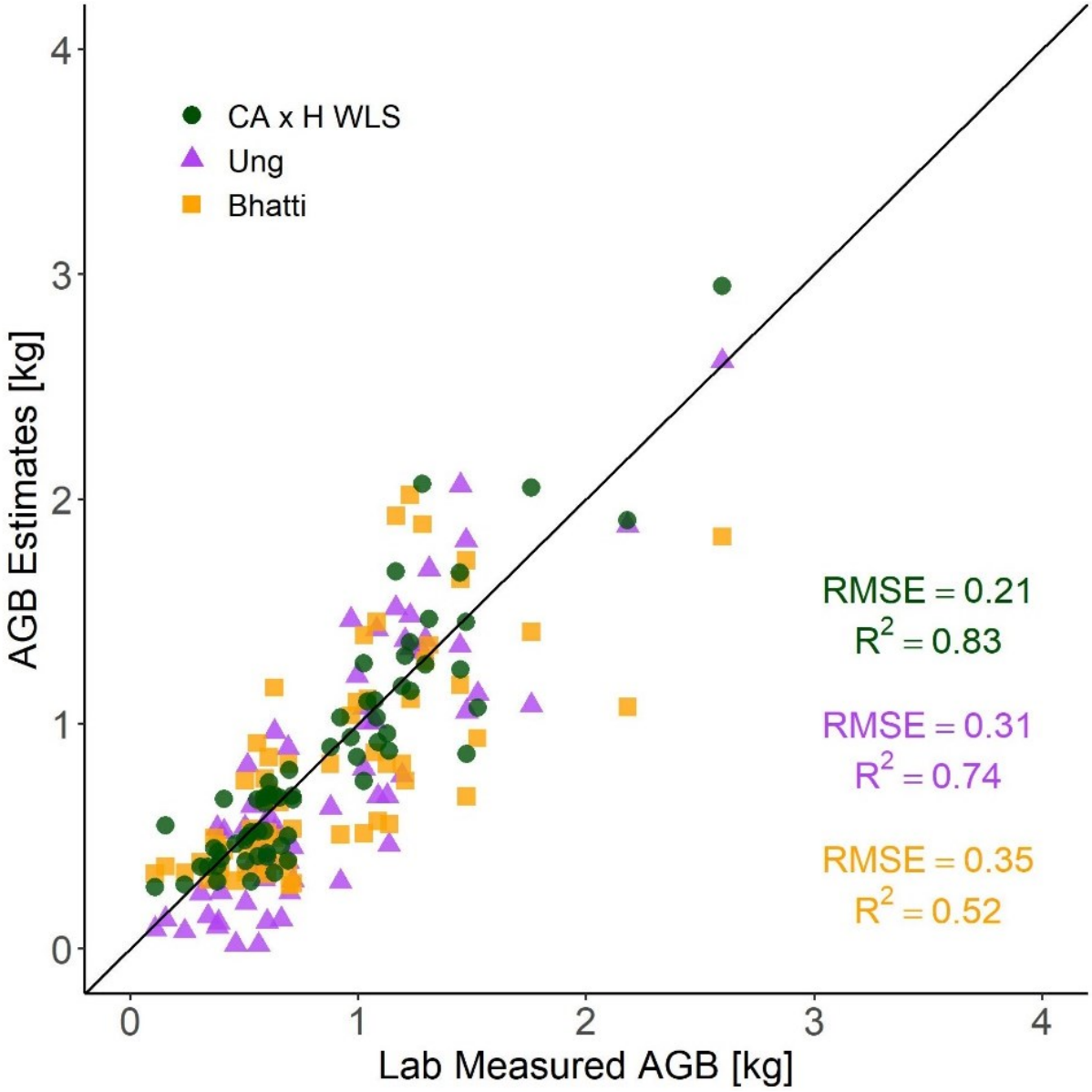
CA x H WLS
Ung
Bhatti
AGB Estimates [kg]
Lab Measured AGB [kg]
0
1
2
3
4
RMSE = 0.21
R2 = 0.83
RMSE = 0.31
R2 = 0.74
RMSE = 0.35
R2 = 0.52

Figure 16.

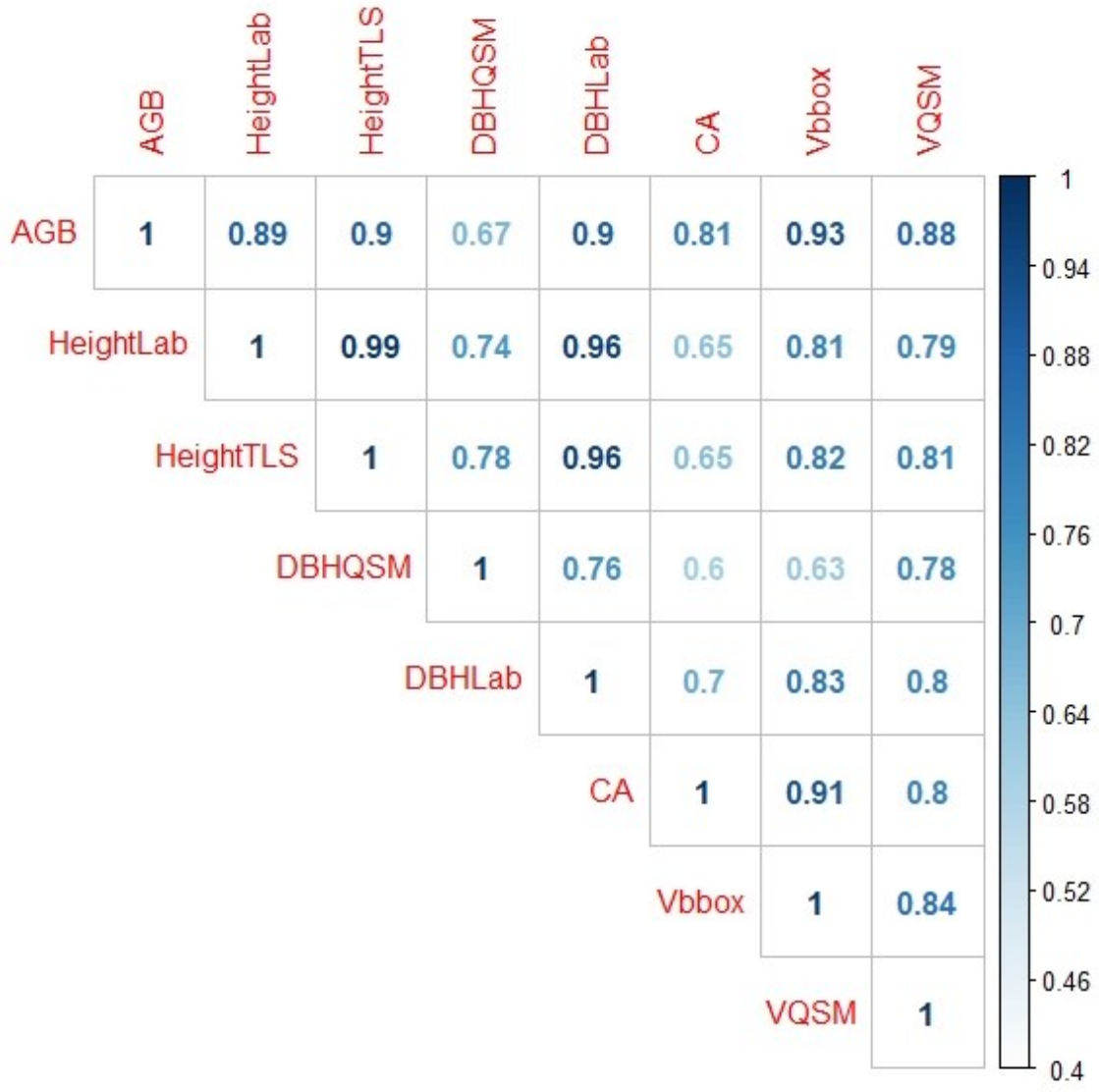
AGB
HeightLab
HeightTLS
DBHQSM
DBHLab
CA
Vbbox
VQSM
AGB 1 0.89 0.9 0.67 0.9 0.81 0.93 0.88
HeightLab 1 0.99 0.74 0.96 0.65 0.81 0.79
HeightTLS 1 0.78 0.96 0.65 0.82 0.81
DBHQSM 1 0.76 0.6 0.63 0.78
DBHLab 1 0.7 0.83 0.8
CA 1 0.91 0.8
Vbbox 1 0.84
VQSM 1
1
0.94
0.88
0.82
0.76
0.7
0.64
0.58
0.52
0.46
0.4

Figure 17.

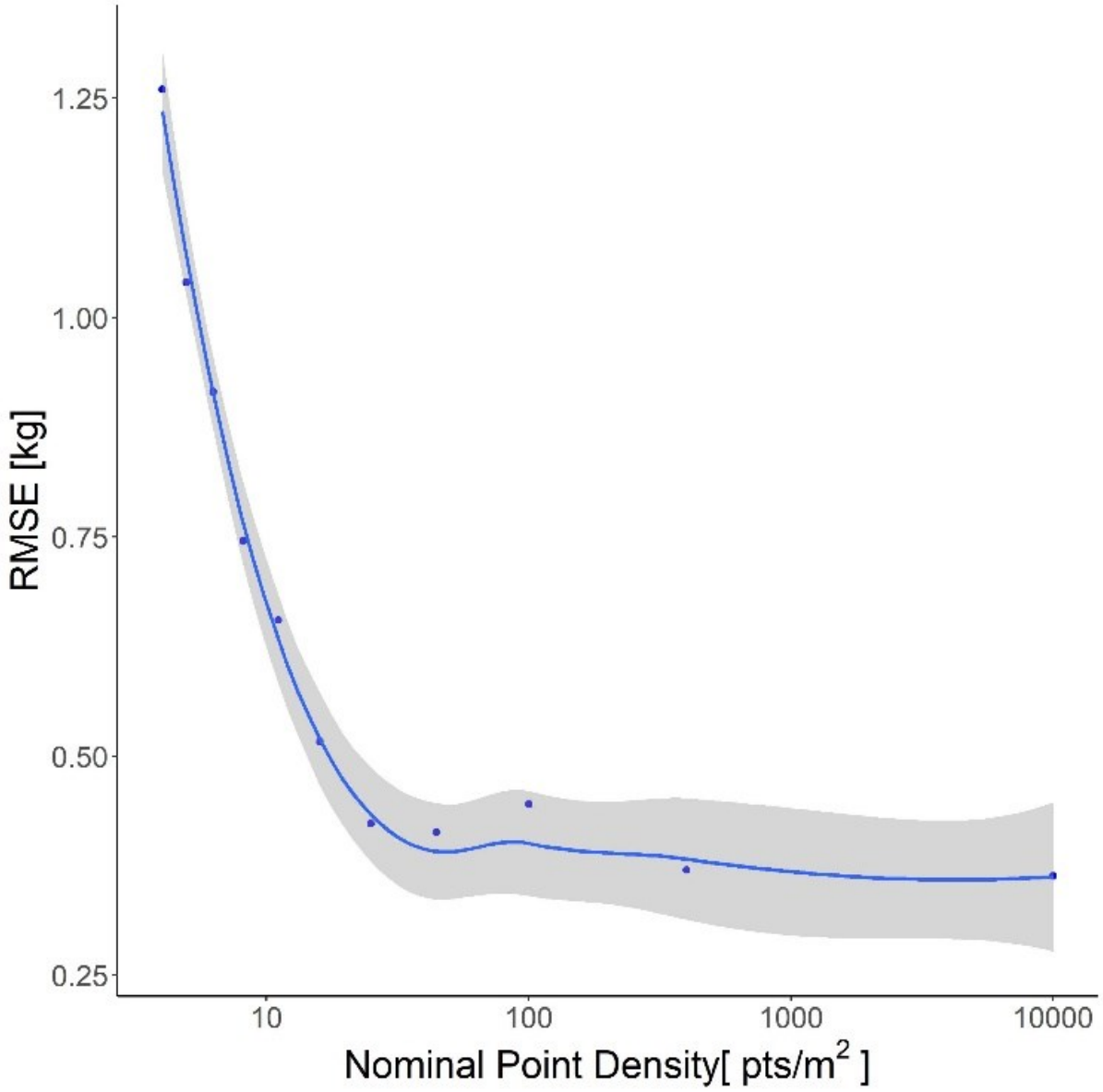
1.25
1.00
0.75
0.50
0.25
RMSE [kg]
10
100
1000
10000
Nominal Point Density[pts/m^2]

Figure 18.

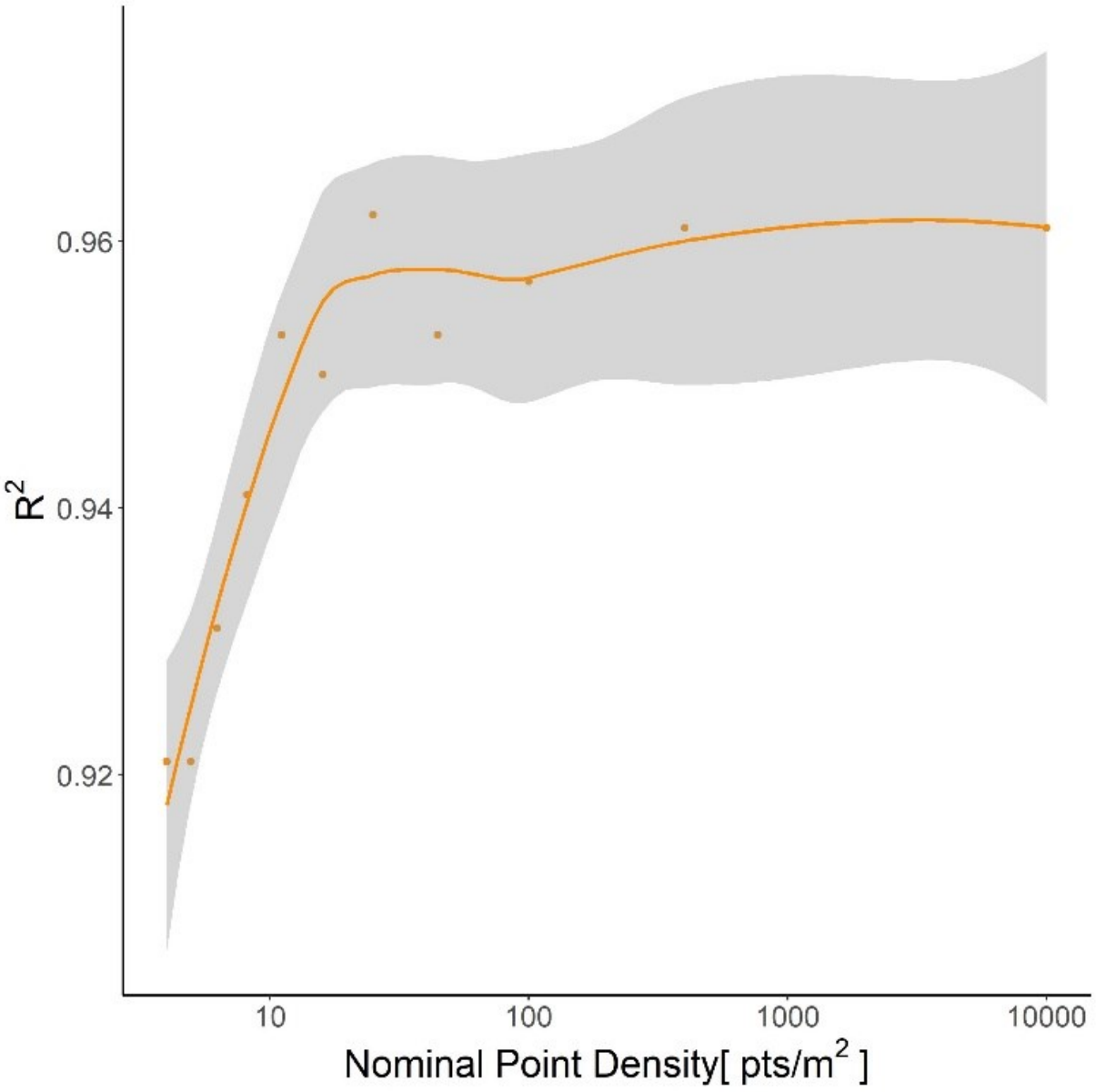

2.8 References

Abegg, M., Kükenbrink, D., Zell, J., Schaepman, M. E., & Morsdorf, F. (2017). Terrestrial Laser Scanning for Forest Inventories—Tree Diameter Distribution and Scanner Location Impact on Occlusion. *Forests (19994907)*, *8*(6), 184. https://doi.org/10.3390/f8060184

Alemdag, I. S. (1983). Mass Equations and Merchantability Factors for Ontario Softwoods. *Canadian Forestry Service*, *Information Report*, 1–24.

Baskerville, G. L. (1972). Use of Logarithmic Regression in the Estimation of Plant Biomass. *Canadian Journal of Forest Research*. https://doi.org/10.1139/x72-009

Bhatti, J. S., Errington, R. C., Bauer, I. E., & Hurdle, P. A. (2006). Carbon stock trends along forested peatland margins in central Saskatchewan. *Canadian Journal of Soil Science*, *86*(Special Issue), 321–333. https://doi.org/10.4141/S05-085

Bona, K. A., Hilger, A., Burgess, M., Wozney, N., & Shaw, C. (2018). A peatland productivity and decomposition parameter database. *Ecology*, *99*(10), 2406–2406. https://doi.org/10.1002/ecy.2462

Bona, K. A., Shaw, C., Thompson, D. K., Hararuk, O., Webster, K., Zhang, G., Voicu, M., & Kurz, W. A. (2020). The Canadian model for peatlands (CaMP): A peatland carbon model for national greenhouse gas reporting. *Ecological Modelling*, *431*, 109164. https://doi.org/10.1016/j.ecolmodel.2020.109164

Brede, B., Calders, K., Lau, A., Raumonen, P., Bartholomeus, H. M., Herold, M., & Kooistra, L. (2019). Non-destructive tree volume estimation through quantitative structure modelling: Comparing UAV laser scanning with terrestrial LIDAR. *Remote Sensing of Environment*, *233*, 111355. https://doi.org/10.1016/j.rse.2019.111355

Breusch, T. S., & Pagan, A. R. (1979). A Simple Test for Heteroscedasticity and Random Coefficient Variation. *Econometrica*, *47*(5), 1287–1294. https://doi.org/10.2307/1911963

Budei, B. C., St-Onge, B., Hopkinson, C., & Audet, F.-A. (2018). Identifying the genus or species of individual trees using a three-wavelength airborne lidar system. *Remote Sensing of Environment*, *204*, 632–647. https://doi.org/10.1016/j.rse.2017.09.037

Burt, A., Disney, M. I., Raumonen, P., Armston, J., Calders, K., & Lewis, P. (2013). Rapid characterisation of forest structure from TLS and 3D modelling. *2013 IEEE International Geoscience and Remote Sensing Symposium - IGARSS*, 3387–3390. https://doi.org/10.1109/IGARSS.2013.6723555

Calders, K., Newnham, G., Burt, A., Murphy, S., Raumonen, P., Herold, M., Culvenor, D., Avitabile, V., Disney, M., Armston, J., & Kaasalainen, M. (2015). Nondestructive estimates of above-ground biomass using terrestrial laser scanning. *Methods in Ecology and Evolution*, *6*(2), 198–208. https://doi.org/10.1111/2041-210X.12301

Calders, K., Wilkes, P., Disney, M., Armston, J., Schaefer, M., & Woodgate, W. (2018). Chapter 19. Terrestrial LiDAR for measuring above-ground biomass and forest structure. In *Effective Field Calibration and Validation Practices*. (pp. 321-336). TERN.

Carlson, M., Roberts, D., & Wells, J. (2009). *The carbon the world forgot: Conserving the capacity of Canada's boreal forest region to mitigate and adapt to climate change* (Alberta Government Library - Internet Internet Access). Boreal Songbird Initiative. https://login.ezproxy.library.ualberta.ca/login?url=https://search.ebscohost.com/login.aspx?direct=true&db=cat03710a&AN=alb.9341038&site=eds-live&scope=site

Chen, X., YE, C., Li, J., & Chapman, M. A. (2018). Quantifying the Carbon Storage in Urban Trees Using Multispectral ALS Data. *IEEE Journal of Selected Topics in Applied Earth*

Observations and Remote Sensing, *11*(9), 3358–3365. https://doi.org/10.1109/JSTARS.2018.2859957

Ciais, P., Sabine, C., Bala, G., Bopp, L., Brovkin, V., Canadell, J., Chhabra, A., DeFries, R., Galloway, J., Heimann, M., Jones, C., Le Quere, C., Myneni, R. B., Piao, S., & Thornton, P. (2013). Carbon and Other Biogeochemical Cycles. In T. F. Stocker, D. Qin, G.-K. Plattner, M. Tignor, S. K. Allen, J. Boschung, A. Nauels, Y. Xia, V. Bex, & P. M. Midgley (Eds.), *Carbon and Other Biogeochemical Cycles. In: Climate Change 2013: The Physical Science Basis. Contribution of Working Group I to the Fifth Assessment Report of the Intergovernmental Panel on Climate Change*. Cambridge University Press.

CloudCompare (v2.11.1). (n.d.). Retrieved March 28, 2021, from https://www.danielgm.net/cc/

Disney, M., Boni Vicari, M., Burt, A., Calders, K., Lewis, S. L., Raumonen, P., & Wilkes, P. (2018). Weighing trees with lasers: Advances, challenges and opportunities. *Interface Focus*, *8*(2), 20170048. https://doi.org/10.1098/rsfs.2017.0048

Disney, M., Burt, A., Calders, K., Schaaf, C., & Stovall, A. (2019). Innovations in Ground and Airborne Technologies as Reference and for Training and Validation: Terrestrial Laser Scanning (TLS). *Surveys in Geophysics*, *40*(4), 937–958. https://doi.org/10.1007/s10712-019-09527-x

Ecosystem Classification Group, Northwest Territories, & Department of Environment and Natural Resources. (2009). *Ecological regions of the Northwest Territories: Taiga Plains*. Dept. of Environment and Natural Resources, Govt. of the Northwest Territories.

Environment and Natural Resources. (n.d.). *Ecosystem Classification* [Information]. Government of the Northwest Territories. Retrieved February 9, 2021, from https://www.enr.gov.nt.ca/en/node/351

Ferguson, C. R., Pan, M., & Oki, T. (2018). The Effect of Global Warming on Future Water Availability: CMIP5 Synthesis. *Water Resources Research*, *54*(10), 7791–7819. https://doi.org/10.1029/2018WR022792

Flade, L., Hopkinson, C., & Chasmer, L. (2020). Allometric Equations for Shrub and Short-Stature Tree Aboveground Biomass within Boreal Ecosystems of Northwestern Canada. *Forests*, *11*(11), 1207. https://doi.org/10.3390/f11111207

Forrester, D. I., Dumbrell, I. C., Elms, S. R., Paul, K. I., Pinkard, E. A., Roxburgh, S. H., & Baker, T. G. (2021). Can crown variables increase the generality of individual tree biomass equations? *Trees*, *35*(1), 15–26. https://doi.org/10.1007/s00468-020-02006-6

Gettelman, A., & Rood, R. B. (2016). Essence of a Climate Model. In A. Gettelman & R. B. Rood (Eds.), *Demystifying Climate Models: A Users Guide to Earth System Models* (pp. 37–58). Springer. https://doi.org/10.1007/978-3-662-48959-8_4

Ghimire, S., Xystrakis, F., & Koutsias, N. (2017). Using Terrestrial Laser Scanning to Measure Forest Inventory Parameters in a Mediterranean Coniferous Stand of Western Greece. *PFG – Journal of Photogrammetry, Remote Sensing and Geoinformation Science*, *85*(4), 213–225. https://doi.org/10.1007/s41064-017-0024-1

Gibbs, M., & Latzko, E. (Eds.). (1979). *Photosynthesis II*. Springer Berlin Heidelberg. https://doi.org/10.1007/978-3-642-67242-2

Gonzalez de Tanago, J., Lau, A., Bartholomeus, H., Herold, M., Avitabile, V., Raumonen, P., Martius, C., Goodman, R. C., Disney, M., Manuri, S., Burt, A., Calders, K., & Kriticos, D. (2017). Estimation of above-ground biomass of large tropical trees with terrestrial LiDAR. *Methods in Ecology & Evolution*, *9*(2), 223–234. https://doi.org/10.1111/2041-210X.12904

Goodman, R. C., Phillips, O. L., & Baker, T. R. (2014). The importance of crown dimensions to improve tropical tree biomass estimates. *Ecological Applications*, *24*(4), 680–698. https://doi.org/10.1890/13-0070.1

Harikumar, A., Bovolo, F., & Bruzzone, L. (2017). An approach to conifer stem localization and modeling in high density airborne LiDAR data. *Image and Signal Processing for Remote Sensing XXIII*, *10427*, 104270Q. https://doi.org/10.1117/12.2279526

Harikumar, A., Paris, C., Bovolo, F., & Bruzzone, L. (2021). A Crown Quantization-Based Approach to Tree-Species Classification Using High-Density Airborne Laser Scanning Data. *IEEE Transactions on Geoscience and Remote Sensing*, *59*(5), 4444–4453. https://doi.org/10.1109/TGRS.2020.3012343

Heinzel, J., & Huber, M. O. (2017). Tree Stem Diameter Estimation From Volumetric TLS Image Data. *Remote Sensing*, *9*(6), 614. https://doi.org/10.3390/rs9060614

Houghton, R. A. (2008). Biomass. In S. E. Jørgensen & B. D. Fath (Eds.), *Encyclopedia of Ecology* (pp. 448–453). Academic Press. https://doi.org/10.1016/B978-008045405-4.00462-6

Jucker, T., Caspersen, J., Chave, J., Antin, C., Barbier, N., Bongers, F., Dalponte, M., Ewijk, K. Y. van, Forrester, D. I., Haeni, M., Higgins, S. I., Holdaway, R. J., Iida, Y., Lorimer, C., Marshall, P. L., Momo, S., Moncrieff, G. R., Ploton, P., Poorter, L., … Coomes, D. A. (2017). Allometric equations for integrating remote sensing imagery into forest monitoring programmes. *Global Change Biology*, *23*(1), 177–190. https://doi.org/10.1111/gcb.13388

Kalwar, O. P. P., Hussin, Y. A., Weir, M. J. C., Bie, C. A. J. M. de, & Karna, Y. (2021). Deriving forest plot inventory parameters using terrestrial laser scanning in the tropical

rainforest of Malaysia. *International Journal of Remote Sensing*, *42*(3), 884–901. https://doi.org/10.1080/01431161.2020.1817606

Kurz, W. A., Shaw, C. H., Boisvenue, C., Stinson, G., Metsaranta, J., Leckie, D., Dyk, A., Smyth, C., & Neilson, E. T. (2013). Carbon in Canada's boreal forest—A synthesis. *Environmental Reviews*, *21*(4), 260–292. https://doi.org/10.1139/er-2013-0041

Lambert, M.-C., Ung, C.-H., & Raulier, F. (2005). Canadian national tree aboveground biomass equations. *Canadian Journal of Forest Research*. https://doi.org/10.1139/x05-112

Lau, A., Bentley, L. P., Martius, C., Shenkin, A., Bartholomeus, H., Raumonen, P., Malhi, Y., Jackson, T., & Herold, M. (2018). Quantifying branch architecture of tropical trees using terrestrial LiDAR and 3D modelling. *Trees*, *32*(5), 1219–1231. https://doi.org/10.1007/s00468-018-1704-1

Lau, A., Calders, K., Bartholomeus, H., Martius, C., Raumonen, P., Herold, M., Vicari, M., Sukhdeo, H., Singh, J., & Goodman, R. (2019). Tree Biomass Equations from Terrestrial LiDAR: A Case Study in Guyana. *Forests*, *10*(6), 527. https://doi.org/10.3390/f10060527

Leica Cyclone 3D Point Cloud Processing Software. (n.d.). Retrieved June 13, 2021, from https://leica-geosystems.com/products/laser-scanners/software/leica-cyclone

Liang, X., Hyyppä, J., Kaartinen, H., Lehtomäki, M., Pyörälä, J., Pfeifer, N., Holopainen, M., Brolly, G., Francesco, P., Hackenberg, J., Huang, H., Jo, H.-W., Katoh, M., Liu, L., Mokroš, M., Morel, J., Olofsson, K., Poveda-Lopez, J., Trochta, J., … Wang, Y. (2018). International benchmarking of terrestrial laser scanning approaches for forest inventories. *ISPRS Journal of Photogrammetry and Remote Sensing*, *144*, 137–179. https://doi.org/10.1016/j.isprsjprs.2018.06.021

Liang, X., Kankare, V., Hyyppä, J., Wang, Y., Kukko, A., Haggrén, H., Yu, X., Kaartinen, H., Jaakkola, A., Guan, F., Holopainen, M., & Vastaranta, M. (2016). Terrestrial laser scanning in forest inventories. *ISPRS Journal of Photogrammetry and Remote Sensing*, *115*, 63–77. https://doi.org/10.1016/j.isprsjprs.2016.01.006

Lieffers, V. J. (1986). Stand Structure, Variability in Growth and Intraspecific Competition in a Peatland Stand of Black Spruce Picea mariana. *Holarctic Ecology*, *9*(1), 58–64.

Liu, G., Wang, J., Dong, P., Chen, Y., & Liu, Z. (2018). Estimating Individual Tree Height and Diameter at Breast Height (DBH) from Terrestrial Laser Scanning (TLS) Data at Plot Level. *Forests*, *9*(7), 398. https://doi.org/10.3390/f9070398

Lorenz, K., & Lal, R. (2010). The Natural Dynamic of Carbon in Forest Ecosystems. In K. Lorenz & R. Lal (Eds.), *Carbon Sequestration in Forest Ecosystems* (pp. 23–101). Springer Netherlands. https://doi.org/10.1007/978-90-481-3266-9_2

Malek S, Miglietta F, Gobakken T, Næsset E, Gianelle D, & Dalponte M. (2019). Prediction of stem diameter and biomass at individual tree crown level with advanced machine learning techniques. *IForest - Biogeosciences and Forestry*, *12*(1), 323–329. https://doi.org/10.3832/ifor2980-012

Mascaro, J., Litton, C. M., Hughes, R. F., Uowolo, A., & Schnitzer, S. A. (2014). Is logarithmic transformation necessary in allometry? Ten, one-hundred, *one-thousand-times yes*: Yes, We Need the Logarithm in Allometry. *Biological Journal of the Linnean Society*, *111*(1), 230–233. https://doi.org/10.1111/bij.12177

McFarland, E. L., Hunt, J. L., & Campbell, J. L. (2007). *Energy, physics and the environment*. Cengage Learning.

Modzelewska, A., Fassnacht, F. E., & Stereńczak, K. (2020). Tree species identification within an extensive forest area with diverse management regimes using airborne hyperspectral data. *International Journal of Applied Earth Observation and Geoinformation*, *84*, 101960. https://doi.org/10.1016/j.jag.2019.101960

Moskal, L. M., & Zheng, G. (2011). Retrieving Forest Inventory Variables with Terrestrial Laser Scanning (TLS) in Urban Heterogeneous Forest. *Remote Sensing*, *4*(1), 1–20. https://doi.org/10.3390/rs4010001

Natural Resources Canada. (2013, July 11). *Boreal forest*. Natural Resources Canada. https://www.nrcan.gc.ca/our-natural-resources/forests/sustainable-forest-management/boreal-forest/13071

Novotný, J., Navrátilová, B., Janoutová, R., Oulehle, F., & Homolová, L. (2020). Influence of Site-Specific Conditions on Estimation of Forest above Ground Biomass from Airborne Laser Scanning. *Forests*, *11*(3), 268–268. https://doi.org/10.3390/f11030268

Nwanganga, F., & Chapple, M. (2020). Practical Machine Learning in R. *John Wiley & Sons*, 311–312.

Peng, X., Zhao, A., Chen, Y., Chen, Q., & Liu, H. (2021). Tree Height Measurements in Degraded Tropical Forests Based on UAV-LiDAR Data of Different Point Cloud Densities: A Case Study on Dacrydium pierrei in China. *Forests*, *12*(3), 328. https://doi.org/10.3390/f12030328

Prošek, J., & Šímová, P. (2019). UAV for mapping shrubland vegetation: Does fusion of spectral and vertical information derived from a single sensor increase the classification accuracy? *International Journal of Applied Earth Observation and Geoinformation*, *75*, 151–162. https://doi.org/10.1016/j.jag.2018.10.009

R Core Team. (2020). *R: A Language and Environment for Statistical Computing*. R Foundation for Statistical Computing. https://www.R-project.org/

Raumonen, P., Kaasalainen, M., Åkerblom, M., Kaasalainen, S., Kaartinen, H., Vastaranta, M., Holopainen, M., Disney, M., & Lewis, P. (2013). Fast Automatic Precision Tree Models from Terrestrial Laser Scanner Data. *Remote Sensing*, *5*(2), 491–520. https://doi.org/10.3390/rs5020491

Reese, H., Nyström, M., Nordkvist, K., & Olsson, H. (2014). Combining airborne laser scanning data and optical satellite data for classification of alpine vegetation. *International Journal of Applied Earth Observation and Geoinformation*, *27*, 81–90. https://doi.org/10.1016/j.jag.2013.05.003

Rencz, A. N., & Auclair, A. N. D. (1978). Biomass distribution in a subarctic *Picea mariana – Cladonia alpestris* woodland. *Canadian Journal of Forest Research*, *8*(2), 168–176. https://doi.org/10.1139/x78-027

Shruthi Srinivasan, Sorin C. Popescu, Marian Eriksson, Ryan D. Sheridan, & Nian-Wei Ku. (2015). Terrestrial Laser Scanning as an Effective Tool to Retrieve Tree Level Height, Crown Width, and Stem Diameter. *Remote Sensing*, *7*(2), 1877–1896. https://doi.org/10.3390/rs70201877

Singh, T. (1984). *Biomass Equations for Six Major Tree Species of the Northwest Territories* (pp. 1–30). Environment Canada, Canadian Forestry Service.

Soma, M., Pimont, F., Allard, D., Fournier, R., & Dupuy, J.-L. (2020). Mitigating occlusion effects in Leaf Area Density estimates from Terrestrial LiDAR through a specific kriging method. *Remote Sensing of Environment*, *245*, 111836. https://doi.org/10.1016/j.rse.2020.111836

Tansey, K., Selmes, N., Anstee, A., Tate, N. J., & Denniss, A. (2009). Estimating tree and stand variables in a Corsican Pine woodland from terrestrial laser scanner data. *International Journal of Remote Sensing*, *30*(19), 5195–5209. https://doi.org/10.1080/01431160902882587

Tarnocai, C., Kettles, I. M., & Lacelle, B. (2011). Peatlands of Canada Database. *Geological Survey of Canada*, *Open File 6561 (digital database)*, 10.

Thomas, V. (2017). *Climate Change and Natural Disasters: Transforming Economies and Policies for a Sustainable Future*. Routledge. http://ebookcentral.proquest.com/lib/ualberta/detail.action?docID=4785158

Thompson, D. K., Schroeder, D., Wilkinson, S. L., Barber, Q., Baxter, G., Cameron, H., Hsieh, R., Marshall, G., Moore, B., Refai, R., Rodell, C., Schiks, T., Verkaik, G. J., & Zerb, J. (2020). Recent Crown Thinning in a Boreal Black Spruce Forest Does Not Reduce Spread Rate nor Total Fuel Consumption: Results from an Experimental Crown Fire in Alberta, Canada. *Fire*, *3*(3), 28. https://doi.org/10.3390/fire3030028

Thompson, D. K., Simpson, B. N., & Beaudoin, A. (2016). Using forest structure to predict the distribution of treed boreal peatlands in Canada. *Forest Ecology and Management*, *372*, 19–27. https://doi.org/10.1016/j.foreco.2016.03.056

Ung, C.-H., Bernier, P., & Guo, X.-J. (2008). Canadian national biomass equations: New parameter estimates that include British Columbia data. *Canadian Journal of Forest Research*, *38*(5), 1123–1132. https://doi.org/10.1139/X07-224

Vashum, K. (2012). Methods to Estimate Above-Ground Biomass and Carbon Stock in Natural Forests—A Review. *Journal of Ecosystem & Ecography*, *02*. https://doi.org/10.4172/2157-7625.1000116

Wang, D., Takoudjou, S. M., & Casella, E. (2020). LeWoS: A universal leaf-wood classification method to facilitate the 3D modelling of large tropical trees using terrestrial LiDAR. *Methods in Ecology and Evolution*, *11*(3), 376–389. https://doi.org/10.1111/2041-210X.13342

Wang, Y., Pyörälä, J., Liang, X., Lehtomäki, M., Kukko, A., Yu, X., Kaartinen, H., & Hyyppä, J. (2019). In situ biomass estimation at tree and plot levels: What did data record and what did algorithms derive from terrestrial and aerial point clouds in boreal forest. *Remote Sensing of Environment*, *232*, 111309. https://doi.org/10.1016/j.rse.2019.111309

Warner, B. G., & Asada, T. (2006). Biological diversity of peatlands in Canada. *Aquatic Sciences*, *68*(3), 240–253. https://doi.org/10.1007/s00027-006-0853-2

Watt, P. J., & Donoghue, D. N. M. (2005). Measuring forest structure with terrestrial laser scanning. *International Journal of Remote Sensing*, *26*(7), 1437–1446. https://doi.org/10.1080/01431160512331337961

Wells, J. V., Dawson, N., Culver, N., Reid, F. A., & Morgan Siegers, S. (2020). The State of Conservation in North America's Boreal Forest: Issues and Opportunities. *Frontiers in Forests and Global Change*, *3*. https://doi.org/10.3389/ffgc.2020.00090

Wenger, S. J., & Olden, J. D. (2012). Assessing transferability of ecological models: An underappreciated aspect of statistical validation. *Methods in Ecology & Evolution*, *3*(2), 260–267. https://doi.org/10.1111/j.2041-210X.2011.00170.x

White, J. C., Coops, N. C., Wulder, M. A., Vastaranta, M., Hilker, T., & Tompalski, P. (2016). Remote Sensing Technologies for Enhancing Forest Inventories: A Review. *Canadian Journal of Remote Sensing*, *42*(5), 619–641. https://doi.org/10.1080/07038992.2016.1207484

Wieder, R. K., Vitt, D. H., & Jackson, R. B. (2006). *Boreal Peatland Ecosystems*. Springer Berlin / Heidelberg. http://ebookcentral.proquest.com/lib/ualberta/detail.action?docID=603642

Wieder, R., Vitt, D., & Benscoter, B. (2006). Peatlands and the Boreal Forest. In *Ecol. Stud.* (Vol. 188, pp. 1–8). https://doi.org/10.1007/978-3-540-31913-9_1

Wu, B., Zheng, G., & Chen, Y. (2020). An Improved Convolution Neural Network-Based Model for Classifying Foliage and Woody Components from Terrestrial Laser Scanning Data. *Remote Sensing*, *12*(6), 1010. https://doi.org/10.3390/rs12061010

Zanhouo, D. A. K., & Nana, A. B. I. (2019). Modeling Climate Change Impact on Health and Population Migration: A Systematic Review. *Economics Literature*, *1*(1), 51–65. https://doi.org/10.22440/elit.1.1.4

Zeileis, A., & Hothorn, T. (2002). Diagnostic Checking in Regression Relationships. *R News*, *2*(3), 7–10.

Zhao, B., Zhuang, Q., Shurpali, N., Köster, K., Berninger, F., & Pumpanen, J. (2021). North American boreal forests are a large carbon source due to wildfires from 1986 to 2016. *Scientific Reports*, *11*(1). https://doi.org/10.1038/s41598-021-87343-3

Zhouxin Xi, Chris Hopkinson, & Laura Chasmer. (2018). Filtering Stems and Branches from Terrestrial Laser Scanning Point Clouds Using Deep 3-D Fully Convolutional Networks. *Remote Sensing*, *10*(8), 1215–1215. https://doi.org/10.3390/rs10081215

Chapter 3 -- Conclusions

The object of this thesis was to develop models that could estimate the above ground biomass (AGB) of small black spruce trees in peatland environments of the Canadian boreal forest. While multiple allometric biomass equations exist for many tree species around the world, including black spruce, they often rely on diameter at breast height (DBH) and height as predictors (Alemdag, 1983; Bhatti et al., 2006; Ung et al., 2008) or are not suitable for the small trees that are often found in boreal forest peatlands (Singh, 1984). The Northwest Territories is home to many peatlands that offer a good representation of the boreal ecosystems we were interested in estimating AGB for across the Taiga Plains ecozone that was focused on in Chapter 2. In this thesis, 42 models were fitted using tree attributes measured in Terrestrial Laser Scanning (TLS) point clouds as predictors of AGB. The best performing models are not only comparable to the methods currently being used by the National Forest Inventory to predict AGB for black spruce but outperform them for small trees in peatland environments. Included in the best performing models are ones that use crown size (crown area or crown diameter) and height as predictors, removing the necessity of DBH measurements altogether. These models help improve the understanding of how TLS can be used to measure the AGB of small trees and they lay the framework for testing with airborne- and UAV- laser scanning systems (ALS and ULS respectively). The end result is the creation of models that have the potential to create high-quality, accurate AGB data for individual trees over large peatland areas using airborne scanning methods.

3.1 Significance of Findings

The objectives of this thesis were to:

1. Assess how well TLS point clouds can be used to measure tree attributes for small black spruce trees.
2. Fit AGB estimation models using the predictor variables measured by TLS.
3. Compare the fitted models to already established models using ground truth data to determine if the models presented in this thesis represent a viable alternative for AGB estimation.

To address the first objective, this thesis showed that there are both advantages and disadvantages to using TLS to measure physical attributes of small trees. Quantitative structure

models (QSMs) have been shown to be valuable tools for measuring attributes of larger trees that can be used to estimate AGB, including DBH, height, and volume (Brede et al., 2019; Calders et al., 2015; Takoudjou et al., 2018). This did not translate well for the trees used in the study presented in this thesis, however, likely because of their relatively small DBHs and the fact that many of the plots used in the study were densely populated, creating occlusion not just from other tree stems, but from lower branches around 1.3 metres high as well. Because QSMs rely on the accuracy of the cylinders being fit to the points of the point cloud, the inaccuracies present in the DBHs measured by QSM were propagated into the volume estimates. As a result, we found that models using QSM-derived volume as a predictor of AGB in small black spruce trees did not perform as well as some of the other predictors used. These findings are significant because they provide further evidence that the performance of QSMs is limited by the size of the structures being measured and provide further evidence that measurement accuracy for structures with a diameter smaller than 7 cm (the largest DBH used in Chapter 2) can be unreliable. As such, this thesis provides a case study for why QSMs should not be recommended to estimate DBH and volume for small, coniferous trees. Although the QSMs did not provide the kind of accuracy seen in other studies that used larger trees, other TLS measurements performed quite well. The work done in Chapter 2 shows that height can be measured to a high degree of accuracy for small trees using TLS. It has already been shown that as trees grow larger and stands become more densely populated, occlusion of treetops becomes more likely, which can lead to underestimation of tree height (Holopainen et al., 2013; Liang et al., 2018), so this is important information that reinforces the notion that tree height estimation from TLS is more accurate for smaller trees.

Exploring the second objective required the fitting of models for multiple different predictors and combinations of predictors, as well as using different types of model (quadratic-, power-, and multiple regression power models). Analyses were performed to assess which models performed the best, based on three commonly used model performance metrics: RMSE, adjusted R^2, and mean average error. The cross-validation methods used to obtain these metrics provide confidence in the transferability of these models to be used in any similar peatland environments found through the boreal forest. As part of the model fitting and tree attribute measuring processes, this thesis also provides methods for calculating crown area using TLS that are scalable for varying point densities by simply adjusting the cell size of the rasters used to

reflect the average space between points in the point cloud being used. The best performing models in Chapter 2 used crown area values measured with these methods (or crown diameter values derived from the crown area) and height as predictors. Because crown area and height are both attributes that can be measured from above the tree canopy, these models could represent a substantial step towards biomass estimation methods that have the potential to be applicable with point clouds acquired using ALS and ULS. Individual-tree-based forest inventory practices in particular could benefit from the findings presented in this thesis. They use ALS to measure tree height, crown size, and species before deriving measurements of other tree attributes like DBH based on the directly measured attributes (Hyyppä et al., 2008; Yu et al., 2010). By eliminating the need to derive other tree attributes to fit existing AGB models, uncertainties in the final AGB estimations can be reduced.

The third objective involved comparing the best models created in this thesis to other established methods. Comparisons between AGB estimates from the best models presented here and those given using the methods in Ung et al. (2008) and Bhatti et al. (2006) showed that the new models produce slightly better estimates than the previously established ones. They also do not require DBH measurements, making them potentially usable with ALS and ULS data, which is a significant advantage over the models currently used.

Beyond the main objectives, there are other things to consider regarding the models presented here. They are specific to a species of tree that is abundant in one of the most common ecosystems of the Canadian boreal forest. While it is true that these models have only been tested using data in one portion of the boreal forest, the cross-validation methods used indicate that they should perform consistently in peatlands of different locations. Further testing must be conducted to confirm this, but due to the widespread distribution of peatlands in Canada (roughly a quarter of the Canadian boreal forest, (Wieder et al., 2006)) it could represent a significant contribution to the scientific literature surrounding biomass estimation and monitoring in boreal forests. Furthermore, when these models were compared to other established models, such as those in Ung et al. (2008) and Bhatti et al. (2006), the established models used lab-measured attributes to make AGB estimates, while our models used TLS-derived measurements of tree attributes. The fact that the TLS-based models outperform the ones that used lab-based measurements further demonstrates TLS's ability to create high quality data that can be used for the accurate estimation of tree parameters and AGB.

3.2 Future Work

The work done in this thesis lays the foundation for many other potential future studies. The most important of these is to assess how well these models can be used with ALS and ULS point clouds. The best models in chapter 2 have been shown to perform well with high density TLS point cloud data while focusing on attributes that have the potential to be directly measured from above. Although preliminary tests were performed to allow for some speculation on their usability with ALS and ULS data, due to budget and time constraints, flights were not performed and could not be included in this study. As such, a future mission to scan small black spruce plots in peatland environments with ALS and ULS being flown at varying heights and speeds to obtain a range of point densities is necessary. This would show how well the models are able to translate to airborne scanning methods and could help to determine the true point density at which attribute measurement accuracy decreases for crown area and height. Few models exist that use the directly measurable tree attributes of crown size and height to estimate biomass, with most models requiring DBH as well, so showing that these models can be applied to data acquired with ALS and ULS while still predicting AGB with a high level of accuracy would represent a significant advance in biomass measurements methods using these kinds of laser scanners.

All the models created in Chapter 2 fall into the individual tree-based measurement method category, but area-based approaches can effectively estimate biomass over large areas as well (Lim & Treitz, 2004; Zolkos et al., 2013). Scaling up from individual tree AGB to an area-based approach could allow the models to be more applicable when point density is too low to allow for sufficient individual tree measurements. This would also allow for comparisons between the two approaches to made. Individual tree-based methods are more expensive than area-based approaches, but they have many advantages such as being able to use species-specific models for AGB estimation, as well as the ability to monitor forests in finer detail (Yu et al., 2010). Using point clouds with multiple point densities obtained from flights at various heights could provide valuable insight into the conditions needed for each method to perform better than the other, and at what point the preferred method changes.

Finally, the best models presented in this thesis performed well for the trees used in the study, but it is important to note that only a portion of the boreal forest was represented by the

sample. All plots were located in the Northwest Territories, between Hay River and Fort Simpson, (a distance of approximately 430 km). While this does provide some variation in the peatlands used for plot selection, it does not cover the entirety of boreal forest peatland environments. By applying the equations given by the models presented here on small black spruce found in similar peatland environments located across the boreal forest it could be possible to confirm their transferability.

3.3 Final Remarks

This information presented in this thesis is beneficial in the short term and could have significant implications on future studies. The best models presented here estimate AGB more accurately for the trees used in Chapter 2 than the established DBH and height models currently being used by the Canadian National Forest Inventory. This study offers an excellent case study of how AGB can be measured accurately using measurements of crown size and height as predictors and not requiring DBH at all. Future studies building upon the work done in this thesis could have far-reaching implications on the kinds of variables used in allometric AGB equations in the future. There is also much to be explored about how these models can be used in point clouds made by laser scanning platforms other than TLS, and the conditions necessary to obtain the best results. The work here offers an important contribution in terms of the crown area and height models given for small peatland black spruce trees, but also provides a starting point for other subsequent studies with potential to markedly increase the base of knowledge in Earth sciences and forestry fields.

3.4 References

Alemdag, I. S. (1983). Mass Equations and Merchantability Factors for Ontario Softwoods. *Canadian Forestry Service*, *Information Report*, 1–24.

Bhatti, J. S., Errington, R. C., Bauer, I. E., & Hurdle, P. A. (2006). Carbon stock trends along forested peatland margins in central Saskatchewan. *Canadian Journal of Soil Science*, *86*(Special Issue), 321–333. https://doi.org/10.4141/S05-085

Brede, B., Calders, K., Lau, A., Raumonen, P., Bartholomeus, H. M., Herold, M., & Kooistra, L. (2019). Non-destructive tree volume estimation through quantitative structure modelling: Comparing UAV laser scanning with terrestrial LIDAR. *Remote Sensing of Environment*, *233*, 111355. https://doi.org/10.1016/j.rse.2019.111355

Calders, K., Newnham, G., Burt, A., Murphy, S., Raumonen, P., Herold, M., Culvenor, D., Avitabile, V., Disney, M., Armston, J., & Kaasalainen, M. (2015). Nondestructive estimates of above-ground biomass using terrestrial laser scanning. *Methods in Ecology and Evolution*, *6*(2), 198–208. https://doi.org/10.1111/2041-210X.12301

Holopainen, M., Kankare, V., Vastaranta, M., Liang, X., Lin, Y., Vaaja, M., Yu, X., Hyyppä, J., Hyyppä, H., Kaartinen, H., Kukko, A., Tanhuanpää, T., & Alho, P. (2013). Tree mapping using airborne, terrestrial and mobile laser scanning – A case study in a heterogeneous urban forest. *Urban Forestry & Urban Greening*, *12*(4), 546–553. https://doi.org/10.1016/j.ufug.2013.06.002

Hyyppä, J., Hyyppä, H., Leckie, D., Gougeon, F., Yu, X., & Maltamo, M. (2008). Review of methods of small-footprint airborne laser scanning for extracting forest inventory data in boreal forests. *International Journal of Remote Sensing*, *29*(5), 1339–1366. https://doi.org/10.1080/01431160701736489

Liang, X., Hyyppä, J., Kaartinen, H., Lehtomäki, M., Pyörälä, J., Pfeifer, N., Holopainen, M., Brolly, G., Francesco, P., Hackenberg, J., Huang, H., Jo, H.-W., Katoh, M., Liu, L., Mokroš, M., Morel, J., Olofsson, K., Poveda-Lopez, J., Trochta, J., … Wang, Y. (2018). International benchmarking of terrestrial laser scanning approaches for forest inventories. *ISPRS Journal of Photogrammetry and Remote Sensing*, *144*, 137–179. https://doi.org/10.1016/j.isprsjprs.2018.06.021

Lim, K., & Treitz, P. (2004). Estimation of above ground forest biomass from airborne discrete return laser scanner data using canopy-based quantile estimators. *Scandinavian Journal of Forest Research*, *19*(6), 558–570.

Singh, T. (1984). *Biomass Equations for Six Major Tree Species of the Northwest Territories* (pp. 1–30). Environment Canada, Canadian Forestry Service.

Takoudjou, S. M., Ploton, P., Sonké, B., Hackenberg, J., Griffon, S., Coligny, F. de, Kamdem, N. G., Libalah, M., Mofack, G. I., Moguédec, G. L., Pélissier, R., & Barbier, N. (2018). Using terrestrial laser scanning data to estimate large tropical trees biomass and calibrate allometric models: A comparison with traditional destructive approach. *Methods in Ecology and Evolution*, *9*(4), 905–916. https://doi.org/10.1111/2041-210X.12933

Ung, C.-H., Bernier, P., & Guo, X.-J. (2008). Canadian national biomass equations: New parameter estimates that include British Columbia data. *Canadian Journal of Forest Research*, *38*(5), 1123–1132. https://doi.org/10.1139/X07-224

Wieder, R., Vitt, D., & Benscoter, B. (2006). Peatlands and the Boreal Forest. In *Ecol. Stud.* (Vol. 188, pp. 1–8). https://doi.org/10.1007/978-3-540-31913-9_1

Yu, X., Hyyppä, J., Holopainen, M., & Vastaranta, M. (2010). Comparison of Area-Based and Individual Tree-Based Methods for Predicting Plot-Level Forest Attributes. *Remote. Sens.* https://doi.org/10.3390/rs2061481

Zolkos, S. G., Goetz, S. J., & Dubayah, R. (2013). A meta-analysis of terrestrial aboveground biomass estimation using lidar remote sensing. *Remote Sensing of Environment*, *128*, 289–298. https://doi.org/10.1016/j.rse.2012.10.017

References for Entire Thesis

Abadie, L. M. (2018). Sea level damage risk with probabilistic weighting of IPCC scenarios: An application to major coastal cities. *Journal of Cleaner Production*, *175*, 582–598. https://doi.org/10.1016/j.jclepro.2017.11.069

Abegg, M., Kükenbrink, D., Zell, J., Schaepman, M. E., & Morsdorf, F. (2017). Terrestrial Laser Scanning for Forest Inventories—Tree Diameter Distribution and Scanner Location Impact on Occlusion. *Forests (19994907)*, *8*(6), 184. https://doi.org/10.3390/f8060184

Abich, A., Mucheye, T., Tebikew, M., Gebremariam, Y., & Alemu, A. (2019). Species-specific allometric equations for improving aboveground biomass estimates of dry deciduous woodland ecosystems. *Journal of Forestry Research*, *30*(5), 1619–1632. https://doi.org/10.1007/s11676-018-0707-5

Alemdag, I. S. (1983). Mass Equations and Merchantability Factors for Ontario Softwoods. *Canadian Forestry Service*, *Information Report*, 1–24.

Alexandrov, G. A., Brovkin, V. A., Kleinen, T., & Yu, Z. (2020). The capacity of northern peatlands for long-term carbon sequestration. *Biogeosciences*, *17*(1), 47–54. https://doi.org/10.5194/bg-17-47-2020

Annighöfer, P., Ameztegui, A., Ammer, C., Balandier, P., Bartsch, N., Bolte, A., Coll, L., Collet, C., Ewald, J., Frischbier, N., Gebereyesus, T., Haase, J., Hamm, T., Hirschfelder, B., Huth, F., Kändler, G., Kahl, A., Kawaletz, H., Kuehne, C., … Mund, M. (2016). Species-specific and generic biomass equations for seedlings and saplings of European tree species. *European Journal of Forest Research*, *135*(2), 313–329. https://doi.org/10.1007/s10342-016-0937-z

Bandh, S. A., Shafi, S., Peerzada, M., Rehman, T., Bashir, S., Wani, S. A., & Dar, R. (2021). Multidimensional analysis of global climate change: A review. *Environmental Science and Pollution Research*, *28*(20), 24872–24888. https://doi.org/10.1007/s11356-021-13139-7

Baskerville, G. L. (1972). Use of Logarithmic Regression in the Estimation of Plant Biomass. *Canadian Journal of Forest Research*. https://doi.org/10.1139/x72-009

Beraldin, J.-A., Blais, F., & Lohr, U. (2010). Laser Scanning Technology. In *Airborne and Terrestrial Laser Scanning*. Whittles Publishing. http://ebookcentral.proquest.com/lib/ualberta/detail.action?docID=3417283

Bhatti, J. S., Errington, R. C., Bauer, I. E., & Hurdle, P. A. (2006). Carbon stock trends along forested peatland margins in central Saskatchewan. *Canadian Journal of Soil Science*, *86*(Special Issue), 321–333. https://doi.org/10.4141/S05-085

Bona, K. A., Hilger, A., Burgess, M., Wozney, N., & Shaw, C. (2018). A peatland productivity and decomposition parameter database. *Ecology*, *99*(10), 2406–2406. https://doi.org/10.1002/ecy.2462

Bona, K. A., Shaw, C., Thompson, D. K., Hararuk, O., Webster, K., Zhang, G., Voicu, M., & Kurz, W. A. (2020). The Canadian model for peatlands (CaMP): A peatland carbon model for national greenhouse gas reporting. *Ecological Modelling*, *431*, 109164. https://doi.org/10.1016/j.ecolmodel.2020.109164

Brede, B., Calders, K., Lau, A., Raumonen, P., Bartholomeus, H. M., Herold, M., & Kooistra, L. (2019). Non-destructive tree volume estimation through quantitative structure modelling: Comparing UAV laser scanning with terrestrial LIDAR. *Remote Sensing of Environment*, *233*, 111355. https://doi.org/10.1016/j.rse.2019.111355

Brede, B., Lau, A., Bartholomeus, H. M., & Kooistra, L. (2017). Comparing RIEGL RiCOPTER UAV LiDAR Derived Canopy Height and DBH with Terrestrial LiDAR. *Sensors*, *17*(10), 2371. https://doi.org/10.3390/s17102371

Breusch, T. S., & Pagan, A. R. (1979). A Simple Test for Heteroscedasticity and Random Coefficient Variation. *Econometrica*, *47*(5), 1287–1294. https://doi.org/10.2307/1911963

Brown, S. (1997). *Estimating Biomass and Biomass Change of Tropical Forests: A Primer*. Food & Agriculture Org.

Budei, B. C., St-Onge, B., Hopkinson, C., & Audet, F.-A. (2018). Identifying the genus or species of individual trees using a three-wavelength airborne lidar system. *Remote Sensing of Environment*, *204*, 632–647. https://doi.org/10.1016/j.rse.2017.09.037

Buech, R. R., & Rugg, D. J. (1989). Biomass relations of shrub components and their generality. *Forest Ecology and Management*, *26*(4), 257–264. https://doi.org/10.1016/0378-1127(89)90086-8

Burt, A., Disney, M. I., Raumonen, P., Armston, J., Calders, K., & Lewis, P. (2013). Rapid characterisation of forest structure from TLS and 3D modelling. *2013 IEEE International Geoscience and Remote Sensing Symposium - IGARSS*, 3387–3390. https://doi.org/10.1109/IGARSS.2013.6723555

Butler, J. H., & Montzka, S. A. (2021). *The NOAA Annual Greenhouse Gas Index (AGGI)*. https://gml.noaa.gov/aggi/aggi.html

Cabo, C., Ordóñez, C., López-Sánchez, C. A., & Armesto, J. (2018). Automatic dendrometry: Tree detection, tree height and diameter estimation using terrestrial laser scanning. *International Journal of Applied Earth Observation and Geoinformation*, *69*, 164–174. https://doi.org/10.1016/j.jag.2018.01.011

Calders, K., Adams, J., Armston, J., Bartholomeus, H., Bauwens, S., Bentley, L. P., Chave, J., Danson, F. M., Demol, M., Disney, M., Gaulton, R., Krishna Moorthy, S. M., Levick, S. R., Saarinen, N., Schaaf, C., Stovall, A., Terryn, L., Wilkes, P., & Verbeeck, H. (2020). Terrestrial laser scanning in forest ecology: Expanding the horizon. *Remote Sensing of Environment*, *251*, 112102. https://doi.org/10.1016/j.rse.2020.112102

Calders, K., Newnham, G., Burt, A., Murphy, S., Raumonen, P., Herold, M., Culvenor, D., Avitabile, V., Disney, M., Armston, J., & Kaasalainen, M. (2015). Nondestructive estimates of above-ground biomass using terrestrial laser scanning. *Methods in Ecology and Evolution*, *6*(2), 198–208. https://doi.org/10.1111/2041-210X.12301

Calders, K., Wilkes, P., Disney, M., Armston, J., Schaefer, M., & Woodgate, W. (2018). Chapter 19. Terrestrial LiDAR for measuring above-ground biomass and forest structure. In *Effective Field Calibration and Validation Practices*. (pp. 321-336). TERN.

Carlson, M., Roberts, D., & Wells, J. (2009). *The carbon the world forgot: Conserving the capacity of Canada's boreal forest region to mitigate and adapt to climate change* (Alberta Government Library - Internet Internet Access). Boreal Songbird Initiative. https://login.ezproxy.library.ualberta.ca/login?url=https://search.ebscohost.com/login.aspx?direct=true&db=cat03710a&AN=alb.9341038&site=eds-live&scope=site

Chen, S., Liu, H., Feng, Z., Shen, C., & Chen, P. (2019). Applicability of personal laser scanning in forestry inventory. *PLOS ONE*, *14*(2), e0211392. https://doi.org/10.1371/journal.pone.0211392

Chen, X., YE, C., Li, J., & Chapman, M. A. (2018). Quantifying the Carbon Storage in Urban Trees Using Multispectral ALS Data. *IEEE Journal of Selected Topics in Applied Earth*

Observations and Remote Sensing, *11*(9), 3358–3365. https://doi.org/10.1109/JSTARS.2018.2859957

Ciais, P., Sabine, C., Bala, G., Bopp, L., Brovkin, V., Canadell, J., Chhabra, A., DeFries, R., Galloway, J., Heimann, M., Jones, C., Le Quere, C., Myneni, R. B., Piao, S., & Thornton, P. (2013). Carbon and Other Biogeochemical Cycles. In T. F. Stocker, D. Qin, G.-K. Plattner, M. Tignor, S. K. Allen, J. Boschung, A. Nauels, Y. Xia, V. Bex, & P. M. Midgley (Eds.), *Carbon and Other Biogeochemical Cycles. In: Climate Change 2013: The Physical Science Basis. Contribution of Working Group I to the Fifth Assessment Report of the Intergovernmental Panel on Climate Change*. Cambridge University Press.

CloudCompare (v2.11.1). (n.d.). Retrieved March 28, 2021, from https://www.danielgm.net/cc/

Colomina, I., & Molina, P. (2014). Unmanned aerial systems for photogrammetry and remote sensing: A review. *ISPRS Journal of Photogrammetry and Remote Sensing*, *92*, 79–97. https://doi.org/10.1016/j.isprsjprs.2014.02.013

Coumou, D., Robinson, A., & Rahmstorf, S. (2013). Global increase in record-breaking monthly-mean temperatures. *Climatic Change*, *118*(3), 771–782. https://doi.org/10.1007/s10584-012-0668-1

Dasgupta, S., Laplante, B., Meisner, C., Wheeler, D., & Yan, J. (2009). The impact of sea level rise on developing countries: A comparative analysis. *Climatic Change*, *93*(3), 379–388. https://doi.org/10.1007/s10584-008-9499-5

Disney, M., Burt, A., Calders, K., Schaaf, C., & Stovall, A. (2019). Innovations in Ground and Airborne Technologies as Reference and for Training and Validation: Terrestrial Laser Scanning (TLS). *Surveys in Geophysics*, *40*(4), 937–958. https://doi.org/10.1007/s10712-019-09527-x

Disney, M. I., Boni Vicari, M., Burt, A., Calders, K., Lewis, S. L., Raumonen, P., & Wilkes, P. (2018). Weighing trees with lasers: Advances, challenges and opportunities. *Interface Focus*, *8*(2), 20170048. https://doi.org/10.1098/rsfs.2017.0048

Ecosystem Classification Group, Northwest Territories, & Department of Environment and Natural Resources. (2009). *Ecological regions of the Northwest Territories: Taiga Plains*. Dept. of Environment and Natural Resources, Govt. of the Northwest Territories.

FAO. (2020). *Global Forest Resources Assessment 2020: Main report*. FAO. https://doi.org/10.4060/ca9825en

Fearnside, P. M. (2000). Global Warming and Tropical Land-Use Change: Greenhouse Gas Emissions from Biomass Burning, Decomposition and Soils in Forest Conversion, Shifting Cultivation and Secondary Vegetation. *Climatic Change*, *46*(1), 115–158. https://doi.org/10.1023/A:1005569915357

Ferguson, C. R., Pan, M., & Oki, T. (2018). The Effect of Global Warming on Future Water Availability: CMIP5 Synthesis. *Water Resources Research*, *54*(10), 7791–7819. https://doi.org/10.1029/2018WR022792

Flade, L., Hopkinson, C., & Chasmer, L. (2020). Allometric Equations for Shrub and Short-Stature Tree Aboveground Biomass within Boreal Ecosystems of Northwestern Canada. *Forests*, *11*(11), 1207. https://doi.org/10.3390/f11111207

Forrester, D. I., Dumbrell, I. C., Elms, S. R., Paul, K. I., Pinkard, E. A., Roxburgh, S. H., & Baker, T. G. (2021). Can crown variables increase the generality of individual tree biomass equations? *Trees*, *35*(1), 15–26. https://doi.org/10.1007/s00468-020-02006-6

Frederikse, T., Landerer, F., Caron, L., Adhikari, S., Parkes, D., Humphrey, V. W., Dangendorf, S., Hogarth, P., Zanna, L., Cheng, L., & Wu, Y.-H. (2020). The causes of sea-level rise since 1900. *Nature*, *584*(7821), 393–397. https://doi.org/10.1038/s41586-020-2591-3

Friend, A. D., Lucht, W., Rademacher, T. T., Keribin, R., Betts, R., Cadule, P., Ciais, P., Clark, D. B., Dankers, R., Falloon, P. D., Ito, A., Kahana, R., Kleidon, A., Lomas, M. R., Nishina, K., Ostberg, S., Pavlick, R., Peylin, P., Schaphoff, S., … Woodward, F. I. (2014). Carbon residence time dominates uncertainty in terrestrial vegetation responses to future climate and atmospheric CO2. *Proceedings of the National Academy of Sciences*, *111*(9), 3280–3285.

Gettelman, A., & Rood, R. B. (2016). Essence of a Climate Model. In A. Gettelman & R. B. Rood (Eds.), *Demystifying Climate Models: A Users Guide to Earth System Models* (pp. 37–58). Springer. https://doi.org/10.1007/978-3-662-48959-8_4

Ghimire, S., Xystrakis, F., & Koutsias, N. (2017). Using Terrestrial Laser Scanning to Measure Forest Inventory Parameters in a Mediterranean Coniferous Stand of Western Greece. *PFG – Journal of Photogrammetry, Remote Sensing and Geoinformation Science*, *85*(4), 213–225. https://doi.org/10.1007/s41064-017-0024-1

Gibbs, M., & Latzko, E. (Eds.). (1979). *Photosynthesis II*. Springer Berlin Heidelberg. https://doi.org/10.1007/978-3-642-67242-2

Gollob, C., Ritter, T., & Nothdurft, A. (2020a). Forest inventory with long range and high-speed Personal Laser Scanning (PLS) and Simultaneous Localization and Mapping (SLAM) technology. *Remote Sensing*, *12*(9). https://doi.org/10.3390/RS12091509

Gollob, C., Ritter, T., & Nothdurft, A. (2020b). Comparison of 3D Point Clouds Obtained by Terrestrial Laser Scanning and Personal Laser Scanning on Forest Inventory Sample Plots. *Data*, *5*(4), 103. https://doi.org/10.3390/data5040103

Gonzalez de Tanago, J., Lau, A., Bartholomeus, H., Herold, M., Avitabile, V., Raumonen, P., Martius, C., Goodman, R. C., Disney, M., Manuri, S., Burt, A., Calders, K., & Kriticos, D. (2017). Estimation of above-ground biomass of large tropical trees with terrestrial LiDAR. *Methods in Ecology & Evolution*, *9*(2), 223–234. https://doi.org/10.1111/2041-210X.12904

Goodman, R. C., Phillips, O. L., & Baker, T. R. (2014). The importance of crown dimensions to improve tropical tree biomass estimates. *Ecological Applications*, *24*(4), 680–698. https://doi.org/10.1890/13-0070.1

Hackenberg, J., Wassenberg, M., Spiecker, H., & Sun, D. (2015). Non Destructive Method for Biomass Prediction Combining TLS Derived Tree Volume and Wood Density. *Forests*, *6*(4), 1274–1300. https://doi.org/10.3390/f6041274

Harikumar, A., Bovolo, F., & Bruzzone, L. (2017). An approach to conifer stem localization and modeling in high density airborne LiDAR data. *Image and Signal Processing for Remote Sensing XXIII*, *10427*, 104270Q. https://doi.org/10.1117/12.2279526

Harikumar, A., Paris, C., Bovolo, F., & Bruzzone, L. (2021). A Crown Quantization-Based Approach to Tree-Species Classification Using High-Density Airborne Laser Scanning Data. *IEEE Transactions on Geoscience and Remote Sensing*, *59*(5), 4444–4453. https://doi.org/10.1109/TGRS.2020.3012343

Heinzel, J., & Huber, M. O. (2017). Tree Stem Diameter Estimation From Volumetric TLS Image Data. *Remote Sensing*, *9*(6), 614. https://doi.org/10.3390/rs9060614

Hirabayashi, Y., Mahendran, R., Koirala, S., Konoshima, L., Yamazaki, D., Watanabe, S., Kim, H., & Kanae, S. (2013). Global flood risk under climate change. *Nature Climate Change*, *3*(9), 816–821. https://doi.org/10.1038/nclimate1911

Holopainen, M., Kankare, V., Vastaranta, M., Liang, X., Lin, Y., Vaaja, M., Yu, X., Hyyppä, J., Hyyppä, H., Kaartinen, H., Kukko, A., Tanhuanpää, T., & Alho, P. (2013). Tree mapping using airborne, terrestrial and mobile laser scanning – A case study in a heterogeneous urban forest. *Urban Forestry & Urban Greening*, *12*(4), 546–553. https://doi.org/10.1016/j.ufug.2013.06.002

Houghton, R. A. (2008). Biomass. In S. E. Jørgensen & B. D. Fath (Eds.), *Encyclopedia of Ecology* (pp. 448–453). Academic Press. https://doi.org/10.1016/B978-008045405-4.00462-6

Hyyppä, E., Hyyppä, J., Hakala, T., Kukko, A., Wulder, M. A., White, J. C., Pyörälä, J., Yu, X., Wang, Y., Virtanen, J.-P., Pohjavirta, O., Liang, X., Holopainen, M., & Kaartinen, H. (2020). Under-canopy UAV laser scanning for accurate forest field measurements. *ISPRS Journal of Photogrammetry and Remote Sensing*, *164*, 41–60. https://doi.org/10.1016/j.isprsjprs.2020.03.021

Hyyppä, J., Hyyppä, H., Leckie, D., Gougeon, F., Yu, X., & Maltamo, M. (2008). Review of methods of small-footprint airborne laser scanning for extracting forest inventory data in boreal forests. *International Journal of Remote Sensing*, *29*(5), 1339–1366. https://doi.org/10.1080/01431160701736489

IPCC. (2014). *Climate Change 2014: Mitigation of Climate Change. Contribution of Working Group III to the Fifth Assessment Report of the Intergovernmental Panel on Climate Change* (O. Edenhofer, R. Pichs-Madruga, Y. Sokona, E. Farahani, S. Kadner, K. Seyboth,

A. Adler, I. Baum, S. Brunner, P. Eickemeier, B. Kriemann, J. Savolainen, S. Schlömer, C. von Stechow, T. Zwickel, & J. C. Minx, Eds.). Cambridge University Press. https://www.ipcc.ch/report/ar5/wg3/

Jaakkola, A., Hyyppä, J., Yu, X., Kukko, A., Kaartinen, H., Liang, X., Hyyppä, H., & Wang, Y. (2017). Autonomous Collection of Forest Field Reference—The Outlook and a First Step with UAV Laser Scanning. *Remote Sensing*, *9*(8), 785. https://doi.org/10.3390/rs9080785

Johansen, B. E. (2017). *Climate Change: An Encyclopedia of Science, Society, and Solutions [3 Volumes]*. ABC-CLIO, LLC. http://ebookcentral.proquest.com/lib/ualberta/detail.action?docID=5013474

Jucker, T., Caspersen, J., Chave, J., Antin, C., Barbier, N., Bongers, F., Dalponte, M., Ewijk, K. Y. van, Forrester, D. I., Haeni, M., Higgins, S. I., Holdaway, R. J., Iida, Y., Lorimer, C., Marshall, P. L., Momo, S., Moncrieff, G. R., Ploton, P., Poorter, L., … Coomes, D. A. (2017). Allometric equations for integrating remote sensing imagery into forest monitoring programmes. *Global Change Biology*, *23*(1), 177–190. https://doi.org/10.1111/gcb.13388

Kalwar, O. P. P., Hussin, Y. A., Weir, M. J. C., Bie, C. A. J. M. de, & Karna, Y. (2021). Deriving forest plot inventory parameters using terrestrial laser scanning in the tropical rainforest of Malaysia. *International Journal of Remote Sensing*, *42*(3), 884–901. https://doi.org/10.1080/01431161.2020.1817606

Kornhuber, K., & Tamarin-Brodsky, T. (2021). Future Changes in Northern Hemisphere Summer Weather Persistence Linked to Projected Arctic Warming. *Geophysical Research Letters*, *48*(4), e2020GL091603. https://doi.org/10.1029/2020GL091603

Kukko, A., Kaijaluoto, R., Kaartinen, H., Lehtola, V. V., Jaakkola, A., & Hyyppä, J. (2017). Graph SLAM correction for single scanner MLS forest data under boreal forest canopy.

ISPRS Journal of Photogrammetry and Remote Sensing, *132*, 199–209. https://doi.org/10.1016/j.isprsjprs.2017.09.006

Kurz, W. A., Shaw, C. H., Boisvenue, C., Stinson, G., Metsaranta, J., Leckie, D., Dyk, A., Smyth, C., & Neilson, E. T. (2013). Carbon in Canada's boreal forest—A synthesis. *Environmental Reviews*, *21*(4), 260–292. https://doi.org/10.1139/er-2013-0041

Moskal, L. M., & Zheng, G. (2011). Retrieving Forest Inventory Variables with Terrestrial Laser Scanning (TLS) in Urban Heterogeneous Forest. Remote Sensing, 4(1), 1–20. https://doi.org/10.3390/rs4010001

Lambert, M.-C., Ung, C.-H., & Raulier, F. (2005). Canadian national tree aboveground biomass equations. *Canadian Journal of Forest Research*. https://doi.org/10.1139/x05-112

Lau, A. (1, 2), Bartholomeus, H. (1), Herold, M. (1), Calders, K. (3), Martius, C. (4), Raumonen, P. (5), Vicari, M. (6), Sukhdeo, H. (7), Singh, J. (7), & Goodman, R. c. (8). (2019). Tree biomass equations from terrestrial LiDAR: A case study in Guyana. *Forests*, *10*(6). https://doi.org/10.3390/f10060527

Lau, A., Bentley, L. P., Martius, C., Shenkin, A., Bartholomeus, H., Raumonen, P., Malhi, Y., Jackson, T., & Herold, M. (2018). Quantifying branch architecture of tropical trees using terrestrial LiDAR and 3D modelling. *Trees*, *32*(5), 1219–1231. https://doi.org/10.1007/s00468-018-1704-1

Lehmann, J., Coumou, D., & Frieler, K. (2015). Increased record-breaking precipitation events under global warming. *Climatic Change: An Interdisciplinary, International Journal Devoted to the Description, Causes and Implications of Climatic Change*, *132*(4), 501. https://doi.org/10.1007/s10584-015-1434-y

Leica Cyclone 3D Point Cloud Processing Software. (n.d.). Retrieved June 13, 2021, from https://leica-geosystems.com/products/laser-scanners/software/leica-cyclone

Liang, X., Hyyppä, J., Kaartinen, H., Lehtomäki, M., Pyörälä, J., Pfeifer, N., Holopainen, M., Brolly, G., Francesco, P., Hackenberg, J., Huang, H., Jo, H.-W., Katoh, M., Liu, L., Mokroš, M., Morel, J., Olofsson, K., Poveda-Lopez, J., Trochta, J., … Wang, Y. (2018). International benchmarking of terrestrial laser scanning approaches for forest inventories. *ISPRS Journal of Photogrammetry and Remote Sensing*, *144*, 137–179. https://doi.org/10.1016/j.isprsjprs.2018.06.021

Liang, X., Hyyppä, J., Kukko, A., Kaartinen, H., Jaakkola, A., & Yu, X. (2014). The Use of a Mobile Laser Scanning System for Mapping Large Forest Plots. *IEEE Geoscience and Remote Sensing Letters*, *11*(9), 1504–1508. https://doi.org/10.1109/LGRS.2013.2297418

Liang, X., Kankare, V., Hyyppä, J., Wang, Y., Kukko, A., Haggrén, H., Yu, X., Kaartinen, H., Jaakkola, A., Guan, F., Holopainen, M., & Vastaranta, M. (2016). Terrestrial laser scanning in forest inventories. *ISPRS Journal of Photogrammetry and Remote Sensing*, *115*, 63–77. https://doi.org/10.1016/j.isprsjprs.2016.01.006

Liang, X., Kukko, A., Kaartinen, H., Hyyppä, J., Yu, X., Jaakkola, A., & Wang, Y. (2014). Possibilities of a Personal Laser Scanning System for Forest Mapping and Ecosystem Services. *Sensors*, *14*(1), 1228–1248. https://doi.org/10.3390/s140101228

Lieffers, V. J. (1986). Stand Structure, Variability in Growth and Intraspecific Competition in a Peatland Stand of Black Spruce Picea mariana. *Holarctic Ecology*, *9*(1), 58–64.

Lim, K., & Treitz, P. (2004). Estimation of above ground forest biomass from airborne discrete return laser scanner data using canopy-based quantile estimators. *Scandinavian Journal of Forest Research*, *19*(6), 558–570.

Lim, K., Treitz, P., Wulder, M., St-Onge, B., & Flood, M. (2003). LiDAR remote sensing of forest structure. *Progress in Physical Geography: Earth and Environment*, *27*(1), 88–106. https://doi.org/10.1191/0309133303pp360ra

Liu, G., Wang, J., Dong, P., Chen, Y., & Liu, Z. (2018). Estimating Individual Tree Height and Diameter at Breast Height (DBH) from Terrestrial Laser Scanning (TLS) Data at Plot Level. *Forests*, *9*(7), 398. https://doi.org/10.3390/f9070398

Liu, W., Li, Z., Li, Y., Sun, S., & Sotelo, M. A. (2020). Using Weighted Total Least Squares and 3-D Conformal Coordinate Transformation to Improve the Accuracy of Mobile Laser Scanning. *IEEE Transactions on Geoscience and Remote Sensing*, *58*(1), 203–217. https://doi.org/10.1109/TGRS.2019.2935744

Liu, W., Li, Z., Sun, S., Malekian, R., Ma, Z., & Li, W. (2019). Improving Positioning Accuracy of the Mobile Laser Scanning in GPS-Denied Environments: An Experimental Case Study. *IEEE Sensors Journal*, *19*(22), 10753–10763. https://doi.org/10.1109/JSEN.2019.2929142

Lorenz, K., & Lal, R. (2010). The Natural Dynamic of Carbon in Forest Ecosystems. In K. Lorenz & R. Lal (Eds.), *Carbon Sequestration in Forest Ecosystems* (pp. 23–101). Springer Netherlands. https://doi.org/10.1007/978-90-481-3266-9_2

Lucas, R. M., Mitchell, A. L., & Armston, J. (2015). Measurement of Forest Above-Ground Biomass Using Active and Passive Remote Sensing at Large (Subnational to Global) Scales. *Current Forestry Reports*, *1*(3), 162–177. https://doi.org/10.1007/s40725-015-0021-9

Magnan, G., Garneau, M., Le Stum-Boivin, É., Grondin, P., & Bergeron, Y. (2020). Long-Term Carbon Sequestration in Boreal Forested Peatlands in Eastern Canada. *Ecosystems*, *23*(7), 1481–1493. https://doi.org/10.1007/s10021-020-00483-x

Malek S, Miglietta F, Gobakken T, Næsset E, Gianelle D, & Dalponte M. (2019). Prediction of stem diameter and biomass at individual tree crown level with advanced machine learning techniques. *IForest - Biogeosciences and Forestry*, *12*(1), 323–329. https://doi.org/10.3832/ifor2980-012

Mao, Q., Zhang, L., Li, Q., Hu, Q., Yu, J., Shaojun Feng, Washington Ochieng, & Hanlu Gong. (2015). A Least Squares Collocation Method for Accuracy Improvement of Mobile LiDAR Systems. *Remote Sensing*, *7*(6), 7402–7424. https://doi.org/10.3390/rs70607402

Martinez, J., Martínez-Garza, C., & Cámara, L. (2020). Species-specific or generic allometric equations: Which option is better when estimating the biomass of Mexican tropical humid forests? *Carbon Management*, *11*, 1–9. https://doi.org/10.1080/17583004.2020.1738823

Mascaro, J., Litton, C. M., Hughes, R. F., Uowolo, A., & Schnitzer, S. A. (2014). Is logarithmic transformation necessary in allometry? Ten, one-hundred, *one-thousand-times yes*: Yes, We Need the Logarithm in Allometry. *Biological Journal of the Linnean Society*, *111*(1), 230–233. https://doi.org/10.1111/bij.12177

McFarland, E. L., Hunt, J. L., & Campbell, J. L. (2007). *Energy, physics and the environment*. Cengage Learning.

Mielcarek, M., Kaminska, A., & Sterenczak, K. (2020). Digital Aerial Photogrammetry (DAP) and Airborne Laser Scanning (ALS) as Sources of Information about Tree Height: Comparisons of the Accuracy of Remote Sensing Methods for Tree Height Estimation. *REMOTE SENSING*, *12*(11). https://doi.org/10.3390/rs12111808

Modzelewska, A., Fassnacht, F. E., & Stereńczak, K. (2020). Tree species identification within an extensive forest area with diverse management regimes using airborne hyperspectral

data. *International Journal of Applied Earth Observation and Geoinformation*, *84*, 101960. https://doi.org/10.1016/j.jag.2019.101960

NASA Global Climate Change. (2021, June 21). *Carbon Dioxide Concentration | NASA Global Climate Change* [Government]. Climate Change: Vital Signs of the Planet. https://climate.nasa.gov/vital-signs/carbon-dioxide

Natural Resources Canada. (2013, July 11). *Boreal forest*. Natural Resources Canada. https://www.nrcan.gc.ca/our-natural-resources/forests/sustainable-forest-management/boreal-forest/13071

Navar, J. (2010). Methods od Assessment of Aboveground Tree Biomass. In *Biomass*. IntechOpen. https://doi.org/10.5772/9768

Novotný, J., Navrátilová, B., Janoutová, R., Oulehle, F., & Homolová, L. (2020). Influence of Site-Specific Conditions on Estimation of Forest above Ground Biomass from Airborne Laser Scanning. *Forests*, *11*(3), 268–268. https://doi.org/10.3390/f11030268

Nwanganga, F., & Chapple, M. (2020). Practical Machine Learning in R. *John Wiley & Sons*, 311–312.

Peng, X., Zhao, A., Chen, Y., Chen, Q., & Liu, H. (2021). Tree Height Measurements in Degraded Tropical Forests Based on UAV-LiDAR Data of Different Point Cloud Densities: A Case Study on Dacrydium pierrei in China. *Forests*, *12*(3), 328. https://doi.org/10.3390/f12030328

Picard, N., Saint-André, L., & Henry, M. (2012). *Manual for building tree volume and biomass allometric equations from filed measurement to prediction*. Food and Agriculture Organization of the United Nations (FA0). http://www.fao.org/docrep/018/i3058e/i3058e.pdf

Prošek, J., & Šímová, P. (2019). UAV for mapping shrubland vegetation: Does fusion of spectral and vertical information derived from a single sensor increase the classification accuracy? *International Journal of Applied Earth Observation and Geoinformation*, *75*, 151–162. https://doi.org/10.1016/j.jag.2018.10.009

Puc-Kauil, R. (1), Ángeles-Pérez, G. (1), Valdéz-Lazalde, J. r. (1), Reyes-Hernández, V. j. (1), Pérez-Rodríguez, P. (1), Dupuy-Rada, J. m. (2), Schneider, L. (3), & García-Cuevas, X. (4). (2020). Allometric equations to estimate above-ground biomass of small-diameter mixed tree species in secondary tropical forests. *IForest*, *13*(3), 165–174. https://doi.org/10.3832/ifor3167-013

R Core Team. (2020). *R: A Language and Environment for Statistical Computing*. R Foundation for Statistical Computing. https://www.R-project.org/

Raumonen, P., Kaasalainen, M., Åkerblom, M., Kaasalainen, S., Kaartinen, H., Vastaranta, M., Holopainen, M., Disney, M., & Lewis, P. (2013). Fast Automatic Precision Tree Models from Terrestrial Laser Scanner Data. *Remote Sensing*, *5*(2), 491–520. https://doi.org/10.3390/rs5020491

Reese, H., Nyström, M., Nordkvist, K., & Olsson, H. (2014). Combining airborne laser scanning data and optical satellite data for classification of alpine vegetation. *International Journal of Applied Earth Observation and Geoinformation*, *27*, 81–90. https://doi.org/10.1016/j.jag.2013.05.003

Reichstein, M., & Carvalhais, N. (2019). Aspects of Forest Biomass in the Earth System: Its Role and Major Unknowns. *Surveys in Geophysics*, *40*(4), 693–707. https://doi.org/10.1007/s10712-019-09551-x

Rencz, A. N., & Auclair, A. N. D. (1978). Biomass distribution in a subarctic *Picea mariana* – *Cladonia alpestris* woodland. *Canadian Journal of Forest Research*, *8*(2), 168–176. https://doi.org/10.1139/x78-027

Resources, E. and N. (n.d.). *Ecosystem Classification* [Information]. Government of the Northwest Territories. Retrieved February 9, 2021, from https://www.enr.gov.nt.ca/en/node/351

Sah, J. P., Ross, M. S., Koptur, S., & Snyder, J. R. (2004). Estimating aboveground biomass of broadleaved woody plants in the understory of Florida Keys pine forests. *Forest Ecology and Management*, *203*(1), 319–329. https://doi.org/10.1016/j.foreco.2004.07.059

Shao, J., Zhang, W., Mellado, N., Wang, N., Jin, S., Cai, S., Luo, L., Lejemble, T., & Yan, G. (2020). SLAM-aided forest plot mapping combining terrestrial and mobile laser scanning. *ISPRS Journal of Photogrammetry and Remote Sensing*, *163*, 214–230. https://doi.org/10.1016/j.isprsjprs.2020.03.008

Shruthi Srinivasan, Sorin C. Popescu, Marian Eriksson, Ryan D. Sheridan, & Nian-Wei Ku. (2015). Terrestrial Laser Scanning as an Effective Tool to Retrieve Tree Level Height, Crown Width, and Stem Diameter. *Remote Sensing*, *7*(2), 1877–1896. https://doi.org/10.3390/rs70201877

Singh, T. (1984). *Biomass Equations for Six Major Tree Species of the Northwest Territories* (pp. 1–30). Environment Canada, Canadian Forestry Service.

Smith, K. B., Smith, C. E. S., Forest, S. F., & Richard, A. J. (2007). *A Field Guide to the Wetlands of the Boreal Plains Ecozone of Canada*. Ducks Unlimited Canada.

Soma, M., Pimont, F., Allard, D., Fournier, R., & Dupuy, J.-L. (2020). Mitigating occlusion effects in Leaf Area Density estimates from Terrestrial LiDAR through a specific kriging

method. *Remote Sensing of Environment*, *245*, 111836. https://doi.org/10.1016/j.rse.2020.111836

Stal, C., Verbeurgt, J., De Sloover, L., & De Wulf, A. (2021). Assessment of handheld mobile terrestrial laser scanning for estimating tree parameters. *Journal of Forestry Research*, *32*(4), 1503–1513. https://doi.org/10.1007/s11676-020-01214-7

Sun, Y., Zhang, X., Zwiers, F. W., Song, L., Wan, H., Hu, T., Yin, H., & Ren, G. (2014). Rapid increase in the risk of extreme summer heat in Eastern China. *Nature Climate Change*, *4*(12), 1082–1085. https://doi.org/10.1038/nclimate2410

Takoudjou, S. M., Ploton, P., Sonké, B., Hackenberg, J., Griffon, S., Coligny, F. de, Kamdem, N. G., Libalah, M., Mofack, G. I., Moguédec, G. L., Pélissier, R., & Barbier, N. (2018). Using terrestrial laser scanning data to estimate large tropical trees biomass and calibrate allometric models: A comparison with traditional destructive approach. *Methods in Ecology and Evolution*, *9*(4), 905–916. https://doi.org/10.1111/2041-210X.12933

Tansey, K., Selmes, N., Anstee, A., Tate, N. J., & Denniss, A. (2009). Estimating tree and stand variables in a Corsican Pine woodland from terrestrial laser scanner data. *International Journal of Remote Sensing*, *30*(19), 5195–5209. https://doi.org/10.1080/01431160902882587

Tarnocai, C., Canadell, J. G., Schuur, E. a. G., Kuhry, P., Mazhitova, G., & Zimov, S. (2009). Soil organic carbon pools in the northern circumpolar permafrost region. *Global Biogeochemical Cycles*, *23*(2). https://doi.org/10.1029/2008GB003327

Tarnocai, C., Kettles, I. M., & Lacelle, B. (2011). PEATLANDS OF CANADA DATABASE. *Geological Survey of Canada*, *Open File 6561 (digital database)*, 10.

Thomas, V. (2017). *Climate Change and Natural Disasters: Transforming Economies and Policies for a Sustainable Future*. Routledge. http://ebookcentral.proquest.com/lib/ualberta/detail.action?docID=4785158

Thompson, D. K., Schroeder, D., Wilkinson, S. L., Barber, Q., Baxter, G., Cameron, H., Hsieh, R., Marshall, G., Moore, B., Refai, R., Rodell, C., Schiks, T., Verkaik, G. J., & Zerb, J. (2020). Recent Crown Thinning in a Boreal Black Spruce Forest Does Not Reduce Spread Rate nor Total Fuel Consumption: Results from an Experimental Crown Fire in Alberta, Canada. *Fire*, *3*(3), 28. https://doi.org/10.3390/fire3030028

Thompson, D. K., Simpson, B. N., & Beaudoin, A. (2016). Using forest structure to predict the distribution of treed boreal peatlands in Canada. *Forest Ecology and Management*, *372*, 19–27. https://doi.org/10.1016/j.foreco.2016.03.056

Treat, C. C., Kleinen, T., Broothaerts, N., Dalton, A. S., Dommain, R., Douglas, T. A., Drexler, J. Z., Finkelstein, S. A., Grosse, G., Hope, G., Hutchings, J., Jones, M. C., Kuhry, P., Lacourse, T., Lähteenoja, O., Loisel, J., Notebaert, B., Payne, R. J., Peteet, D. M., … Brovkin, V. (2019). Widespread global peatland establishment and persistence over the last 130,000 y. *Proceedings of the National Academy of Sciences*, *116*(11), 4822–4827.

Ung, C.-H., Bernier, P., & Guo, X.-J. (2008). Canadian national biomass equations: New parameter estimates that include British Columbia data. *Canadian Journal of Forest Research*, *38*(5), 1123–1132. https://doi.org/10.1139/X07-224

Vashum, K. (2012). Methods to Estimate Above-Ground Biomass and Carbon Stock in Natural Forests—A Review. *Journal of Ecosystem & Ecography*, *02*. https://doi.org/10.4172/2157-7625.1000116

Vauhkonen, J., Maltamo, M., McRoberts, R. E., & Næsset, E. (2014). Introduction to Forestry Applications of Airborne Laser Scanning. In M. Maltamo, E. Næsset, & J. Vauhkonen (Eds.), *Forestry Applications of Airborne Laser Scanning: Concepts and Case Studies* (pp. 1–16). Springer Netherlands. https://doi.org/10.1007/978-94-017-8663-8_1

Vosselman, G., & Maas, H.-G. (2010). *Airborne and Terrestrial Laser Scanning*. Whittles Publishing. http://ebookcentral.proquest.com/lib/ualberta/detail.action?docID=3417283

Wang, D., Takoudjou, S. M., & Casella, E. (2020). LeWoS: A universal leaf-wood classification method to facilitate the 3D modelling of large tropical trees using terrestrial LiDAR. *Methods in Ecology and Evolution*, *11*(3), 376–389. https://doi.org/10.1111/2041-210X.13342

Wang, Y., Chen, Q., Zhu, Q., Liu, L., Li, C., & Zheng, D. (2019). A Survey of Mobile Laser Scanning Applications and Key Techniques over Urban Areas. *REMOTE SENSING*, *11*(13). https://doi.org/10.3390/rs11131540

Wang, Y., Pyörälä, J., Liang, X., Lehtomäki, M., Kukko, A., Yu, X., Kaartinen, H., & Hyyppä, J. (2019). In situ biomass estimation at tree and plot levels: What did data record and what did algorithms derive from terrestrial and aerial point clouds in boreal forest. *Remote Sensing of Environment*, *232*, 111309. https://doi.org/10.1016/j.rse.2019.111309

Warner, B. G., & Asada, T. (2006). Biological diversity of peatlands in Canada. *Aquatic Sciences*, *68*(3), 240–253. https://doi.org/10.1007/s00027-006-0853-2

Watt, P. J., & Donoghue, D. N. M. (2005). Measuring forest structure with terrestrial laser scanning. *International Journal of Remote Sensing*, *26*(7), 1437–1446. https://doi.org/10.1080/01431160512331337961

Wells, J. V., Dawson, N., Culver, N., Reid, F. A., & Morgan Siegers, S. (2020). The State of Conservation in North America's Boreal Forest: Issues and Opportunities. *Frontiers in Forests and Global Change*, *3*. https://doi.org/10.3389/ffgc.2020.00090

Wenger, S. J., & Olden, J. D. (2012). Assessing transferability of ecological models: An underappreciated aspect of statistical validation. *Methods in Ecology & Evolution*, *3*(2), 260–267. https://doi.org/10.1111/j.2041-210X.2011.00170.x

Westra, S., Alexander, L. V., & Zwiers, F. W. (2013). Global Increasing Trends in Annual Maximum Daily Precipitation. *Journal of Climate*, *26*(11), 3904–3918. https://doi.org/10.1175/JCLI-D-12-00502.1

White, J. C., Coops, N. C., Wulder, M. A., Vastaranta, M., Hilker, T., & Tompalski, P. (2016). Remote Sensing Technologies for Enhancing Forest Inventories: A Review. *Canadian Journal of Remote Sensing*, *42*(5), 619–641. https://doi.org/10.1080/07038992.2016.1207484

Wieder, R. K., Vitt, D. H., & Jackson, R. B. (2006). *Boreal Peatland Ecosystems*. Springer Berlin / Heidelberg. http://ebookcentral.proquest.com/lib/ualberta/detail.action?docID=603642

Wieder, R., Vitt, D., & Benscoter, B. (2006). Peatlands and the Boreal Forest. In *Ecol. Stud.* (Vol. 188, pp. 1–8). https://doi.org/10.1007/978-3-540-31913-9_1

Wu, B., Zheng, G., & Chen, Y. (2020). An Improved Convolution Neural Network-Based Model for Classifying Foliage and Woody Components from Terrestrial Laser Scanning Data. *Remote Sensing*, *12*(6), 1010. https://doi.org/10.3390/rs12061010

Yu, X., Hyyppä, J., Holopainen, M., & Vastaranta, M. (2010). Comparison of Area-Based and Individual Tree-Based Methods for Predicting Plot-Level Forest Attributes. *Remote. Sens.* https://doi.org/10.3390/rs2061481

Zanhouo, D. A. K., & Nana, A. B. I. (2019). Modeling Climate Change Impact on Health and Population Migration: A Systematic Review. *Economics Literature*, *1*(1), 51–65. https://doi.org/10.22440/elit.1.1.4

Zeileis, A., & Hothorn, T. (2002). Diagnostic Checking in Regression Relationships. *R News*, *2*(3), 7–10.

Zhang, J. (2019). Boreal forests and taiga. In *Salem Press Encyclopedia of Science*. Salem Press. https://login.ezproxy.library.ualberta.ca/login?url=https://search.ebscohost.com/login.aspx?direct=true&db=ers&AN=94981257&site=eds-live&scope=site

Zhao, B., Zhuang, Q., Shurpali, N., Köster, K., Berninger, F., & Pumpanen, J. (2021). North American boreal forests are a large carbon source due to wildfires from 1986 to 2016. *Scientific Reports*, *11*(1). https://doi.org/10.1038/s41598-021-87343-3

Zhouxin Xi, Chris Hopkinson, & Laura Chasmer. (2018). Filtering Stems and Branches from Terrestrial Laser Scanning Point Clouds Using Deep 3-D Fully Convolutional Networks. *Remote Sensing*, *10*(8), 1215–1215. https://doi.org/10.3390/rs10081215

Zolkos, S. G., Goetz, S. J., & Dubayah, R. (2013). A meta-analysis of terrestrial aboveground biomass estimation using lidar remote sensing. *Remote Sensing of Environment*, *128*, 289–298. https://doi.org/10.1016/j.rse.2012.10.017

Appendix

Uncertainty Propagation

Final AGB estimates from the models are subject to uncertainties that stem from the model coefficients as well as from the instruments used to measure the variables being used as predictors in the model. These uncertainties can be seen as errorbars on the model estimates in Figures 6-14. These uncertainties were calculated using error propagation formulas as outlined below. When predictors consisted of the product of two variables (ie. $x = y \cdot z$ where x is the predictor and y and z are the two variables used), measurement uncertainties for y and z were measured and combined using equation 7 for propagating errors through multiplication by maintaining the uncertainty percentages of each variable:

$$\delta x = |x| \sqrt{\left(\frac{\delta y}{y}\right)^2 + \left(\frac{\delta z}{z}\right)^2}. \quad \text{(A1)}$$

In the power models, which follow the form $AGB = \beta x^{\alpha}$, where α and β are model coefficients with standard error values of $\delta\alpha$ and $\delta\beta$. The uncertainty of the AGB estimates are represented by equation (7), where y is replaced by β, δy is replaced by $\delta\beta$, δz is replaced by δx^{α} and z is replaced by x^{α}. In order to do this we need to determine the uncertainty of the term x^{α} which can be done by adding the linear approximations of x and α in quadrature. The linear approximation of x can be calculated as

$$\delta x^{\alpha}{}_1 = \alpha \cdot x^{\alpha-1} \cdot \delta x, \quad \text{(A2)}$$

and the linear approximation of α can be calculated as

$$\delta x^{\alpha}{}_2 = x^{\alpha} \cdot ln(x) \cdot \delta\alpha. \quad \text{(A3)}$$

These are then added together as

$$\delta x^{\alpha} = \sqrt{(\delta x_1^{\alpha})^2 + (\delta x_2^{\alpha})^2} \quad \text{(A4)}$$

The same process can be done for the multiple regression power models by expanding equation 7 to encompass a third term (equation 11)

$$\delta x = |x| \sqrt{\left(\frac{\delta m}{m}\right)^2 + \left(\frac{\delta y}{y}\right)^2 + \left(\frac{\delta z}{z}\right)^2}. \quad \text{(A5)}$$

Both terms with variables and coefficients are calculated as described using equations 8, 9, and 10.

Quadratic models follow a similar concept where we compute the uncertainty of each term from the model equation which takes the form

$$AGB = exp(\alpha x^2 + \omega x + \beta), \quad \text{(A6)}$$

where α, ω, and β are model coefficients, and x is the predictor variable. The uncertainty in the first term, αx^2, comes from the model uncertainty in α ($\delta\alpha$) and the measurement uncertainty in x^2 (δx^2). The measurement uncertainty in x^2 can be determined using the linear approximation of x^2 and the measurement uncertainty of x (δx) as shown in equation 12:

$$\delta x^2 = 2x \cdot \delta x. \quad \text{(A7)}$$

The δx^2 and $\delta\alpha$ terms can then be combined in the same fashion as outline in equation 7 to get $\delta\alpha x^2$. Similarly, the $\delta\omega$ and δx uncertainties that apply to the second term can be combined in the same way. These uncertainties are then added in quadrature (equation 13) to get the total uncertainty for the measurements inside the brackets of equation 11.

$$\delta T = \sqrt{(\delta\alpha x^2)^2 + (\delta\omega x)^2 + (\delta\beta)^2}. \quad \text{(A8)}$$

Finally, the uncertainty of the AGB estimates can be found using equation 14:

$$\delta AGB = AGB \cdot \delta T. \quad \text{(A9)}$$